Institute of Thermoelectricity, Academy of Sciences and Ministry of Education and Science of Ukraine

Journal of THERMOELECTRICITY

International Research

Founded in December, 1993

published 6 times a year

No. 2 *2019*

Editorial Board

International Editorial Board

Founders – National Academy of Sciences, Ukraine
Institute of Thermoelectricity of National Academy of Sciences and Ministry of Education and Science of Ukraine

Certificate of state registration № КВ 15496-4068 ПР

Address of editorial office:
Ukraine, 58002, Chernivtsi, General Post Office, P.O. Box 86.
Phone: +(380-372) 90 31 65.
Fax: +(380-3722) 4 19 17.
E-mail: jt@inst.cv.ua
http://www.jt.inst.cv.ua

Signed for publication 26.05.2019. Format 70×108/16. Offset paper №1. Offset printing.
Printer's sheet 11.5. Publisher's signature 9.2. Circulation 400 copies. Order 5.

Printed from the layout original made by "Journal of Thermoelectricity" editorial board
in the printing house of "Bukrek" publishers,
10, Radischev Str., Chernivtsi, 58000, Ukraine

CONTENTS

Rifert V.G., *doct. techn. sciences* [1]
Anatychuk L.I., *acad. National Academy of sciences of Ukraine*[2,3]
Barabash P.O., *cand. techn. sciences* [1]**,**
Usenko V.I., *doct. techn. sciences* [1]
Solomakha A.S., *cand. of techn. sciences* [1,2]
Petrenko V.G., *cand. of techn. sciences* [1]
Prybyla A.V., *cand. phys. - math. sciences* [2,3]
Strikun A.P.[1]

1NTUU KPI, 6 Politekhnicheskaya str, Kyiv, 03056, Ukraine;
[2]Institute of Thermoelectricity, 1 Nauky str.,
Chernivtsi, 58029, Ukraine *e–mail: anatych@gmail.com*
[2]Yu.Fedkovych Chernivtsi National University,
2, Kotsiubynskyi str., Chernivtsi, 58012, Ukraine

EVOLUTION OF CENTRIFUGAL DISTILLATION SYSTEM WITH A THERMOELECTRIC HEAT PUMP FOR SPACE MISSIONS

Part 2. Study of the variable characteristics of a multi-stage distillation system with a thermoelectric heat pump

The work presents the results of testing a multi-stage (5 stages) centrifugal distiller (CD) with the use of a thermoelectric heat pump (THP) to reduce power consumption. In the experiments, measurements were made of the local (online) data of distillation system, such as the temperature of the liquids (initial and distillate), current production, total salt content, specific power consumption at different speeds of distiller rotor, THP power, and the degree of concentration. The total duration of the tests was more than 700 hours, the amount of processed liquid (NaCl and urine) was more than 2000 kg. The study of three distillers and two THPs and a comparison of their results showed their identity, which characterizes high quality workmanship of these devices. The obtained operating parameters (revolutions n and THP power) can be used to optimize the design and operating modes of the entire CD + THP system. Bibl. 28, Fig. 8, Tabl. 1.

Key words: thermoelectricity, heat pump, distiller

Introduction

In [1 – 7], information is given on a 3-stage distiller with a thermoelectric heat pump. [8-10] show the results of the development of a five-stage centrifugal distiller with THP and its testing at the benches of the distiller manufacturer - Thermodistillation, Ukraine, and the customer - Honeywell, USA. In the following years, from 2002 to 2015, several articles and reports [11 – 18] were published on CDS tests at the NASA bench during the concentration of various solutions. These results, as well as some methods for improving the performance of the CDS system, are described in more detail in [19 – 26]. A more detailed review of the works is given in the 1st part of the article [27].

The published results quite convincingly describe the uniqueness of the system for its use in the life

support system of manned spacecraft in long space missions and on the International Space Station. However, the majority of publications give the integral characteristics of the CDS operation, namely the production of the Gd system (in distillate), kg/h; specific power consumption SPC, W·h/kg; the degree of water recovery from the original (processed) liquid %; and some indicators of the quality of the water obtained.

To create a theoretical model of CDS with a view to further improve it and optimize the design of the centrifugal distiller and the system as a whole, the data available in the published literature are insufficient. Attempts at modeling CDS were made in [28]. For the development, without proof of their suitability, the authors used some relationships to calculate the heat transfer coefficient during condensation and evaporation and did not take into account the temperature depression that occurs when the initial solutions are evaporated in the distiller. In addition, the thermal resistance of the wall was not taken into account in the calculation of heat transfer, which, as will be shown in part 3 of our article, can make up to 30 % of the total heat transfer. All this leads to a distortion of such important factors in assessing the efficiency of a thermoelectric heat pump (THP) as the difference in the temperature of liquid flows at the inlet of the device Δt_{IN} and the average temperature of liquids in the device Δt_{AV}.

From the data presented in our report [8] it follows that at the same rotational speeds of the distiller rotor, with decreasing THP power, a decrease in the specific energy consumption at CDS is observed, which was also noted in our works [19, 20]. The effect of this factor on the efficiency of THP and the value of system SPC has not been studied in more detail.

An important parameter of the efficiency of CD + THP system is also the degree of recovery. The larger this value, the smaller the amount of residue. In test trials of all works in the period from 1990 to 2017 there is no critical analysis of the possibility of achieving the maximum degree of recovery.

Experimental test bench for the study of integral characteristics of CD with THP

As already mentioned, in the period from 2000 to 2007, three identical five-stage centrifugal distillers were developed and manufactured by “TD” Co: the first one, in 2001, the second in 2002 and the third in 2006. Also, two thermoelectric heat pumps, developed and manufactured by the Institute of Thermoelectricity of the NAS and MES of Ukraine (ITE), were transferred to Honeywell International Inc. These devices were then tested in various versions at several test benches in the United States, including the NASA test bench.

Before shipment to the USA, the devices were tested at the “TD” Co. test bench.

Fig. 1 is a diagram of the test bench which was used by “TD” Co. for testing three distillers and two heat pumps.

The main and auxiliary equipment of the bench is combined by a system of pipelines that form two circulation circuits. In one of them (“hot”) the evaporated solution circulates, and in the other (“cold”) - distillate.

The test bench works as follows. The engine of the distiller 1 is switched on, providing given revolutions of the distiller rotor. The vacuum pump 7 sets the required pressure in the apparatus, which corresponds to the required boiling point of the solution. From the tank 13, the cold circuit is filled with distillate, in which the distillate is circulated through the distiller condenser 1, salimeter 9, rotameter 14, the cold side of the THP 2, heat exchanger-cooler 3 and again the distiller condenser. The “hot” circuit is filled from the tank 4 to the level set by the control valve 6. In the hot circuit, the solution circulates from the evaporator of the distiller 1 through the rotameter 14 to the hot side of the THP 2 and again to the evaporator of the distiller 1. When the electric power is supplied to the THP 2, the condensate is cooled in the "cold" circuit and the solution is heated in the "hot" circuit. The solution superheated in THP 2 relative

to the saturation temperature in the evaporator of distiller 1 partially evaporates, and the obtained steam is used as a heating agent in the next stage of distillation evaporation, the steam obtained in the last stage of the distiller is condensed in the contact condenser of distiller 1. Excess distillate from the cold circuit is automatically discharged into the distillate tank 5.

Valve 6 compensates with the fresh solution the evaporated part of the solution circulating in the hot circuit. At the same time, an increase in the concentration of dissolved substances occurs in it. Due to the fact that in THP 2 $Qr = mr \cdot cpr(t2 - t1) > Qx = mx \cdot cpx(t4 - t3)$, to ensure the stationarity of the process, the excess heat is removed by the heat exchanger-cooler 3 to the environment.

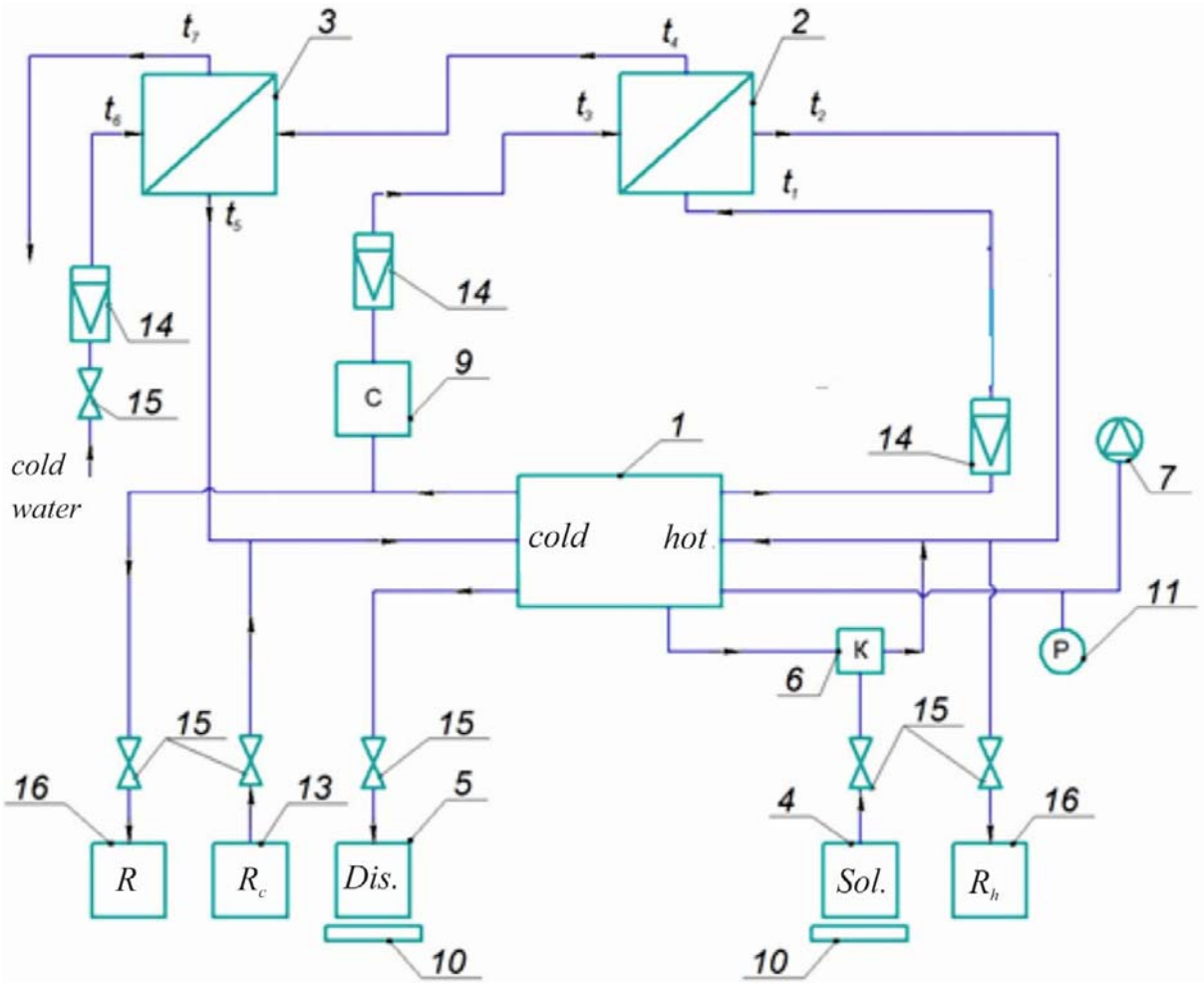

Fig.1. Diagram of the experimental test bench
1 – centrifugal vacuum distiller; 2 – thermoelectric heat pump;
3 – heat-exchanger-cooler; 4 – outlet solution; 5 – distillate collector;
6 – system power control valve; 7 –vacuum pump; 9 –salimeter; 10 –electronic balance;
11 – vacuum gauge; 13 – distillate container for refueling; 14 - rotameters;
15 –shut-off valve; 16 – circuit emptying containers.

After the experiment, the THP 2 power supply is turned off, and the cold and hot circuits are emptied into the corresponding containers 16.

The temperature was measured at the inlet and outlet of the thermal battery on the hot (t_1, t_2) and cold sides (t_3, t_4), behind the heat exchanger-cooler in the cold circuit (t_5) and at the inlet and outlet of the heat exchanger-cooler on the cooling side (t_6, t_7). The temperatures in the hot and cold circuits were measured with chromel-kopel thermocouples at an accuracy of ± 0.1 °C.

The pressure in the apparatus was measured with a vacuum gauge 11 with a measuring scale of -1 ... 0 bar (accuracy class 1.0) complete with a barometer.

The mass of the obtained distillate (product) and the initial solution was measured by electronic balance, the measurement accuracy of ± 2 g, the measurement range of ± 10 kg.

The salinity in the cold circuit was measured with a Hanna salimeter (0 ... 999ppm).

The drive power of the engine and heat pump was measured on the basis of voltmeters and ammeters, accuracy class 0.5. Revolutions were measured with a tachometer with an accuracy of ± 1 rpm.

Calculated values

Production in kilograms per hour:

$$G_d = \Sigma G_d / \Delta\tau, \quad (1)$$

where ΣG_d is the total mass of the obtained distillate in the tank 13, measured by the weights; $\Delta\tau$ is the measurement time interval.

Power consumption in watts for the main components of the CDS test product:

$$W = W_{THP} + W_{CD} \ , \quad (2)$$

where W_{THP} and W_{CD} is the average power consumed by THP and CD, respectively, over the period from the start to the stop of the distiller. The energy consumption of the vacuum pump was not taken into account at this stage.

Specific power consumption (*SPC*), W·h per kg of produced water:

$$SPC = W/G, \text{ W·h/kg}. \quad (3)$$

Degree of recovery:

$$R = G_d / G_{in}, \quad (4)$$

where $G_{in} = \Sigma G_{in}/\Delta\tau$ is the mass of the consumed solution during the experiment, calculated by the weights in the tank 16.

Heat pump efficiency:

$$COP = Q_r / W_{THP} \ , \quad (5)$$

where $Q_r = G_r \cdot C_p(t_2 - t_1)$, W, G_r is flow rate of the liquid (solution) in the hot circuit; C_p is the average isobaric heat capacity of the solution, kJ/(kg·K).

Test results

Table presents a typical list of measured key indicators when concentrating urine.

Here, production stands for distiller capacity, TDS is total number of dissolved solids.

Table

Typical table of measured values (urine, n=)1200 rpm

Time	Drive			THP			Weight		TDS	Flow		Product ion	SPC	Temperature				
	U	*I*	*W*	*U*	*I*	*W*	in	out		hot	Cold			Hot in THP	Hot out THP	Cold in THP	Cold out THP	
Min	V	A	W	V	A	W	r		mg/l	l/h		kg/h	W h/kg	^{0}C				
0	24.2	3.1	75.0	20.5	10.08	206.6	0	0	12	60	82	0.00	0.0	23.2	23.1	22.9	22.9	
6	24.2	3.1	75.0	22.5	10.9	245.3	288	184	22	60	82	1.84	174.1	31.8	43.7	23.4	22.7	
12	24.2	3.1	75.0	28.5	14.3	407.6	634	602	38	60	82	4.18	174.1	37.5	48.3	24.5	22.4	
18	24.2	3.1	75.0	29.2	14	408.8	1122	1070	51	60	82	4.68	103.4	38.7	49.4	25.1	22.3	
24	24.2	3.1	75.0	32	14.4	460.8	1584	1528	61	60	82	4.58	117.0	38.8	50.8	25.1	22.0	
30	24.2	3.1	75.0	31.8	15.2	483.4	2078	2006	67	60	82	4.78	116.8	39.4	51.5	25.2	22.1	
36	24.2	3.1	75.0	32.3	14.22	459.3	2592	2502	73	60	82	4.96	107.7	40.0	52.2	25.4	22.1	
42	24.2	3.1	75.0	32.1	15.24	489.2	3110	3004	76	60	82	5.02	112.4	40.0	52.2	25.4	22.3	
48	24.2	3.1	75.0	31.9	15.2	484.9	3628	3500	79	61	82	4.96	112.9	40.1	52.1	24.9	22.0	
54	24.2	3.1	75.0	32.4	15.36	497.7	4136	3990	82	61	83	4.90	116.9	40.3	52.2	25.1	22.1	
60	24.2	3.1	75.0	33	15.6	514.8	4656	4492	84	62	83	5.02	117.5	40.7	53.5	24.9	22.0	
66	24.2	3.1	75.0	33.2	15.64	519.2	5182	5006	87	62	83	5.14	115.6	40.9	53.2	24.9	22.1	
72	24.2	3.1	75.0	33.1	15.56	515.0	5702	5508	90	63	83	5.02	117.5	40.9	53.1	24.9	22.0	
78	24.2	3.1	75.0	33	15.58	514.1	6220	6010	92	64	83	5.02	117.4	40.9	53.2	24.9	22.0	
84	24.2	3.1	75.0	33.2	15.72	521.9	6740	6510	94	65	83	5.00	119.4	41.0	53.5	24.8	22.0	
90	24.2	3.1	75.0	33.2	15.46	513.3	7250	7010	96	67	83	5.00	117.7	41.0	53.5	24.8	22.0	
96	24.2	3.1	75.0	32.8	15.34	503.2	7755	7500	97	68	83	4.90	118.0	41.0	53.1	24.6	22.0	
102	24.2	3.1	75.0	32.9	15.4	506.7	8175	8000	98	71	83	5.00	116.3	41.0	53.1	24.8	22.0	
108	24.2	3.1	75.0	0	0	0.0	8280	8205	96	71	83							
Average	24.2	3	75.0			492.8			75			4.93	115.1					
Total							8280	8205										

The identity of performance of three models of multi-stage centrifugal distillers with two THPs

Figs. 2 and 3 show the results of the concentration of urine from three distiller models with a heat pump power of N = 400 W and a rotational speed of 1200 rpm for 60 minutes. It can be seen from the figures that the production G_d and the specific power consumption *SPC* of all three samples of centrifugal distillers are close. The discrepancy of data on these indicators at the same time τ does not exceed 5 %.

This result allows us in the further analysis of the results of the various tests not to indicate the distiller number.

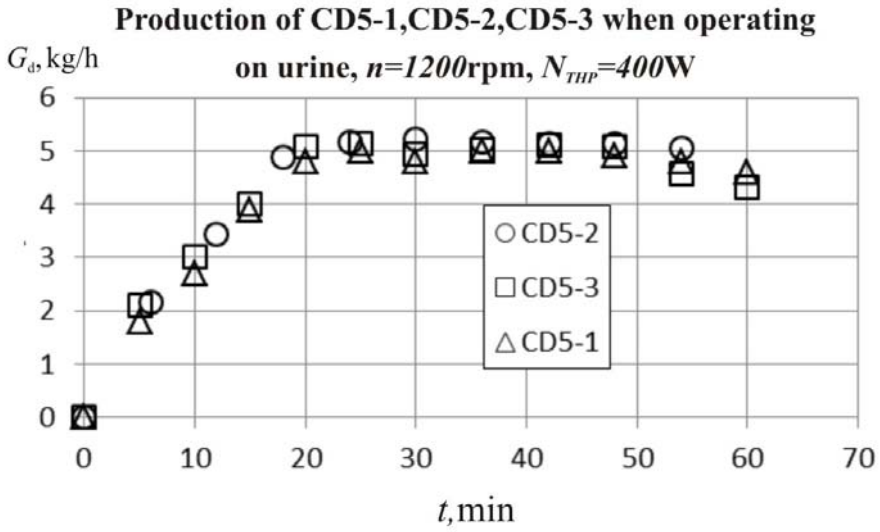

Fig.2 Time dependence of production for different distillers

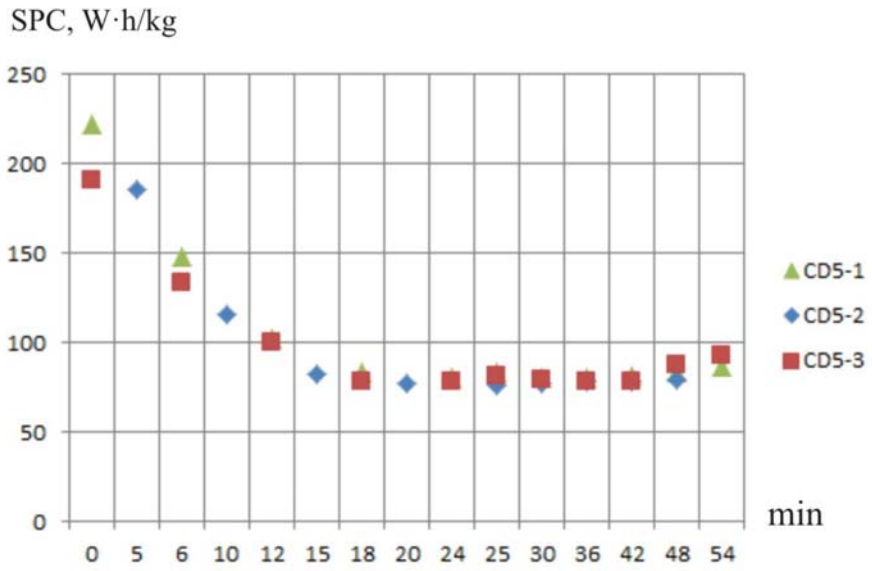

Fig.3 Time dependence of specific power consumption for different distillers, W = 400 W (without account of engine)

The identity of the THP is shown in Fig. 4, from which it follows that when operating on the same sample of the CD5-3 distiller with different heat pumps THP-1 and THP-2, the production with the same heat pump power is identical.

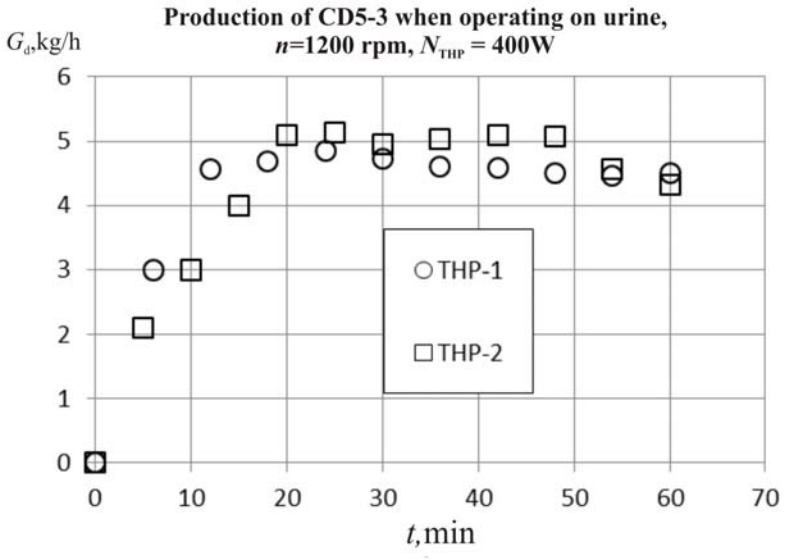

Fig.4. Time dependence of system production for two samples of thermoelectric heat pumps

Temperatures

Fig. 5 shows temperature change in online mode when processing urine with the initial concentration C = 5 %, rotations n = 1100 rpm and heat pump power N_{THP} = 400 W.

After turning on the distiller, after 10 minutes, the temperatures of the liquids in the hot and cold circuits reach the operating value.

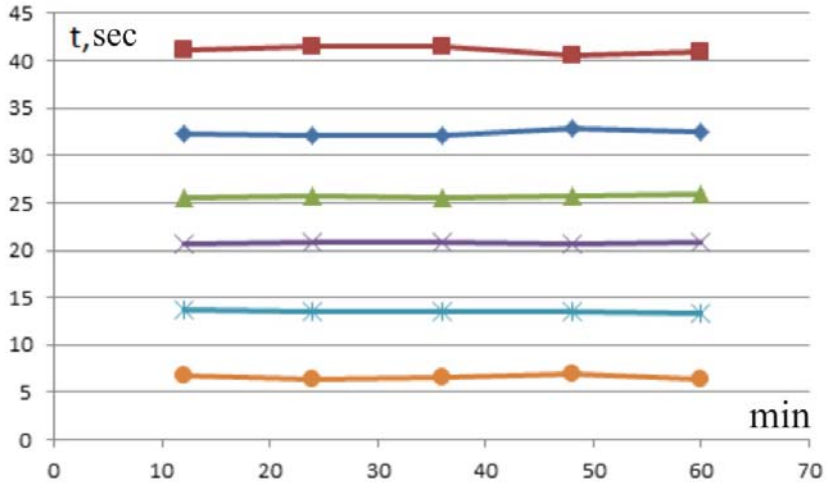

Fig.5a The dependence of temperatures on the time of the experiment (Water)

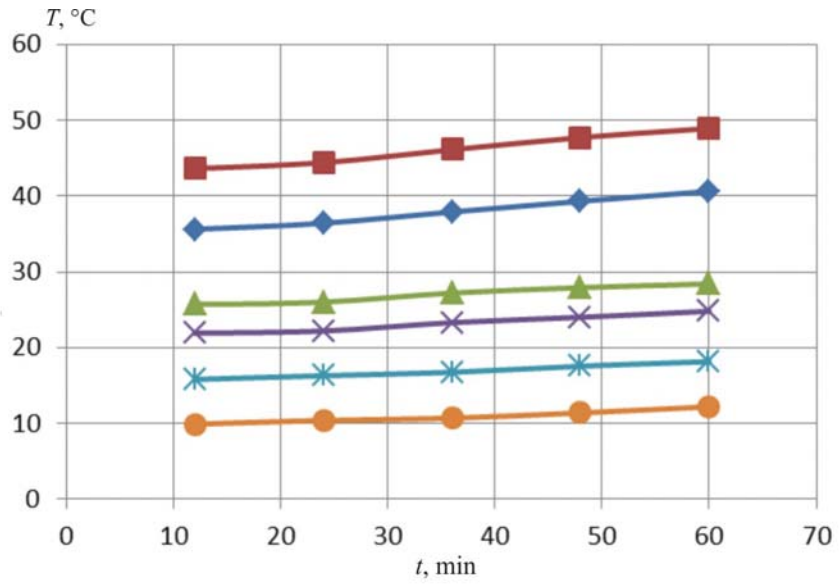

Fig.5b The dependence of temperatures on the time of the experiment (Urine)

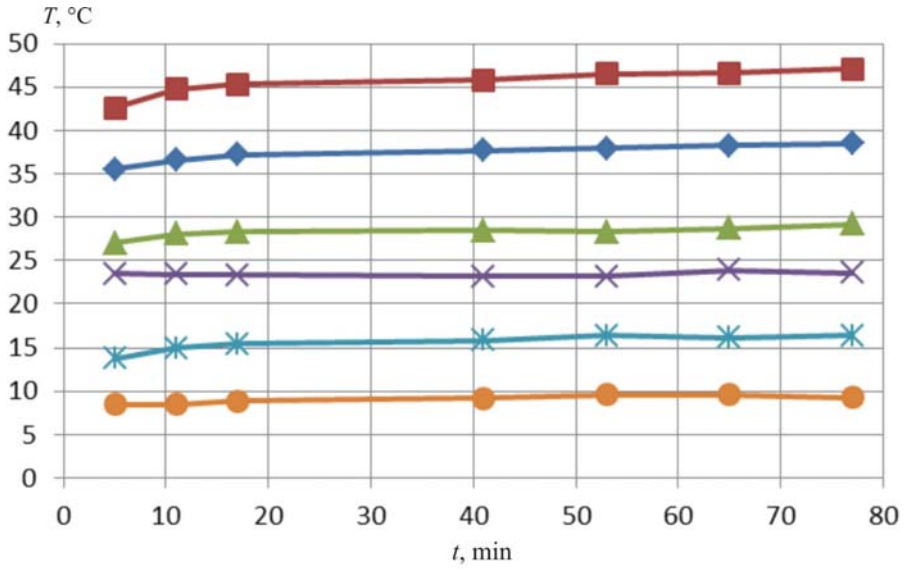

Fig.5c The dependence of temperatures on the time of the experiment (NaCl)

hot-in — *solution temperature at the inlet to the heat pump in the "hot" circuit (t_1), °C;*

hot-out — *solution temperature at the outlet of the heat pump in the "hot" circuit (t_2), °C;*

cold-in — *distillate temperature at the inlet to the heat pump in the "cold" circuit (t_3), °C;*

cold-out — *distillate temperature at the outlet of the heat pump in the "cold" circuit (t_4), °C;*

Δt — *average temperature head at the heat pump, $\Delta t_{av} = 0{,}5(t_1 + t_2) - 0{,}5(t_3 + t_4)$, °C;*

Δt_in — *average temperature head at the inlet to the heat pump, $\Delta t_{in} = t_1 - t_3$, °C;*

When concentrating a *NaCl* solution and urine, the temperatures in the hot circuit increase throughout the experiment due to an increase in the physical-chemical temperature depression during

evaporation. In turn, this increases the overall average temperature head at the heat pump (Δt_{av}) and the average temperature head at the inlet to the heat pump (Δt_{in}), which affects the efficiency of the heat pump.

Production

It can be seen from Fig. 6 that when *NaCl* and urine are concentrated, the production is lower than that obtained when working on the distillate and decreases during the experiment due to an increase in temperature depression.

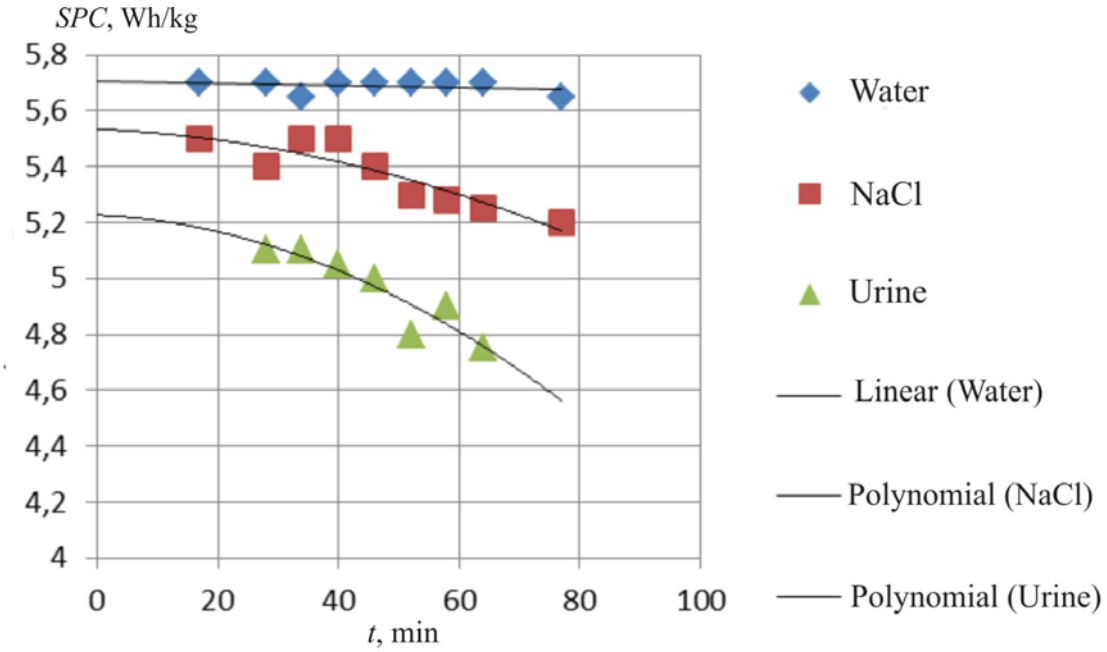

Fig. 6 The production of the distiller depending on the type of processed solution (n = 1100 rpm; N = 400 W).

Figure 7 shows the effect of heat pump power on the production of the distiller. The experiments were performed on urine at the same distillation speed (n = 1000 rpm). The amount of distillate obtained in all experiments was 5 kg, which corresponded to recovery ≈ 0.9. The greater the power of the heat pump, the higher the system production. In so doing, for each power in the initial 15 minutes there is an increase in the production (the device enters the operating mode), after which, due to an increase in the concentration of the solution in the hot circuit, the temperature depression increases and the production decreases. At the same time, the higher the power, the greater effect on the production is produced by temperature depression.

At the same time, as can be seen from Fig. 8, the higher the power supplied to the heat pump, the higher the specific energy consumption for producing one kg of distillate. Thus, from an energy point of view, it is more efficient to work at low heat pump powers.

In all tests performed, the quality of the obtained distillate met all the requirements to potable water. When processing NaCl, TDS in the "cold" circuit did not exceed 10 ppm. When processing urine, TDS < 100 ppm; COD (chemical oxygen demand) < 15 mg/*l*; ammonia NH3 + NH4 <5 mg/*l*.

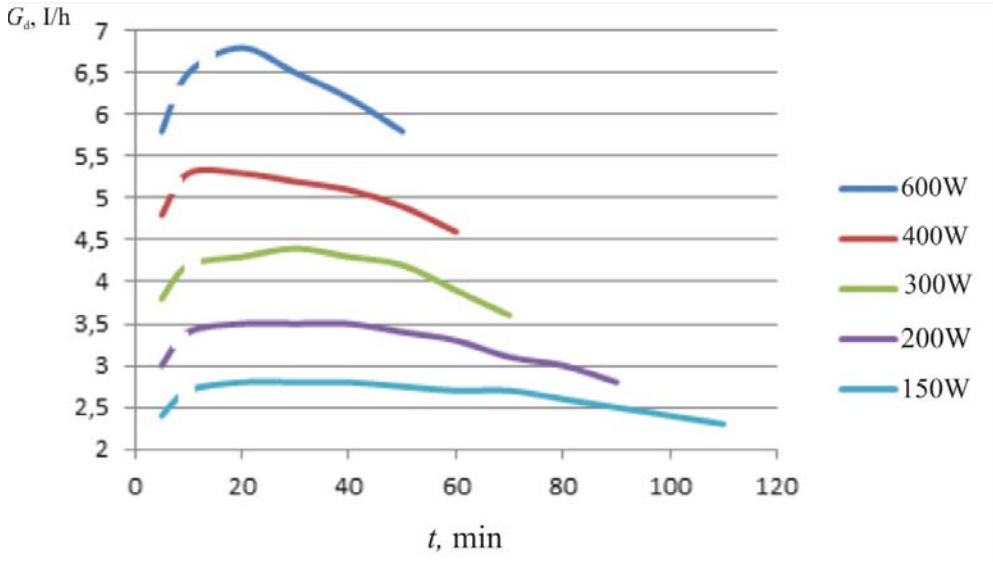

Fig. 7 Effect of heat pump power on the distiller production (n = 1000 rpm)

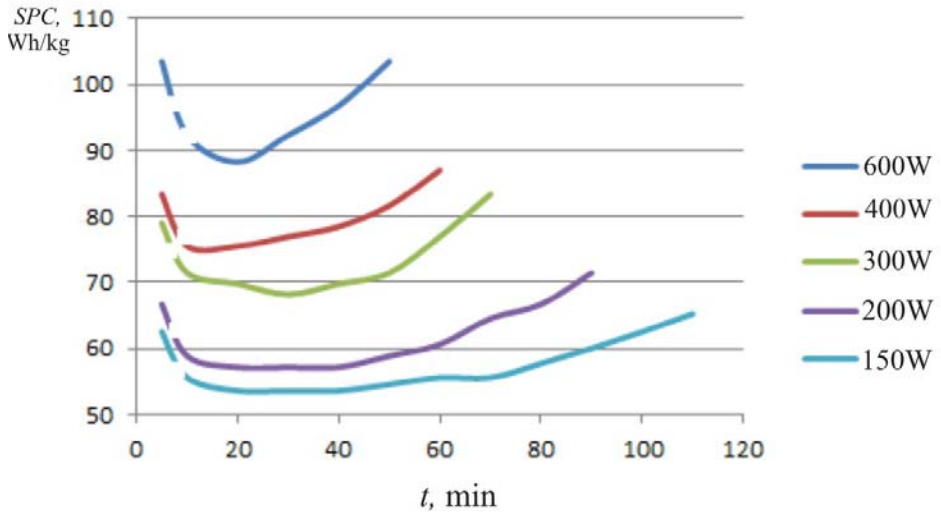

Fig. 8 Effect of heat pump power on the specific power consumption of the distiller without account of engine power (n = 1000 rpm)

Conclusions

1. This paper presents the results of measuring local parameters of distillation system (temperature in the "hot" and "cold" circuits, production, specific power consumption, TDS) in online mode with a change in testing time from 30 to 200 min, rotation speed n = 800…1200 rpm, NTHP = 150…600 W.
2. The identity of three manufactured multi-stage centrifugal distillers with 5 stages and 2 thermoelectric heat pumps is shown.
3. A decrease in SPC with a decrease in NTHP both locally, i.e. at a certain value of time τ, and on the average for the concentration of urine and *NaCl* solution at the same speed and total amount of distillate obtained has been noted.
4. Measured in all the tests, the main characteristics of distillate quality TDS, NH4, TOC meet the requirements to potable water.

References

1. Rifert V., Barabash P., Goliad N. (1990). Methods and processes of thermal distillation of water solutions for closed water supply systems. *SAE Paper 901249, 20th Intersociety Conference on Environmental Systems (Williamsburg, July 1990).*
2. Samsonov N., Bobe L., Novikov V., Rifert V., et al. (1994). Systems for water reclamation from humidity condensate and urine for space station. *SAE Paper 941536, 24th International society Conference on Environmental Systems (June, 1994).*
3. Samsonov N.M., Bobe L.S, Novikov V., Rifert V.G., Barabash P.A, et al (1995). Development of urine processor distillation hardware for space stations. *SAE Paper 951605, 25th International Conference on Environmental Systems (San Diego, July 1995).*
4. Samsonov, N.M., Bobe, L.S, Novikov, V., Rifert, V.G., et al. (1997). Updated systems for water recovery from humidity condensate and urine for the international space station. *SAE Paper 972559, 27th International Conference on Environmental Systems (Nevada, July 1997).*
5. Samsonov N.M., Bobe L.S, Novikov V., Rifert V.G., et al. (1999). Development and testing of a vacuum distillation subsystem for water reclamation from urine. *SAE Paper 1999-01-1993, 29th International Conference on Environmental Systems, 1999.*
6. Rifert V., Usenko V., Zolotukhin I., MacKnight A., Lubman A. (1999). Comparison of secondary water processors using distillation for space applications. *SAE Paper 99-70466, 29th International Conference on Environmental Systems (Denver, July 1999).*
7. Rifert V, Stricun, A., Usenko, V. (2000). Study of dynamic and extreme performances of multistage centrifugal distiller with the thermoelectric heat pump. *SAE Technical Papers 2000. 30th International Conference on Environmental Systems (Toulouse; France, 10-13 July 2000).*
8. Rifert, V., V. Usenko, I. Zolotukhin, A. MacKnight and A. Lubman (2001). Design optimisation of cascade rotary distiller with the heat pump for water reclamation from urine. (2001). *SAE Paper 2001-01-2248, 31st International Conference on Environmental Systems (Orlando, July 2001).*
9. Rifert, V. G., Usenko V.I., Zolotukhin I.V., MacKnight A. and Lubman A. (2003). Cascaded distillation technology for water processing in space. *SAE Paper 2003-01-2625. 34st International Conference on Environmental Systems (Orlando, July 2003).*
10. Lubman A, MacKnight A, Rifert V, Zolotukhin I. and Pickering K. (2006). Wastewater processing cascade distillation subsystem. design and evaluation. *SAE International, 2006-01-2273. July 2006.*
11. Lubman A., MacKnight A., Rifert V. and Barabash, P. (2007). Cascade distillation subsystem hardware development for verification testing. *SAE International, 2007-01-3177, July 2007.*
12. Callahan M., Lubman A., MacKnight A., Thomas H. and Pickering K. (2008). Cascade distillation subsystem development testing. (2008). *SAE International, 2008-01-2195, July 2008.*
13. Callahan M., Lubman A. and Pickering K. (2009). Cascade distillation subsystem development: progress toward a distillation comparison test. (2009). *SAE International, 2009-01 -2401, July 2009.*
14. Callahan M., Patel V. and Pickering K. (2010). Cascade distillation subsystem development: early results from the exploration life support distillation technology comparison test. *American Institute of Aeronautics and Astronautics, 2010-6149, July 2010.*
15. McQuillan Jeff, Pickering Karn D., Anderson Molly, Carter Layne, Flynn Michael, Callahan Michael, Vega Leticia, Allada Rama and Yeh Jannivine. Distillation technology down-selection for the exploration life support (ELS) water recovery systems element. *40th International Conference on Environmental Systems, AIAA 2010-6125 (Barcelona, Spain. July 2010). .*
16. Patel V., Au H., Shull S., Sargusingh M., Callahan M.. (2014). Cascade distillation system – a water recovery system for deep space missions. *ICES-2014-12, 44 International Conference on*

Environmental Systems (Tucson, Arizona, July 2014).
17. Loeftelholz David, Baginski Ben, Patel Vipul, MacKnight Allen, Schull Sarah, Sargusingh Miriam, Callahan Michael. (2014). Unit operation performance testing of cascade distillation subsystem. *44th International Conference on Environmental Systems, 13-17 July 2014 (Tucson. Arizona). ICES-2014-0014.*
18. Callahan Michael R., Sargusingh Miriam J. (2014). Honeywell cascade distiller system performance testing interim results. American Institute of Aeronautics and Astronautics.
19. Rifert V.G., Anatychuk L.I., Barabash P.A, Usenko V.I., Strikun A.P., Prybyla A.V. (2017). Improvement of the distillation methods by using centrifugal forces for water recovery in space flight applications. *J.Thermoelectricity*, 1, 71-83.
20. Rifert Vladimir G., Barabash Petr A., Usenko Vladimir, Solomakha Andrii S., Anatychuk Lukyan I., Prybyla A.V. (2017). Improvement of the cascade distillation system for long-term space flights. 68th International Astronautical Congress (IAC) (Adelaide, Australia, 25-29 September 2017). IAC-17-A1.IP.25.
21. Anatychuk L.I.., Prybyla A.V. (2015). Optimization of thermal connections in thermoelectric liquid-liquid heat pumps for water purification systems of space application. *J.Thermoelectricity*, 4, 45 – 51.
22. Anatychuk L.I., Prybyla A.V. (2015). Optimization of power supply system of thermoelectric liquid-liquid heat pump. *J.Thermoelectricity*, 6, 53 – 58.
23. Anatychuk L.I., Rozver Yu.Yu., Prybyla A.V. (2017). Experimental study of thermoelectric liquid-liquid heat pump. *J.Thermoelectricity*, 3, C. 33 – 39.
24. Anatychuk L.I., Prybyla A.V. (2017). Limiting possibilities of thermoelectric liquid-liquid heat pump. *J.Thermoelectricity*, 4, 33 – 39.
25. Anatychuk L.I., Prybyla A.V. (2017). The influence of quality of heat exchangers on the properties of thermoelectric liquid-liquid heat pumps. *J.Thermoelectricity*, 5, 33 – 39.
26. Anatychuk L.I., Prybyla A.V. (2017). On the coefficient of performance of thermoelectric liquid-liquid heat pumps with regard to energy loss for heat carrier transfer. *J.Thermoelectricity*, 6, 33 – 39.
27. Rifert V.G., Anatychuk L.I., Barabash P.O., Usenko V.I., Strikun A.P, Solomakha A.S., Petrenko V.G., Prybyla A.V. (2019). Evolution of centrifugal distillation system with a thermoelectric heat pump for space missions. Part 1. Review of publications on centrifugal distillation in the period of 1990 – 2017. J.Thermoelectricity, 1, 5–15.
28. Perry Bruce A., Anderson Molly S. (2015). Improved dynamic modeling of the cascade distillation subsystem and analysis of factors affecting its performance. *45th International Conference on Environmental Systems 12-16 July 2015 (Bellevue, Washington). ICES-2015-216.*

Submitted 30.04.2019

Риферт В.Г., *док. техн. наук* [1]
Анатичук Л.І., *акад. НАН України*[2]
Барабаш П.О., *канд. техн. наук*[1]
Усенко В.І., *док. техн. наук*[1]
Соломаха А.С., *канд. техн. наук*[1,2]
Петренко В.Г., *канд. техн. наук*[1]
Прибула А.В., *канд. фіз.-мат. наук* [1]
Стрикун А.П.[1]

[1]НТУ «КПИ», вул. Політехнічна, 6,
Київ, 03056, Україна;
[2]Інститут термоелектрики, вул. Науки, 1,
Чернівці, 58029, Україна;
e–mail: anatych@gmail.com

ЕВОЛЮЦІЯ СИСТЕМИ ВІДЦЕНТРОВОЇ ДИСТИЛЯЦІЇ З ТЕРМОЕЛЕКТРИЧНИМ ТЕПЛОВИМ НАСОСОМ ДЛЯ КОСМІЧНИХ МІСІЙ

Частина 2. Дослідження змінних характеристик системи багатоступінчастої дистиляції (СМЕД) з термоелектричним тепловим насосом (ТНР)

У роботі наведені результати випробувань багатоступінчастого (5 щаблів) відцентрового дистилятора (СМЕД) з використанням для зниження енергоспоживання термоелектричного теплового насоса (ТНР). У досвідах заміряли локальні (у режимі он-лайн) дані системи дистиляції, такі як температура рідин (вихідної й дистиляту) продуктивність, що тече, загальний солевміст, питому витрату енергії при різних швидкостях обертання ротора дистилятора, потужності ТНР, ступінь концентрування. Загальна тривалість випробувань склала більш 700 годин, кількість переробленої рідини (NaCl і урини) склала більш 2000 кг. Дослідження трьох дистиляторів і двох ТНР і порівняння їх результатів показало їхню ідентичність, що характеризує висока якість виготовлення цих пристроїв. Отримані дані параметрів експлуатації (оберти n і потужність ТНР), можуть бути використані для оптимізації конструкції й режимів експлуатації роботи всієї системи СД + ТНР. Бібл. 28, рис. 8, табл. 1.

Ключові слова: термоелектрика, тепловий насос, дистилятор

Риферт В.Г., *док. техн. наук* [1]
Анатычук Л.И., *акад. НАН Украины*[2]
Барабаш П.О. *канд. техн. наук*[1]
Усенко В.И. *док. техн. наук*[1]
Соломаха А. С., *канд. техн. наук*[1,2]
Петренко В. Г., *канд. техн. наук*[1]
Прибила А. В. *канд. физ.-мат. наук* [1]
Стрикун А.П.[1]

[1]НТУ «КПИ», вул. Политехническая, 6,
Киев, 03056, Украина;
[2]Институт термоэлектричества НАН и МОН Украины,
ул. Науки, 1, Черновцы, 58029, Украина,
e–mail: anatych@gmail.com

ЭВОЛЮЦИЯ СИСТЕМЫ ЦЕНТРОБЕЖНОЙ ДИСТИЛЛЯЦИИ С ТЕРМОЭЛЕКТРИЧЕСКИМ ТЕПЛОВЫМ НАСОСОМ ДЛЯ КОСМИЧЕСКИХ МИССИЙ

Часть 2. Исследование переменных характеристик системы многоступенчатой дистилляции (СМЕД) с термоэлектрическим тепловым насосом (THP)

В работе приведены результаты испытаний многоступенчатого (5 ступеней) центробежного дистиллятора (СМЕД) с использованием для снижения энергопотребления термоэлектрического теплового насоса (THP). В опытах замеряли локальные (в режиме он-лайн) данные системы дистилляции, такие как температура жидкостей (исходной и дистиллята), текущую производительность, общее солесодержание, удельный расход энергии при разных скоростях вращения ротора дистиллятора, мощности THP, степень концентрирования. Общая продолжительность испытаний составила более 700 часов, количество переработанной жидкости (NaCl и урины) составила более 2000 кг. Исследование трех дистилляторов и двух THP и сравнение их результатов показало их идентичность, что характеризует высокое качество изготовления этих устройств. Получены данные параметров эксплуатации (обороты n и мощность THP), могут быть использованы для оптимизации конструкции и режимов эксплуатации работы всей системы СД + THP. Библ. 28, рис. 8, табл. 1.
Ключевые слова: термоэлектричество, тепловой насос, дистилятор.

References

1. Rifert V., Barabash P., Goliad N. (1990). Methods and processes of thermal distillation of water solutions for closed water supply systems. *SAE Paper 901249, 20th Intersociety Conference on Environmental Systems (Williamsburg, July 1990).*
2. Samsonov N., Bobe L., Novikov V., Rifert V., et al. (1994). Systems for water reclamation from humidity condensate and urine for space station. *SAE Paper 941536, 24th International society Conference on Environmental Systems (June, 1994).*
3. Samsonov N.M., Bobe L.S, Novikov V., Rifert V.G., Barabash P.A, et al (1995). Development of urine processor distillation hardware for space stations. *SAE Paper 951605, 25th International Conference on Environmental Systems (San Diego, July 1995).*
4. Samsonov, N.M., Bobe, L.S, Novikov, V., Rifert, V.G., et al. (1997). Updated systems for water recovery from humidity condensate and urine for the international space station. *SAE Paper 972559, 27th International Conference on Environmental Systems (Nevada, July 1997).*
5. Samsonov N.M., Bobe L.S, Novikov V., Rifert V.G., et al. (1999). Development and testing of a vacuum distillation subsystem for water reclamation from urine. *SAE Paper 1999-01-1993, 29th International Conference on Environmental Systems, 1999.*
6. Rifert V., Usenko V., Zolotukhin I., MacKnight A., Lubman A. (1999). Comparison of secondary water processors using distillation for space applications. *SAE Paper 99-70466, 29th International Conference on Environmental Systems (Denver, July 1999).*
7. Rifert V, Stricun, A., Usenko, V. (2000). Study of dynamic and extreme performances of multistage centrifugal distiller with the thermoelectric heat pump. *SAE Technical Papers 2000. 30th International Conference on Environmental Systems (Toulouse; France, 10-13 July 2000).*
8. Rifert, V., V. Usenko, I. Zolotukhin, A. MacKnight and A. Lubman (2001). Design optimisation of cascade rotary distiller with the heat pump for water reclamation from urine. (2001). *SAE Paper 2001-*

01-2248, 31st International Conference on Environmental Systems (Orlando, July 2001).
9. Rifert, V. G., Usenko V.I., Zolotukhin I.V., MacKnight A. and Lubman A. (2003). Cascaded distillation technology for water processing in space. *SAE Paper 2003-01-2625. 34st International Conference on Environmental Systems (Orlando, July 2003).*
10. Lubman A, MacKnight A, Rifert V, Zolotukhin I. and Pickering K. (2006). Wastewater processing cascade distillation subsystem. design and evaluation. *SAE International, 2006-01-2273. July 2006.*
11. Lubman A., MacKnight A., Rifert V. and Barabash, P. (2007). Cascade distillation subsystem hardware development for verification testing. *SAE International, 2007-01-3177, July 2007.*
12. Callahan M., Lubman A., MacKnight A., Thomas H. and Pickering K. (2008). Cascade distillation subsystem development testing. (2008). *SAE International, 2008-01-2195, July 2008.*
13. Callahan M., Lubman A. and Pickering K. (2009). Cascade distillation subsystem development: progress toward a distillation comparison test. (2009). *SAE International, 2009-01 -2401, July 2009.*
14. Callahan M., Patel V. and Pickering K. (2010). Cascade distillation subsystem development: early results from the exploration life support distillation technology comparison test. *American Institute of Aeronautics and Astronautics, 2010-6149, July 2010.*
15. McQuillan Jeff, Pickering Karn D., Anderson Molly, Carter Layne, Flynn Michael, Callahan Michael, Vega Leticia, Allada Rama and Yeh Jannivine. Distillation technology down-selection for the exploration life support (ELS) water recovery systems element. *40th International Conference on Environmental Systems, AIAA 2010-6125 (Barcelona, Spain. July 2010). .*
16. Patel V., Au H., Shull S., Sargusingh M., Callahan M.. (2014). Cascade distillation system – a water recovery system for deep space missions. *ICES-2014-12, 44 International Conference on Environmental Systems (Tucson, Arizona, July 2014).*
17. Loeftelholz David, Baginski Ben, Patel Vipul, MacKnight Allen, Schull Sarah, Sargusingh Miriam, Callahan Michael. (2014). Unit operation performance testing of cascade distillation subsystem. *44th International Conference on Environmental Systems, 13-17 July 2014 (Tucson. Arizona). ICES-2014-0014.*
18. Callahan Michael R., Sargusingh Miriam J. (2014). Honeywell cascade distiller system performance testing interim results. American Institute of Aeronautics and Astronautics.
19. Rifert V.G., Anatychuk L.I., Barabash P.A, Usenko V.I., Strikun A.P., Prybyla A.V. (2017). Improvement of the distillation methods by using centrifugal forces for water recovery in space flight applications. *J.Thermoelectricity*, 1, 71-83.
20. Rifert Vladimir G., Barabash Petr A., Usenko Vladimir, Solomakha Andrii S., Anatychuk Lukyan I., Prybyla A.V. (2017). Improvement of the cascade distillation system for long-term space flights. 68th International Astronautical Congress (IAC) (Adelaide, Australia, 25-29 September 2017). IAC-17-A1.IP.25.
21. Anatychuk L.I.., Prybyla A.V. (2015). Optimization of thermal connections in thermoelectric liquid-liquid heat pumps for water purification systems of space application. *J.Thermoelectricity*, 4, 45 – 51.
22. Anatychuk L.I., Prybyla A.V. (2015). Optimization of power supply system of thermoelectric liquid-liquid heat pump. *J.Thermoelectricity*, 6, 53 – 58.
23. Anatychuk L.I., Rozver Yu.Yu., Prybyla A.V. (2017). Experimental study of thermoelectric liquid-liquid heat pump. *J.Thermoelectricity*, 3, C. 33 – 39.
24. Anatychuk L.I., Prybyla A.V. (2017). Limiting possibilities of thermoelectric liquid-liquid heat pump. *J.Thermoelectricity*, 4, 33 – 39.
25. Anatychuk L.I., Prybyla A.V. (2017). The influence of quality of heat exchangers on the properties of thermoelectric liquid-liquid heat pumps. *J.Thermoelectricity*, 5, 33 – 39.

26. Anatychuk L.I., Prybyla A.V. (2017). On the coefficient of performance of thermoelectric liquid-liquid heat pumps with regard to energy loss for heat carrier transfer. *J.Thermoelectricity*, 6, 33 – 39.
27. Rifert V.G., Anatychuk L.I., Barabash P.O., Usenko V.I., Strikun A.P, Solomakha A.S., Petrenko V.G., Prybyla A.V. (2019). Evolution of centrifugal distillation system with a thermoelectric heat pump for space missions. Part 1. Review of publications on centrifugal distillation in the period of 1990 – 2017. J.Thermoelectricity, 1, 5–15.
28. Perry Bruce A., Anderson Molly S. (2015). Improved dynamic modeling of the cascade distillation subsystem and analysis of factors affecting its performance. *45th International Conference on Environmental Systems 12-16 July 2015 (Bellevue, Washington). ICES-2015-216.*

Submitted 30.04.2019

Anatychuk L.I. *acad. National Academy of sciences of Ukraine*[1,2],
Kobylianskyi R.R. *cand. Phys.-math. sciences*[1,2],
Fedoriv R.V.[2]

[1]Institute of Thermoelectricity of the NAS and MES of Ukraine,
1, Nauky str., Chernivtsi, 58029, Ukraine;
[2]Yu.Fedkovych Chernivtsi National University,
2, Kotsiubynskyi str., Chernivtsi, 58012, Ukraine

COMPUTER SIMULATION OF HUMAN SKIN CRYODESTRUCTION PROCESS DURING THERMOELECTRIC COOLING

The paper presents the results of computer simulation of human skin cryodestruction process with regard to thermophysical processes, blood circulation, heat transfer, metabolic processes and phase transition. The physical, mathematical and computer models were built for human skin, on the surface of which there is a cooling element at a temperature of -50 ° C. The distribution of temperature and heat fluxes in human skin was determined in cooling mode. The obtained results make it possible to predict the depth of freezing of the skin and, accordingly, biological tissue at a given temperature effect.

Key words: human skin, temperature exposure, cryodestruction, phase transition, computer simulation.

Introduction

It is well known in medical practice that temperature exposure is an important factor in the treatment of many diseases of human body [1-3]. One of the promising lines is cryodestruction - a set of surgical treatment methods based on local freezing of the biological tissue of human body. Such cooling is mainly realized using special cryotools using liquid nitrogen [4 8]. However, the use of liquid nitrogen has several drawbacks: nitrogen does not provide the ability to provide cooling with the necessary accuracy of maintaining the temperature; there are also risks of hypothermia with negative consequences. In addition, liquid nitrogen is a rather dangerous substance and requires proper care when used, and the delivery of liquid nitrogen is not always available, which limits the possibility of using this method. An alternative to nitrogen cooling can be thermoelectric, which implements a decrease in temperature to 0 ÷ -80 ° C. Thermoelectric medical devices make it possible to precisely set the required temperature of the working tool, the time of temperature effect on the corresponding part of human body and provide a cyclic change of cooling and heating modes [1 – 2, 9 – 12].

Computer models created so far for human skin, on the surface of which there is a cooling element, make it possible to simulate thermophysical processes taking into account blood circulation, heat transfer, and metabolic processes [13 19]. However, existing computer models do not take into account the phase transition in the biological tissue when it is cooled, which leads to errors in computer simulation of temperatures and heat fluxes.

Therefore, *the purpose of this work* is to take into account the phase transition in the biological tissue during computer simulation of human skin cryodestruction process.

Physical model

According to physical 2D model with axial symmetry (Fig. 1), the biological tissue of human body is a structure of three skin layers (epidermis 1, dermis 2, subcutis 3) and the internal biological tissue 4, and is characterized by the following thermophysical properties: thermal conductivity κ_i, specific heat C_i, density ρ_i, blood perfusion rate ω_{bi}, blood density ρ_b, blood temperature T_b, specific heat of blood C_b and specific heat release Q_{meti} due to metabolic processes and latent phase transition heat L. The thermophysical properties of the skin and the biological tissue of human body in the normal and frozen states are given in [20 – 27]. The respective layers of the biological tissue 1-4 are considered as volumetric heat sources q_i, where:

$$q_i = Q_{meti} + \rho_b \cdot C_b \cdot \omega_{bi} \cdot (T_b - T), \quad i = 1..4 . \tag{1}$$

On the surface of the skin there is a cooling element 5. The geometric dimensions of each such layer 1-4 are a_i, b_i, and, respectively, of cooling element 5 – c, d. The temperatures at the boundaries of the respective layers 1-4 and cooling element 5 are T_1, T_2, T_3, T_4, T_5, T_6. The temperature inside the biological tissue is T_1 = +37°C. The temperature of the cooling element is T_7 = -50°C. The ambient temperature is T_8 = +22°C. The surface of human skin with a temperature of T_6 is in a state of heat exchange with the environment (heat transfer coefficient α and emissivity ε) at temperature T_8. The lateral surface of the skin is adiabatically isolated.

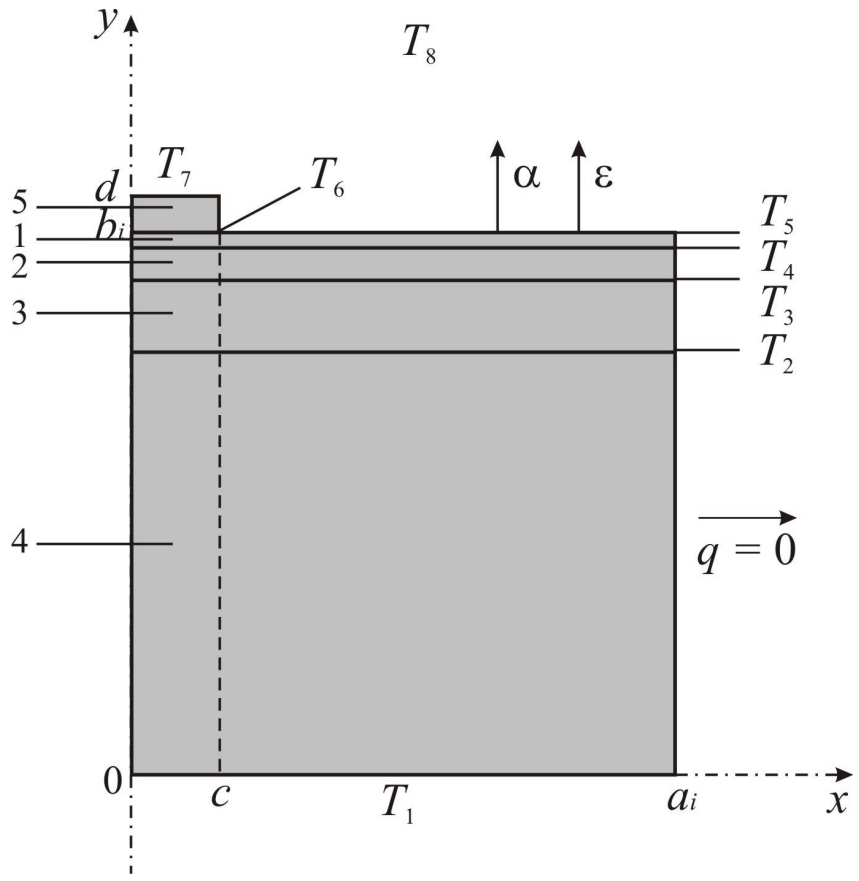

Fig.1. Physical 2D model of human skin with axial symmetry:
1 – epidermis, 2 – dermis, 3 – subcutis; 4 – internal biological tissue,
5 – cooling element

Mathematical model

In general, the equation of heat transfer in the biological tissue is given by [20-27]:

$$C_i \cdot \frac{\partial T}{\partial t} = \nabla \cdot (\kappa_i \cdot \nabla T) + \rho_b \cdot C_b \cdot \omega_{bi} \cdot (T_b - T) + Q_{meti}, \quad i = 1..4, \tag{2}$$

where C, κ are specific heat and thermal conductivity of the biological tissue, ρ_b is blood density, C_b is specific heat of blood, ω_b is blood perfusion of corresponding layers, T_b is blood temperature, T is temperature of the biological tissue; Q_{met} is heat which is released due to metabolic processes in each layer.

The term on the left side of equation (2) is the rate of change of thermal energy contained in a unit volume of the biological tissue. The three terms on the right side of this equation represent, respectively, the rate of change of thermal energy due to thermal conductivity, blood perfusion, and metabolic heat.

The equation of heat transfer in the biological tissue (2) is solved with the corresponding boundary conditions. The temperature on the surface of cooling element is T_7 = -50°C. The temperature inside the biological tissue is T_1 = + 37 ° C. The lateral surfaces of the biological tissue are adiabatically isolated (q = 0), and the upper surface of the skin is in a state of heat exchange (heat transfer coefficient α and emissivity ε) with the environment at a temperature of T_8.

$$q(x,y,t)\Big|_{\substack{c\le x\le a \\ y=b_i}} = \alpha \cdot (T_8 - T_5) + \varepsilon \cdot \sigma \cdot (T_8^4 - T_5^4), \tag{3}$$

where α is coefficient of convective heat exchange of the surface of the skin with the environment, ε is emissivity, σ is the Boltzmann constant, T_5 is the temperature of the biological tissue surface, T_8 is ambient temperature (T_8=+22°C).

At the initial time t = 0 s, it is believed that the temperature in the bulk of the biological tissue is T = + 37 °C, that is, the initial conditions for solving equation (2) are as follows:

$$T(x,y,0) = T_b. \tag{4}$$

As a result of solving the initial boundary value problem (2) - (4), the distributions of temperature $T(x, y, t)$ and heat fluxes in the respective skin layers are determined at an arbitrary time. As an example, in this paper we consider a case in which the temperature of cooling element is T_7 = -50 °C. However, it should be noted that the proposed method allows considering cases where the temperature of cooling element $T_f(t)$ changes in any temperature range or according to a predetermined function.

During the freezing, the cells will undergo a phase change at the freezing point, with the loss of the phase transition heat (L), and the temperature in these cells will not change. The phase transition in the biological cells occurs in the temperature range (-1 ÷ -8) °C. The properties of the skin and the biological tissue in the normal and frozen states are shown [20 – 27]. In the temperature range (-1 ÷ -8) °C, when cells are frozen, the heat of the phase transition is absorbed, which can be simulated by adding an appropriate value to the heat capacity [26, 27].

When the biological tissue is frozen, the vessels in the capillaries are narrowed to freeze all blood in the capillaries, and the value ω_{bi} tends to zero. In addition, the cells will not be able to generate metabolic heat when frozen and Q_{met} will be zero at a temperature below zero.

In the frozen state the properties of the skin and the biological tissue will have the following values (5) – (8):

$$C_i = \begin{cases} C_1 & T \geq -1°C \\ \dfrac{L}{-1-(-8)} + \dfrac{C_1 + C_2}{2} & -8°C \leq T \leq -1°C \\ C_2 & T \leq -8°C \end{cases} \quad (5)$$

$$\kappa_i = \begin{cases} \kappa_1 & T \geq -1°C \\ \dfrac{\kappa_1 + \kappa_2}{2} & -8°C \leq T \leq -1°C \\ \kappa_2 & T \leq -8°C \end{cases} \quad (6)$$

$$Q_{met_i} = \begin{cases} 420 & T \geq -1°C \\ 0 & -8°C \leq T \leq -1°C \\ 0 & T \leq -8°C \end{cases} \quad (7)$$

$$\omega_{b_i} = \begin{cases} 0,0005 & T \geq -1°C \\ 0 & -8°C \leq T \leq -1°C \\ 0 & T \leq -8°C \end{cases} \quad (8)$$

Computer model

A computer model of human skin was created on the surface of which there is a cooling element. To build a computer model, the Comsol Multiphysics application package was used [28], which makes it possible to simulate thermophysical processes in the biological tissue taking into account blood circulation, heat transfer, metabolic processes, and phase transition.

The distribution of temperatures and heat fluxes in the human skin and, accordingly, the biological tissue was calculated by the finite element method, the essence of which is that the object under study is divided into a large number of finite elements, and in each of them the value of a function is sought that satisfies given second-order differential equations with the corresponding boundary conditions. The accuracy of solving the problem depends on the level of partitioning and is ensured by the use of a large number of finite elements [28].

As an example, Figs. 2-3 show the distribution of temperature and isothermal surfaces in the bulk of human skin, on the surface of which a cooling element is placed at a temperature of T = -50 °C.

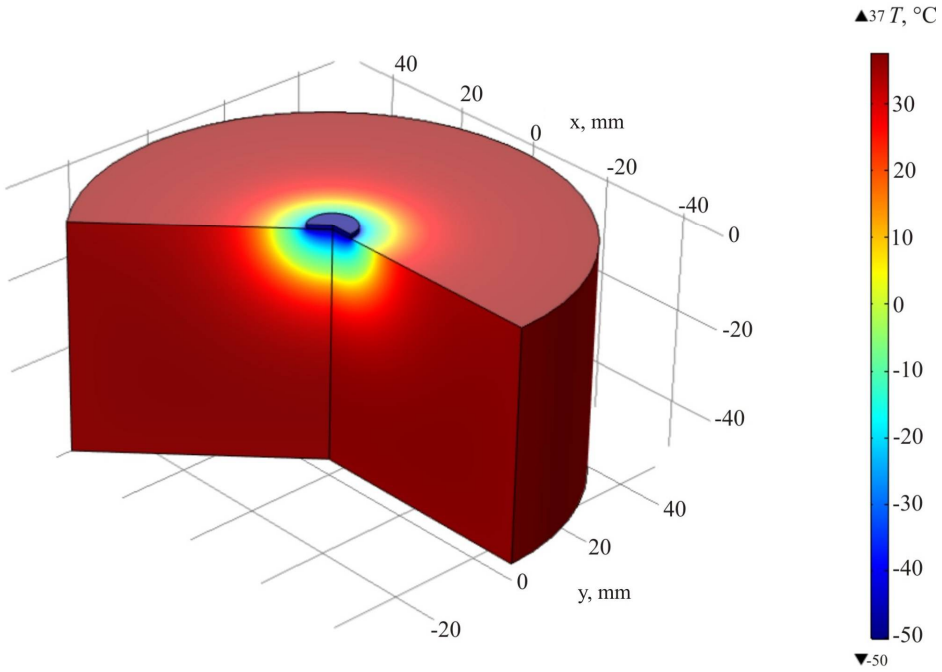

Fig.2. Temperature distribution in the bulk of human skin on the surface of which there is a cooling element at a temperature of T = -50°C

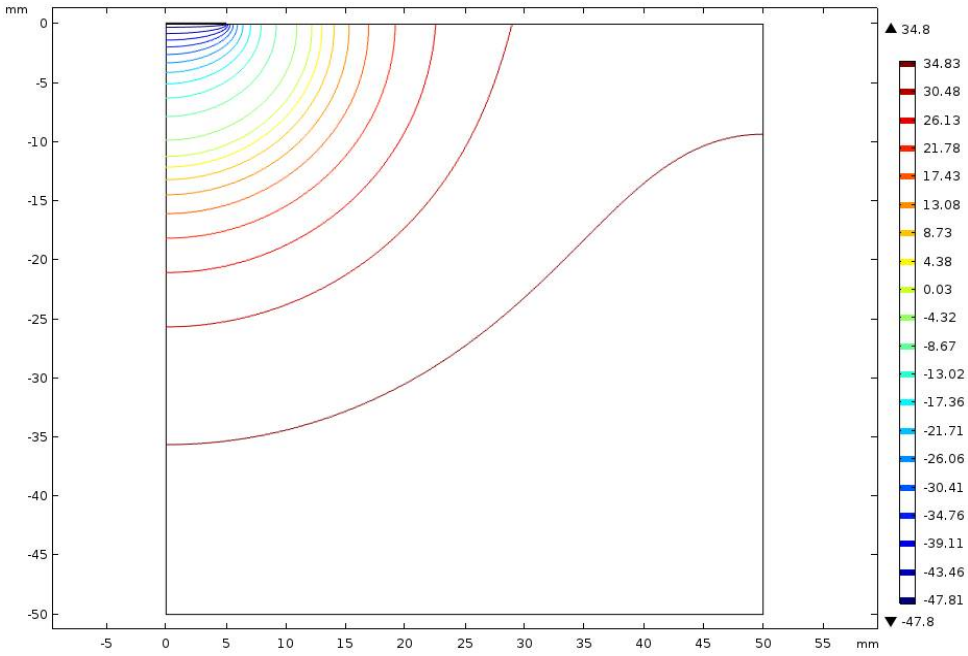

Fig. 3. Isothermal surfaces in the bulk of human skin on the surface of which there is a cooling element at a temperature of T = -50°C

Computer simulation results

Figs.4 *a*, *b*, *c*, *d*, *e*, *f* show temperature distributions in the section of human skin on the surface of which there is a cooling element at a temperature of $T = -50°C$ at different time moments

t = 10, 60, 180, 300, 600, 1200 *s*. In so doing, l_1 is temperature level T = -8°C and l_2 is temperature level T = -1°C.

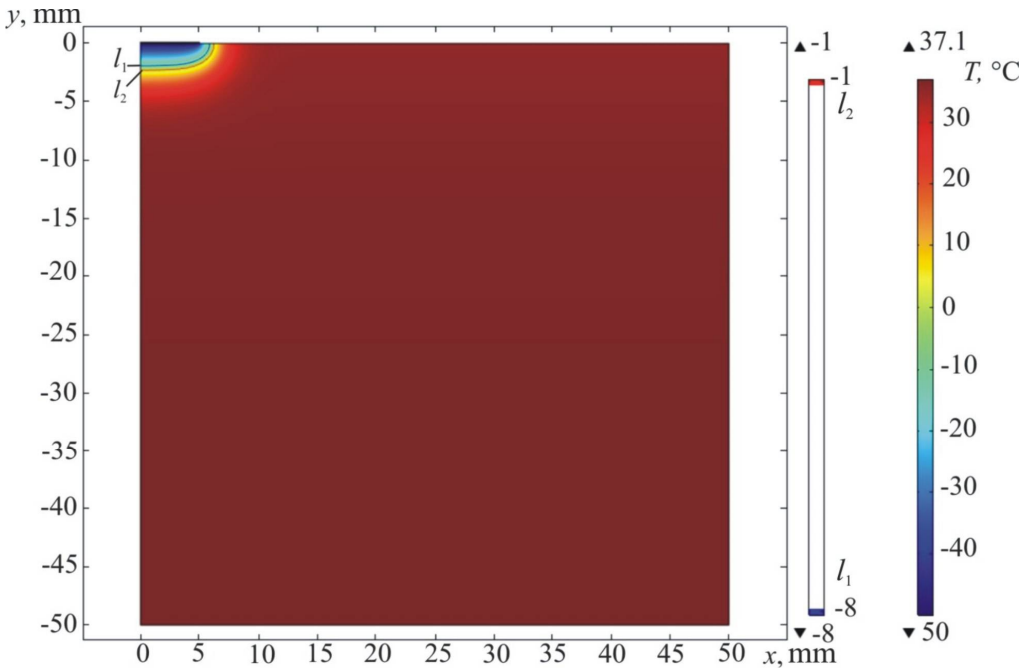

a) t = 10 s

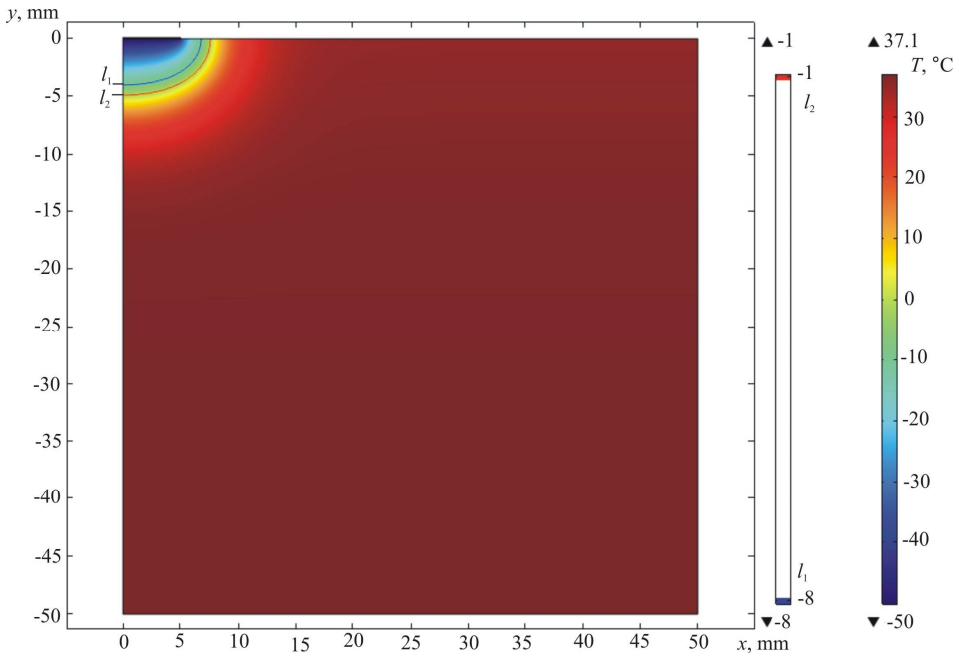

b) t = 60 s

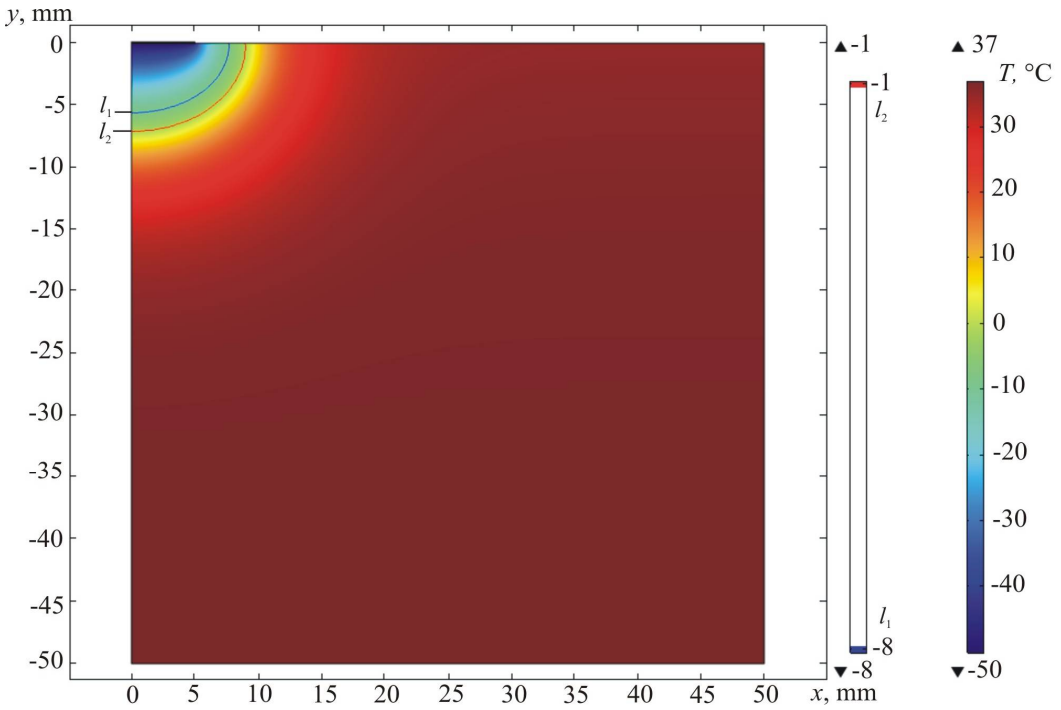

c) t = 180 s

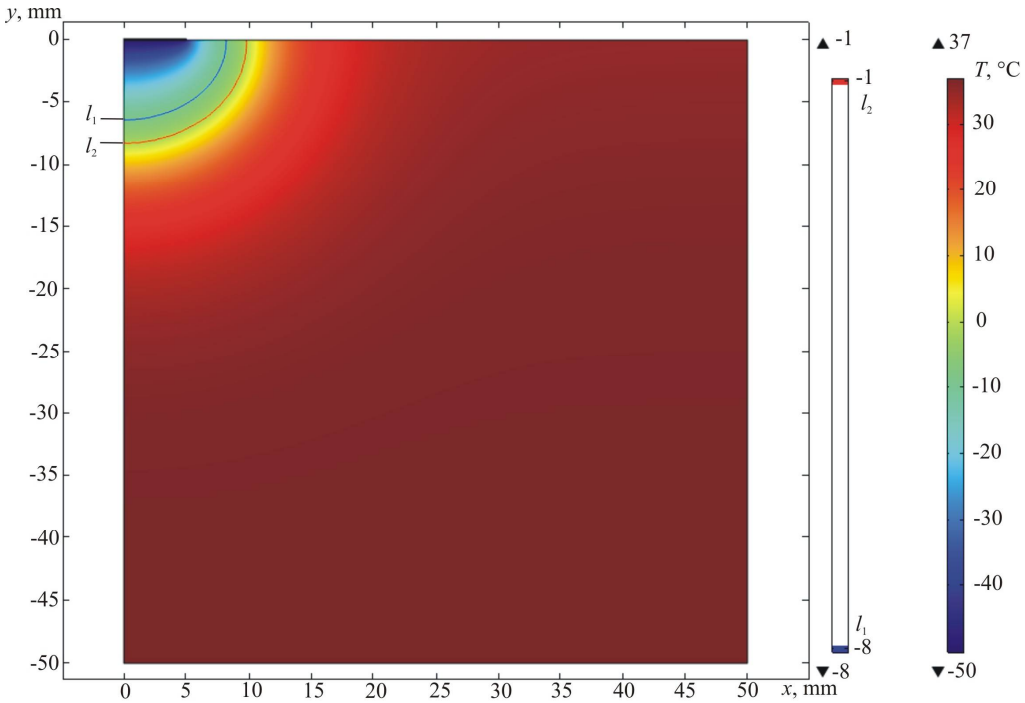

d) t = 300 s

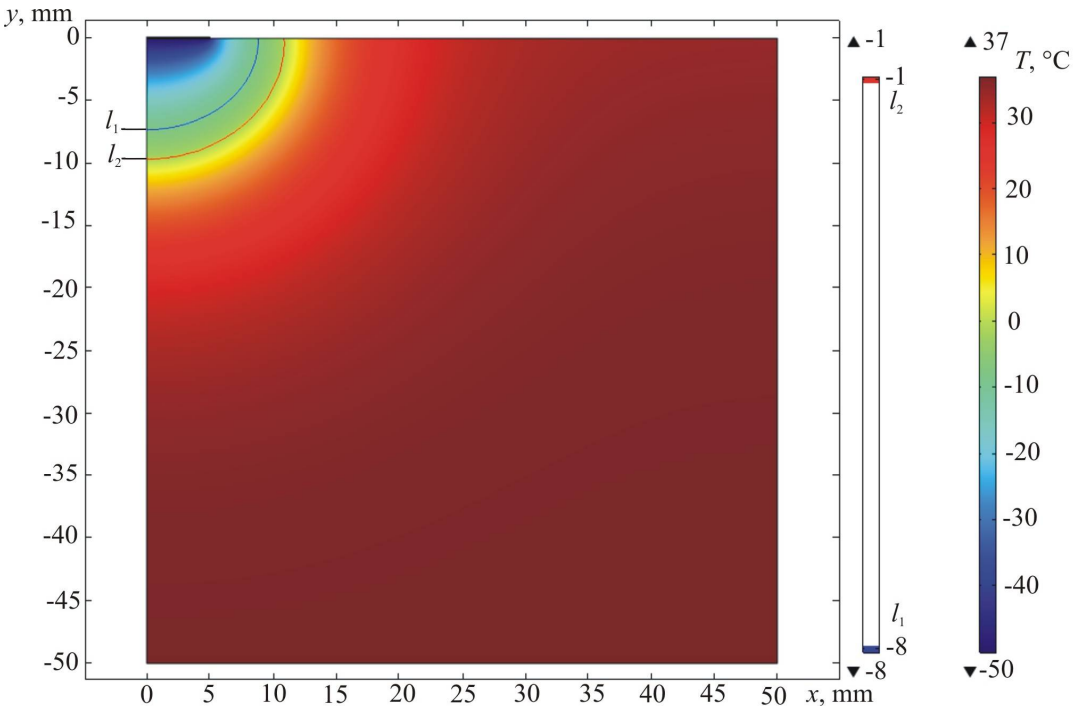

e) t = 600 s

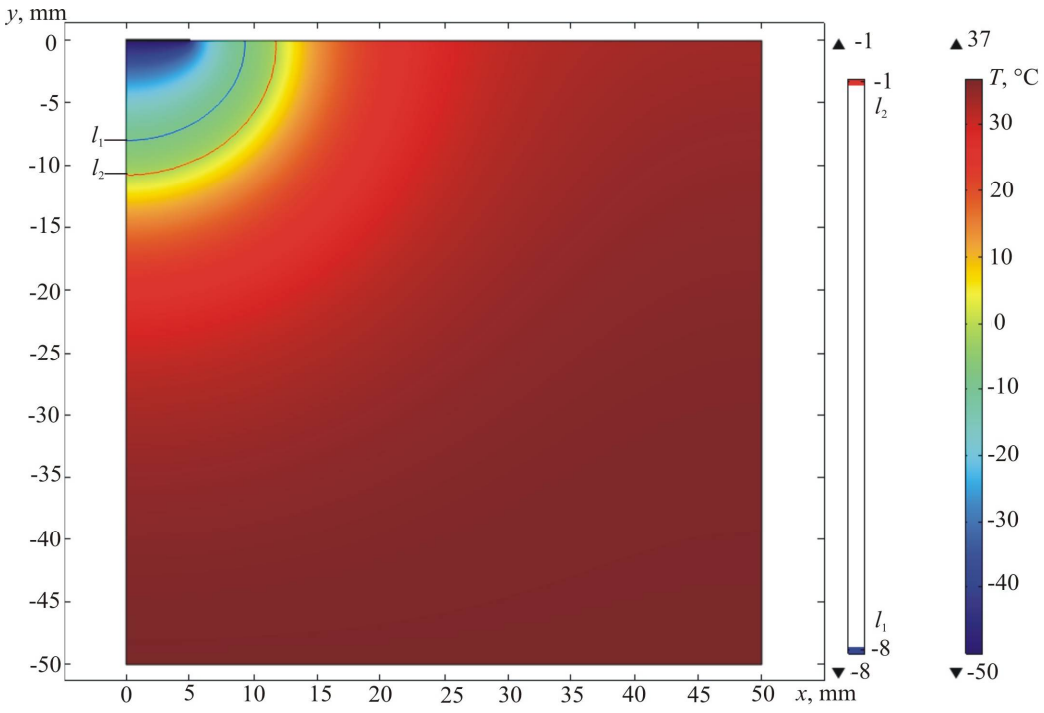

f) t = 1200 s

Fig.4 a, b, c, d, e, f. Temperature distributions in the section of human skin on the surface of which there is a cooling element at a temperature of T = -50°C, at different time moments: a) t = 10 s, b) t = 60 s, c) t = 180 s, d) t = 300 s, e) t = 600 s, f) t = 1200 s, where l_1 is temperature level T = -8°C and l_2 is temperature level T = -1°C

Fig. 5 shows the dependence of the movement of the phase transition zone (crystallization zone of the biological tissue) on the time of temperature exposure. From Fig. 5 it is obvious that the maximum freezing depth of human skin and, accordingly, the biological tissue is about l ≈ 10 mm at a temperature of cooling element T = 50 ° C.

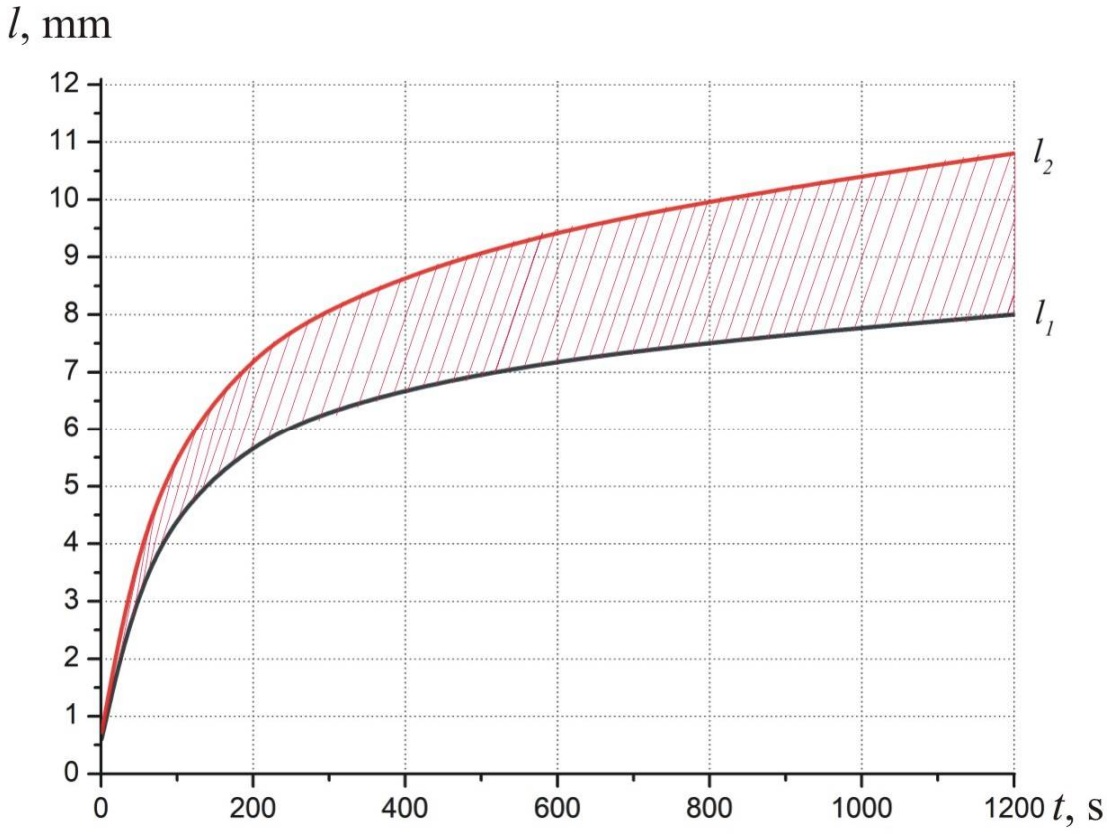

Fig. 5. Dependence of the movement of the phase transition zone (crystallization zone of the biological tissue) on the time of temperature exposure at a temperature of cooling element T = -50°C: l_1 – temperature level T = -8°C and l_2 – temperature level T = -1°C

Using computer simulation, we determined the dependence of the depth of freezing of human skin on temperature at different times (Fig. 6) and on the time of temperature exposure at a temperature of cooling element T = -50 ° C (Fig. 7).

Figs. 6, 7 show that at t = 60 s the biological tissue is cooled to a temperature of T = 10 ° C at a depth of l ≈ 3.5 mm, at t = 180 s - at a depth of l ≈ 5 mm, and at t = 600 s - at a depth of l ≈ 7 mm and at t = 1200 s - at a depth of l ≈ 7.5 mm.

It is established that with increasing temperature exposure, a deeper cooling of human skin is achieved. That is, with a prolonged temperature exposure (T = -50 °C), a destruction of the corresponding area of human skin can be achieved.

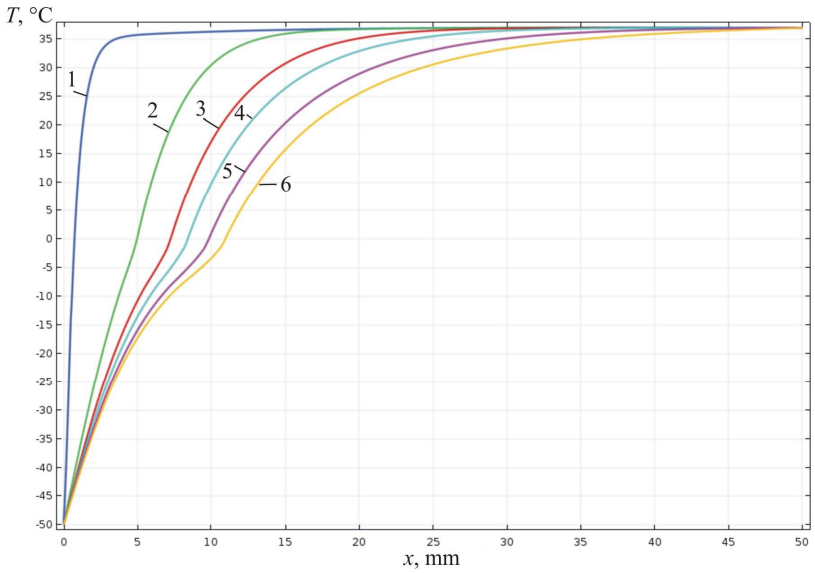

Fig. 6. Temperature distribution in human skin at different time moments of temperature exposure: 1 – t = 1 s; 2 – t = 60 s; 3 – t = 180 s; 4 – t = 300 s; 5 – t = 600 s; 6 – t = 1200 s

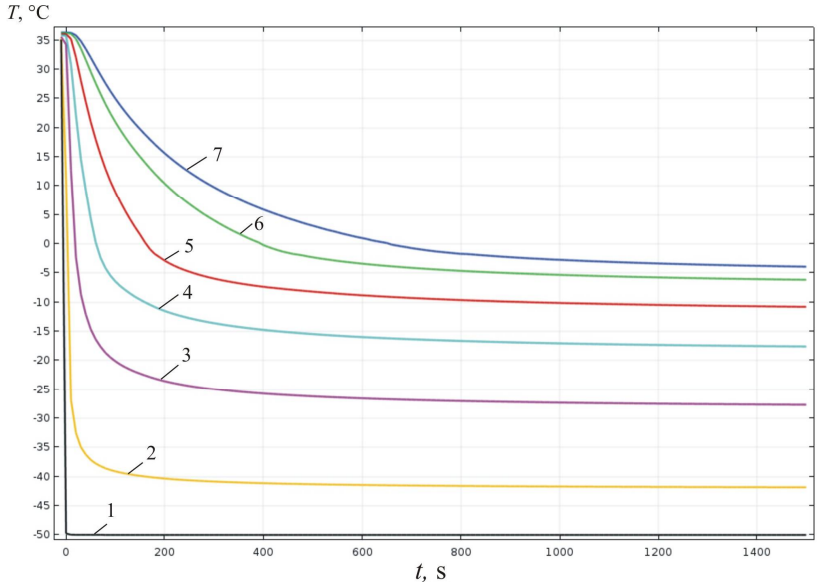

Fig. 7. Temporal dependence of temperature at different depth h of human skin at a temperature of cooling element T = -50°C: 1 – h = 0; 2 – h = 1 mm; 3 – h = 3 mm; 4 – h = 5 mm; 5 – h = 7 mm; 6 – h = 9 mm; 7 – h = 10 mm

Thus, a technique was developed for taking into account the phase transition in human skin during computer –aided simulation of cryodestruction process, which makes it possible to predict the results of local temperature effect on the biological tissue and to determine the temperature and heat flux distributions at any time moment with a predetermined arbitrary time function of change in the temperature of cooling element $T_f(t)$ [29].

It should be noted that the obtained results make it possible to predict the depth of freezing of the skin, and, accordingly, the biological tissue at a given temperature exposure, taking into account the phase transition to achieve the maximum effect during cryodestruction of human skin. They are also necessary for the design of thermoelectric refrigerators for cryodestruction of the skin and providing the necessary cooling modes.

Conclusion

1. A physical, mathematical and computer models of human skin, on the surface of which there is a cooling element at a temperature of T = -50°C were created with regard to thermophysical processes, blood circulation, heat transfer, metabolic and phase transition processes.
2. Using computer simulation, the distribution of temperature and heat fluxes in various skin layers was determined taking into account the phase transition in the process of cryodestruction of human skin. The dependence of the freezing depth of human skin on the temperature of cooling element and the time of the temperature exposure was established. The maximum freezing depth of the skin was determined which is $l \approx 10$ mm at a temperature of cooling element T=50° C.

References

1. Anatychuk L.I. (1979). *Termoelementy i termoelektricheskiie ustroistva. Spravochnik [Thermoelements and thermoelectric devices. Reference book]*. Kyiv: Naukova Dumka [in Russian].
2. Kolenko E.A. (1967). *Termoelektricheskiie okhlazhdaiushchiie pribory [Thermoelectric cooling devices]. 2nd ed.* Leningrad: Nauka [in Russian].
3. Anatychuk L.I., Denisenko O.I., Kobylianskyi R.R., Kadeniuk T.Ya., Perepichka M.P. (2017). Modern methods of cryotherapy in dermatological practice. *Klinichna ta eksperymental'na patologiia - Clinical and experimental pathology*, XVI, (59), 150-156.
4. Denkov V. (1988). At the edge of life. Moscow: Znaniie [Russian transl.]
5. Maruyama S., Nakagawa K., Takeda H.(2008). The flexible cryoprobe using Peltier effect for heat transfer control. *Journal of Biomechanical Science and Engineering*, 138-150.
6. Kochenov V.I. (2000). *Kriokhirurgicheskaia profilakticheskaia onkologiia [Cryosurgical preventive oncology]*. Nizhnii Novgorod [in Russian].
7. Kochenov V.I. (2003). *Kriologicheskaia profilakticheskaia onkologiia: kratkoie uchebnoie I metodicheskoie posibiie dlia vrachei i studentov [Cryological preventive oncology: brief educational and methodological manual for doctors and students]*. 2nd revised ed. Nizhnii Novgorod [in Russian].
8. Kochenov V.I. (1982). Adhesive effect in cryosurgery. *Abstract in the International Abstract Journal*, IV, 8.
9. Moskalyk, I.A., Manyk O.M. (2013). On the use of thermoelectric cooling in cryodestruction practice. *J.Thermoelectricity*, 6, 84-92.
10. Anatychuk L.I., Denisenko O.I., Kobylianskyi R.R., Kadeniuk T.Ya. (2015). On the use of thermoelectric cooling in dermatology and cosmetology. *J.Thermoelectricity*, 3, 57-71.
11. Moskalyk I.A. (2015). On the use of thermoelectric devices in cryosurgery. *Physics and Chemistry of the Solid State,* 4, 742-746.
12. Kobylianskyi R.R., Kadeniuk T.Ya. (2016) Pro perspektyvy vykorystannia termoelektryky dlia likuvannia zakhvoriuvan' shkiry kholodom [On the prospects of using thermoelectricity for treatment of skin diseases with cold]. *Naukovy visnyk Chernivetskogo universitetu: zbirnyk naukovykh ptrats. Fizyka. Elektronika - Scientific Bulletin of Chernivtsi University: Collection of Scientific Papers. Physics. Electronics,* 5, 1, 67 – 72 [in Ukrainian].
13. Anatychuk L.I., Vikhor L.M., Kotsur M.P., Kobylianskyi R.R., Kadeniuk T.Ya. (2016). Optimal control of time dependence of cooling temperature in thermoelectric devices. *J.Thermoelectricity*, 5, 5-11.

14. Anatychuk L.I., Kobylianskyi R.R., Kadeniuk T.Ya. (2017). Computer simulation of local thermal effect on human skin. *J.Thermoelectricity*, 1, 69-79.
15. Anatychuk L.I., Vikhor L.M., Kobylianskyi R.R., Kadeniuk T.Ya. (2017). Computer simulation and optimization of the dynamic operating modes of thermoelectric device for treatment of skin diseases. *J.Thermoelectricity*, 2, 44-57.
16. Anatychuk L.I.., Vikhor L.M., Kobylianskyi R.R., Kadeniuk T.Ya., Zvarich O.V. (2017). Computer simulation and optimization of the dynamic operating modes of thermoelectric device for reflexotherapy. *J.Thermoelectricity*, 3, 68-78.
17. Anatychuk L.I., Vikhor L.M., Kobylianskyi R.R., Kadeniuk T.Ya. (2017). Computer simulation and optimization of the dynamic operating modes of thermoelectric device for cryodestruction. *Physics and Chemistry of the Solid State*, 18 (4), 455-459.
18. Anatychuk L., Vikhor L, Kotsur M., Kobylianskyi R., Kadeniuk T. (2018). Optimal control of time dependence of temperature in thermoelectric devices for medical purposes. *International Journal of Thermophysics 3*9:108. https://doi.org/10.1007/s10765-018-2430-z.
19. Anatychuk L.I., Vikhor L.M., Kobylianskyi R.R., Kadeniuk T.Ya. (2018). Kompiuterne modeliuvannia lokalnoho temperaturnoho vplyvu na shkiru liudyny v dynamichnomu rezhymi [Computer simulation of local temperature effect on human skin in the dynamic mode]. *Visnyk Natsionalnogo universitetu "Lvivska Politechnica". Physical and mathematical sciences – Bulletin of National university "Lvivska Politechnica." Physical and mathematical sciences.* Lviv: Lvivska Politechnical Publ., 898, 78-82.
20. Pennes H.H. (1948). Analysis of tissue and arterial blood temperatures in the resting forearm *J. Appl. Physiol*. 1(2), 93 – 122.
21. Jiang S.C., Ma N., Li H.J. and Zhang X.X. (2002). Effects of thermal properties and geometrical dimensions on skin burn injuries. *Burns* 28, 713 – 717.
22. Cetingul M.P., Herman C. (2008). Identification of skin lesions from the transient thermal response using infrared imaging technique. *IEEE*, 1219 – 1222.
23. Ciesielski M., Mochnacki B. and Szopa R. (2011). Numerical modeling of biological tissue heating. Admissible thermal dose. *Scientific Research of the Institute of Mathematics and Computer Science* 1 (10), 11 – 20.
24. Filipoiu Florin, Bogdan Andrei Ioan and Carstea Iulia Maria (2010). Computer-aided analysis of the heat transfer in skin tissue. *Proceedings of the 3rd WSEAS Int. Conference on Finite Differences - Finite Elements - Finite Volumes - Boundary Elements,* 53 – 59.
25. Carstea Daniela, Carstea Ion and Carstea Iulia Maria Carstea (2011). Interdisciplinarity in computer-aided analysis of thermal therapies. *WSEAS Transactions on Systems and Control*, 6 (4), 115 – 124.
26. Deng Z.S., Liu J. (2005). Numerical simulation of selective freezing of target biological tissues following injection of solutions with specific thermal properties. *Cryobiology*, 50, 183-192.
27. Han Liang Lim, Venmathi Gunasekaran. Mathematical modeling of heat distribution during cryosurgery // https://isn.ucsd.edu/last/courses/beng221/problems/2011/project10.pdf.
28. COMSOL Multiphysics User's Guide (2018). COMSOLAB.
29. L.I. Anatychuk, R.R Kobylianskyi, R.V. Fedoriv (2019). Method for taking into account the phase transition in biological tissue during computer-aided simulationof cryodestruction process. *J.Thermoelectricity*, 1, 42 – 54.

Submitted 08.04.2019

Анатичук Л.І. *акад. НАН України*[1,2]
Кобилянський Р.Р. *канд. фіз.-мат. наук* [1,2], **Федорів Р.В.**[2]

[1]Інститут термоелектрики НАН і МОН України,
вул. Науки, 1, Чернівці, 58029, Україна;
[2]Чернівецький національний університет
ім. Юрія Федьковича, вул. Коцюбинського 2,
Чернівці, 58012, Україна; *e-mail: anatych@gmail.com*

МЕТОДИКА ВРАХУВАННЯ ФАЗОВОГО ПЕРЕХОДУ В БІОЛОГІЧНІЙ ТКАНИНІ ПРИ КОМП'ЮТЕРНОМУ МОДЕЛЮВАННІ ПРОЦЕСУ КРІОДЕСТРУКЦІЇ

У роботі наведено результати комп'ютерного моделювання процесу кріодеструкції шкіри людини з врахуванням теплофізичних процесів, кровообігу, теплообміну, процесів метаболізму та фазового переходу. Побудовано фізичну, математичну та комп'ютерну моделі шкіри людини, на поверхні якої знаходиться охолоджуючий елемент при температурі -50°C. Визначено розподіли температури і теплових потоків у шкірі людини в режимі охолодження. Отримані результати дають можливість прогнозувати глибину промерзання шкіри і, відповідно, біологічної тканини при заданому температурному впливі. Бібл. 29, рис. 7.

Ключові слова: шкіра людини, температурний вплив, кріодеструкція, фазовий перехід, комп'ютерне моделювання.

Анатичук Л.И. *акад. НАН Украины*[1,2]
Кобылянський Р.Р. *канд. физ.– мат. наук* [1,2], **Федорив Р.В.**[2]

[1]Институт термоэлектричества НАН и МОН Украины, ул. Науки, 1,
Черновцы, 58029, Украина, *e–mail: anatych@gmail.com;*
[2]Черновицкий национальный университет
им. Юрия Федьковича, ул. Коцюбинского, 2,
Черновцы, 58012, Украина

КОМПЬЮТЕРНОЕ МОДЕЛИРОВАНИЕ ПРОЦЕССА КРИОДЕСТРУКЦИИ КОЖИ ЧЕЛОВЕКА ПРИ ТЕРМОЭЛЕКТРИЧЕСКОМ ОХЛАЖДЕНИИ

В работе приведены результаты компьютерного моделирования процесса криодеструкции кожи человека с учетом теплофизических процессов, кровообращения, теплообмена, процессов метаболизма и фазового перехода. Построены физическая, математическая и компьютерная модели кожи человека, на поверхности которой находится охлаждающий

элемент при температуре -50 °C. *Определенно распределения температуры и тепловых потоков в коже человека в режиме охлаждения. Полученные результаты дают возможность прогнозировать глубину промерзания кожи и, соответственно, биологической ткани при заданном температурном воздействии. Библ. 28, рис. 7.*
Ключевые слова: кожа человека, температурное влияние, криодеструкция, фазовый переход, компьютерное моделирование.

References

1. Anatychuk L.I. (1979). *Termoelementy i termoelektricheskiie ustroistva. Spravochnik [Thermoelements and thermoelectric devices. Reference book]*. Kyiv: Naukova Dumka [in Russian].
2. Kolenko E.A. (1967). *Termoelektricheskiie okhlazhdaiushchiie pribory [Thermoelectric cooling devices]*. *2nd ed.* Leningrad: Nauka [in Russian].
3. Anatychuk L.I., Denisenko O.I., Kobylianskyi R.R., Kadeniuk T.Ya., Perepichka M.P. (2017). Modern methods of cryotherapy in dermatological practice. *Klinichna ta eksperymental'na patologiia - Clinical and experimental pathology*, XVI, (59), 150-156.
4. Denkov V. (1988). At the edge of life. Moscow: Znaniie [Russian transl.]
5. Maruyama S., Nakagawa K., Takeda H.(2008). The flexible cryoprobe using Peltier effect for heat transfer control. *Journal of Biomechanical Science and Engineering*, 138-150.
6. Kochenov V.I. (2000). *Kriokhirurgicheskaia profilakticheskaia onkologiia [Cryosurgical preventive oncology]*. Nizhnii Novgorod [in Russian].
7. Kochenov V.I. (2003). *Kriologicheskaia profilakticheskaia onkologiia: kratkoie uchebnoie I metodicheskoie posibiie dlia vrachei i studentov [Cryological preventive oncology: brief educational and methodological manual for doctors and students]*. 2nd revised ed. Nizhnii Novgorod [in Russian].
8. Kochenov V.I. (1982). Adhesive effect in cryosurgery. *Abstract in the International Abstract Journal*, IV, 8.
9. Moskalyk, I.A., Manyk O.M. (2013). On the use of thermoelectric cooling in cryodestruction practice. *J.Thermoelectricity*, 6, 84-92.
10. Anatychuk L.I., Denisenko O.I., Kobylianskyi R.R., Kadeniuk T.Ya. (2015). On the use of thermoelectric cooling in dermatology and cosmetology. *J.Thermoelectricity*, 3, 57-71.
11. Moskalyk I.A. (2015). On the use of thermoelectric devices in cryosurgery. *Physics and Chemistry of the Solid State,* 4, 742-746.
12. Kobylianskyi R.R., Kadeniuk T.Ya. (2016) Pro perspektyvy vykorystannia termoelektryky dlia likuvannia zakhvoriuvan' shkiry kholodom [On the prospects of using thermoelectricity for treatment of skin diseases with cold]. *Naukovy visnyk Chernivetskogo universitetu: zbirnyk naukovykh ptrats. Fizyka. Elektronika - Scientific Bulletin of Chernivtsi University: Collection of Scientific Papers. Physics. Electronics,* 5, 1, 67 – 72 [in Ukrainian].
13. Anatychuk L.I., Vikhor L.M., Kotsur M.P., Kobylianskyi R.R., Kadeniuk T.Ya. (2016). Optimal control of time dependence of cooling temperature in thermoelectric devices. *J.Thermoelectricity*, 5, 5-11.
14. Anatychuk L.I., Kobylianskyi R.R., Kadeniuk T.Ya. (2017). Computer simulation of local thermal effect on human skin. *J.Thermoelectricity*, 1, 69-79.
15. Anatychuk L.I., Vikhor L.M., Kobylianskyi R.R., Kadeniuk T.Ya. (2017). Computer simulation and optimization of the dynamic operating modes of thermoelectric device for treatment of skin diseases. *J.Thermoelectricity*, 2, 44-57.

16. Anatychuk L.I.., Vikhor L.M., Kobylianskyi R.R., Kadeniuk T.Ya., Zvarich O.V. (2017). Computer simulation and optimization of the dynamic operating modes of thermoelectric device for reflexotherapy. *J.Thermoelectricity*, 3, 68-78.
17. Anatychuk L.I., Vikhor L.M., Kobylianskyi R.R., Kadeniuk T.Ya. (2017). Computer simulation and optimization of the dynamic operating modes of thermoelectric device for cryodestruction. *Physics and Chemistry of the Solid State*, 18 (4), 455-459.
18. Anatychuk L., Vikhor L, Kotsur M., Kobylianskyi R., Kadeniuk T. (2018). Optimal control of time dependence of temperature in thermoelectric devices for medical purposes. *International Journal of Thermophysics 3*9:108. https://doi.org/10.1007/s10765-018-2430-z.
19. Anatychuk L.I., Vikhor L.M., Kobylianskyi R.R., Kadeniuk T.Ya. (2018). Kompiuterne modeliuvannia lokalnoho temperaturnoho vplyvu na shkiru liudyny v dynamichnomu rezhymi [Computer simulation of local temperature effect on human skin in the dynamic mode]. *Visnyk Natsionalnogo universitetu "Lvivska Politechnica". Physical and mathematical sciences – Bulletin of National university "Lvivska Politechnica." Physical and mathematical sciences.* Lviv: Lvivska Politechnical Publ., 898, 78-82.
20. Pennes H.H. (1948). Analysis of tissue and arterial blood temperatures in the resting forearm *J. Appl. Physiol*. 1(2), 93 – 122.
21. Jiang S.C., Ma N., Li H.J. and Zhang X.X. (2002). Effects of thermal properties and geometrical dimensions on skin burn injuries. *Burns* 28, 713 – 717.
22. Cetingul M.P., Herman C. (2008). Identification of skin lesions from the transient thermal response using infrared imaging technique. *IEEE*, 1219 – 1222.
23. Ciesielski M., Mochnacki B. and Szopa R. (2011). Numerical modeling of biological tissue heating. Admissible thermal dose. *Scientific Research of the Institute of Mathematics and Computer Science* 1 (10), 11 – 20.
24. Filipoiu Florin, Bogdan Andrei Ioan and Carstea Iulia Maria (2010). Computer-aided analysis of the heat transfer in skin tissue. *Proceedings of the 3rd WSEAS Int. Conference on Finite Differences - Finite Elements - Finite Volumes - Boundary Elements,* 53 – 59.
25. Carstea Daniela, Carstea Ion and Carstea Iulia Maria Carstea (2011). Interdisciplinarity in computer-aided analysis of thermal therapies. *WSEAS Transactions on Systems and Control*, 6 (4), 115 – 124.
26. Deng Z.S., Liu J. (2005). Numerical simulation of selective freezing of target biological tissues following injection of solutions with specific thermal properties. *Cryobiology*, 50, 183-192.
27. Han Liang Lim, Venmathi Gunasekaran. Mathematical modeling of heat distribution during cryosurgery // https://isn.ucsd.edu/last/courses/beng221/problems/2011/project10.pdf.
28. COMSOL Multiphysics User's Guide (2018). COMSOLAB.
29. L.I. Anatychuk, R.R Kobylianskyi, R.V. Fedoriv (2019). Method for taking into account the phase transition in biological tissue during computer-aided simulation of cryodestruction process. *J.Thermoelectricity*, 1, 42 – 54.

Submitted 08.04.2019


P.V. Gorskiy

P.V. Gorskiy *doctor phys.-math. science*[1,2],
Mytskaniuk N.V.[1,2]

[1]Institute of Thermoelectricity of the NAS and MES of Ukraine, 1, Nauky str, Chernivtsi, 58029, Ukraine;
e-mail: anatych@gmail.com
[2]Yu.Fedkovych Chernivtsi National University,
2, Kotsiubynskyi str., Chernivtsi, 58000, Ukraine


Мыцканюк Н.В.

ON THE TEMPERATURE DEPENDENCES OF THERMOELECTRIC CHARACTERISTICS OF THERMOELECTRIC MATERIAL-METAL TRANSIENT LAYER WITHOUT REGARD TO PERCOLATION EFFECT

The basic relationships are obtained by calculation, which determine the temperature dependences of thermoelectric characteristics of thermoelectric material-metal transient contact layers without regard to percolation theory. Specific quantitative results and plots of the temperature dependences of the electrical and thermal contact resistances, the thermoEMF, the power factor, and the dimensionless thermoelectric figure of merit are given for bismuth telluride – nickel contact pair. It has been established that with uneven distribution of metal atoms in the temperature range of 200 - 400 K, the intensity of metal atoms entering transient layer, which corresponds to a change in the distribution of metal atoms by the thickness of transient layer from linear to square and the thickness range of transient layer from 20 to 150 μm, the electrical contact resistance varies from 1.8 · 10-7 to 4.8 · 10-6 Ohm·cm^2, the thermal contact resistance - from 0.022 to 0.35 K·cm^2/W, the thermoEMF - from 155 to 235 μV/K, the power factor - from 1.6·10^{-4} òo 2.9·10^{-4} W/(m·K^2), the dimensionless thermoelectric figure of merit - from 0.55 to 1.7. Bibl. 34, Fig. 21.

Key words: thermoelectric material-metal contact, near-contact transient layer, electrical contact resistance, thermal contact resistance, thermoEMF, power factor, dimensionless thermoelectric figure of merit, temperature dependences.

Introduction

The efficiency of thermoelectric modules, which is mainly determined by the figure of merit of thermoelement leg materials, essentially depends on the electrical contact resistance at the boundaries between semiconductor materials of legs with metal interconnect layers. Contact resistance is one of the main reasons for the fact that in thermoelectric coolers and generators the properties of materials are not fully realized [1 – 3]. It is well known that the Joule heat, which is released on contact resistances, reduces the energy efficiency of thermoelectric converters and leads to the dependence of their characteristics on the height of thermoelement legs [4]. The influence of contact resistance on the characteristics of thermoelectric devices becomes more significant under conditions of miniaturization of thermoelectric legs, when the thickness of thermoelectric material-metal transient contact layers along the electric current directions becomes comparable with the height of thermoelectric legs [5, 6] Miniaturization of thermoelectric power converters is a modern trend of their improvement [7 – 12], aimed primarily at reducing the expenses for thermoelectric materials and thereby cheapening the thermoelectric modules. Therefore, studies of the electrical properties of TEM-metal transient layers, aimed at reducing the contact

resistance and thereby preserving the high values of the characteristics of thermoelectric converters under miniaturization conditions, are currently central.

To design thermoelectric modules and calculate their characteristics, the experimentally established contact resistance values are used. As a rule, to measure these values, rather complicated methods and installations are employed [13 – 17]. Contact resistance depends on the technology for producing thermoelectric materials, methods for forming their contacts with metal layers, pre-processing of the surfaces of semiconductor crystals [16, 18 – 20] and other factors. Therefore, the experimental values of contact resistance for specific TEM-metal pairs can differ significantly, which complicates the analysis and optimization of the structure of transient contact layers. Theoretical methods for modeling TEM-metal contacts are practically absent.

Therefore, *the purpose of this work* is to develop a model of the structure of TEM-metal transient contact layers and methods for estimating the electrical contact resistance of such a structure, to calculate the temperature dependences of contact resistance for thermoelements of traditional materials based on BiTe with a view to their further application for the design of thermoelectric power converters, on particular with microminiature legs.

Physical model of TEM-metal transient layer

In thermoelectric modules manufactured by traditional technology, connection of *n*- and *p*-type legs in thermoelements is carried out by interconnect plates made of highly conductive metal, in particular copper. The contact of the semiconductor material with metal interconnects, as a rule, is provided by soldering or connection using a special electrically conductive paste. To restrict the diffusion of interconnect elements and solder or paste into the bulk of a semiconductor leg, a thin anti-diffusion layer of metal, usually nickel, is applied to its surface [21 – 26], which, in addition to low diffusion of elements, provides high adhesion and a reliable electrical contact. After applying the metal to the surface of the thermoelectric material, a transient TEM-metal contact layer arises at the interface. Physical processes in the transient layer are the main cause for contact resistance that occurs when an electric current passes through a thermoelement.

For the effective operation of thermoelectric modules, the contacts must be ohmic [21 – 27]. In ohmic contacts, current carriers pass from semiconductor to metal, overcoming the potential barrier at the TEM – metal interface, which is created due to the difference in the energy band structure of semiconductor and metal [28, 29]. The main characteristic of an ohmic contact is its resistance, reduced to a unit area [30]. This resistance has two main components. The first is the resistance r_l of transient near-contact area, the second – the resistance r_b associated with the transition of charge carriers through the potential barrier at the boundary between the semiconductor and the metal. This second component is commonly called the boundary electrical resistance [31]. However, the purpose of this paper is to calculate the temperature dependences of thermoelectric characteristics of transient layer without taking into account the presence of a potential barrier.

General formulae for thermoelectric characteristics of transient layer

The electrical resistance of transient layer is affected by its composition and structure, which depend on the technology of fabrication of TEM-metal contact. The most common methods of metal deposition on the surface of a semiconductor are the technologies of fusion, sputtering, electroplating, and epitaxy. The structure of transient layer is determined by two basic physical processes. It is mutual diffusion of atoms (molecules) of contacting materials and their chemical interaction [32]. Traditionally, the application of

nickel diffusion layers on the surface of thermoelectric material is carried out by electroplating. As stated in [22,23,32], under the conditions of such technology, the structure of transient layer is characterized by the absence of any chemical compounds of metal atoms with atoms (molecules) of the semiconductor. In this case, the main factor determining the electrical properties of transient layer is considered to be the effect of semiconductor doping with metal due to mutual diffusion [32], which occurs under the conditions of the operating modes of thermoelements. It should be noted that transient layer differs from the bulk thermoelectric material by the inhomogeneous spatial distribution of metal impurity atoms, which leads to the dependence of the electrical conductivity $\sigma_l(x)$ of transient layer on the dimensionless coordinate $x = \tilde{x}/h$ where h is the thickness of transient layer, $x \in [0,1]$. Suppose that electrical conductivity varies continuously from its value σ_m in metal to the value σ_s in thermoelectric material, i.e., function $\sigma_l(x)$ satisfies the requirements.

$$\sigma_m=\sigma_l(0), \quad \sigma_s=\sigma_l(1). \tag{1}$$

To determine the appearance of the dependence $\sigma_l(x)$, we use the concept of the distribution of the volume fraction of an impurity metal in the material of the near-contact transient layer, which is determined by the ratio of the volumes of impurity atoms to all atoms (molecules) of transient layer, which are in the elementary volume of thickness *dx* at a distance *x* from the metal surface *x = 0* and is calculated by the relation

$$v(x) = \frac{\left(A_m/\gamma_m\right)n(x)}{\left(A_m/\gamma_m\right)n(x)+\left(A_s/\gamma_s\right)\left(n_0-n(x)\right)}, \tag{2}$$

where A_s, A_m is the atomic or molecular weight, γ_s, γ_m is the density of semiconductor thermoelectric material and metal, respectively, $n(x)$ is the distribution of the concentration of metal atoms in transient layer, which is established in the steady-state operating modes of the thermoelement due to diffusion, n_0 is the concentration of metal atoms that can diffuse. Formula (2) is correct, subject that part of the elementary volume of transient layer, unoccupied by metal atoms, is considered to be occupied by atoms (molecules) of thermoelectric material.

Function $n(x)$ is a solution of one-dimensional boundary value problem of steady-state diffusion in the presence of a constant source of metal atoms with the boundary conditions $n(0)=n_0$, $n(1)=0$, which under the condition of constancy of diffusion coefficient D and intensity Q of the source with concentration n_0, looks like:

$$n(x) = n_0\left[1-(1-A)x-Ax^2\right]. \tag{3}$$

where n_0 – concentration of atoms in metal, dimensionless parameter $A = Qd_0^2/2Dn_0$ characterizes the mode and conditions of contact creation.

Under these assumptions, the dimensionless function (2) of the distribution of volume fraction of impurity $v(y)$ takes on the form

$$v(y) = \frac{\left(A_m/\gamma_m\right)\left[1-(1-A)y-Ay^2\right]}{\left(A_m/\gamma_m\right)\left[1-(1-A)y-Ay^2\right]+\left(A_s/\gamma_s\right)\left[(1-A)y+Ay^2\right]}, \tag{4}$$

and the following conditions for it are satisfied

$$v(0)=1, \quad v(1)=0. \tag{5}$$

We assume that electrical conductivity proportional to carrier concentration in the case of doping impurity is proportional to concentration of impurity atoms. As a result, the form of coordinate dependence of electrical conductivity of transient layer $\sigma_l(y)$ will be determined by the coordinate dependence (4) of the volume fraction $v(y)$ of metal impurity. Then $\sigma_l(y)$ without regard to percolation effect, when metal atoms do not form clusters, will be determined through $v(y)$ by the function

$$\sigma_l(y) = \sigma_s + (\sigma_m - \sigma_s)v(y), \tag{6}$$

for which, taking into account (5), the requirements of (1) will be satisfied. Formula (6) coincides with classical formula for generalized composite conduction.

With this approximation, the electrical resistance of the near-contact transient layer can be estimated by the formula

$$r_{ce} = h\int_0^1 \frac{dy}{\sigma_l(y)}. \tag{7}$$

The relation similar to (6) is also valid for thermal conductivity of transient layer:

$$\kappa_l(y) = \kappa_s + (\kappa_m - \kappa_s)v(y), \tag{8}$$

where κ_s and κ_m are thermal conductivities of TEM and metal, respectively, so for electrical contact resistance the following relation is valid:

$$r_{ct} = h\int_0^1 \frac{dy}{\kappa_l(y)}. \tag{9}$$

For thermoEMF the following relation is true:

$$\alpha = \frac{\int_0^1 \{(\alpha_m/\kappa_m)v(y) + (\alpha_s/\kappa_s)[1 - v(y)]\}dy}{\int_0^1 \{\kappa_m^{-1}v(y) + \kappa_s^{-1}[1 - v(y)]\}dy}. \tag{10}$$

Approximation of the temperature dependences of thermoelectric characteristics of material and metal

To calculate the temperature dependences of contact resistance, we will need the temperature dependences of thermoelectric characteristics of TEM and metal. This approximation can be done in two ways, namely by construction of regression models on the basis of experimental data, or purely by calculation, on the basis of certain model assumptions of the microscopic mechanisms of charge and heat transfer in material. In this paper we use the second way.

We start with the thermoelectric characteristics of TEM. Let at some temperature T_0 we know its thermoelectric parameters, namely the thermoEMF α_{s0}, the electrical conductivity σ_{s0} and the thermal conductivity κ_{s0}. To construct their temperature dependences, using this data we make the following model assumptions:

1) zone spectrum of carriers in TEM is parabolic and isotropic with temperature independent effective mass;
2) quasi-elastic scattering of carriers in relevant temperature region occurs on the deformation potential of acoustic phonons with energy independent cross section and mean free path inversely proportional to temperature;
3) lattice thermal conductivity of semiconductor is determined by phonon-phonon scattering with umklapp and is inversely proportional to temperature.

Provided that these assumptions are valid, the carrier scattering index $r = –0.5$. Taking into account its value, the construction of the necessary temperature dependences on the basis of known general relations [33] is carried out in the following order.

From the relation for the thermoEMF

$$\alpha_{s0} = \frac{k}{e}\left[\frac{2F_1(\eta_0)}{F_0(\eta_0)} - \eta_0\right] \tag{11}$$

we find a reduced chemical potential η_0 of carrier gas at temperature T_0.

Using the condition of carrier concentration constancy, from the equation

$$\frac{T^{1.5}F_{0.5}(\eta)}{T_0^{1.5}F_{0.5}(\eta_0)} = 1 \tag{12}$$

we determine the temperature dependence of reduced chemical potential η of carrier gas on temperature T in given temperature range.

From the relation

$$\alpha_s = \frac{k}{e}\left[\frac{2F_1(\eta)}{F_0(\eta)} - \eta\right] \tag{13}$$

we determine the temperature dependence of the thermoEMF of TEM.

From the relation

$$L_s(\eta) = \left(\frac{k}{e}\right)^2\left[\frac{3F_2(\eta)}{F_0(\eta)} - \frac{4F_1^2(\eta)}{F_0^2(\eta)}\right] \tag{14}$$

we determine the temperature dependence of the Lorentz number of TEM.

The temperature dependence of electrical conductivity of TEM for the above model assumptions is determined as:

$$\sigma_s = \sigma_{s0}\left(\frac{T_0}{T}\right)^{1.5}\frac{F_0(\eta)F_{0.5}(\eta_0)}{F_{0.5}(\eta)F_0(\eta_0)}\,. \tag{15}$$

The temperature dependence of thermal conductivity with regard to everything mentioned above is determined as:

$$\kappa_s = \sigma_s L_s(\eta)T + [\kappa_{s0} - \sigma_{s0}L_s(\eta_0)T_0]\frac{T_0}{T}\,. \tag{16}$$

In formulae (11) – (16), $F_m(\eta)$ denote the Fermi integrals that are determined by the following relation:

$$F_m(\eta) = \int_0^\infty x^m \left[\exp(x-\eta)+1\right]^{-1} dx\,. \tag{17}$$

Relations (11)–(17) completely determine the temperature dependences of the thermoEMF, the electrical conductivity and the thermal conductivity of TEM.

Let us pass to approximation of the temperature dependences of the electrical conductivity, the thermal conductivity and the thermoEMF of metal. We assume that in metal, just as in TEM, scattering of free carriers takes place on the deformation potential of acoustic phonons, and in the real temperature region the mean free path of carriers is inversely proportional to temperature. Then, taking into account strong degeneracy of carriers in metal, the temperature dependence of its electrical conductivity will be determined as [34]:

$$\sigma_m = \sigma_{m0} \cdot (T_0/T), \tag{18}$$

and, therefore, taking into account the Wiedemann-Franz relation, the thermal conductivity of the metal κ_m will be considered to be temperature independent. We will also consider the thermoEMF of the metal α_m to be independent of temperature.

Results of calculation of the temperature dependences of thermoelectric characteristics of the TEM-metal transient contact layer and their discussion

The temperature dependences of the electrical and thermal contact resistances, the thermoEMF and the dimensionless thermoelectric figure of merit of the TEM-metal transient contact layer for bismuth telluride-nickel pair obtained in the framework of the calculation procedure described above, provided that the uneven distribution of the metal atoms in the layer is preserved, are shown in Figs. 1–7.

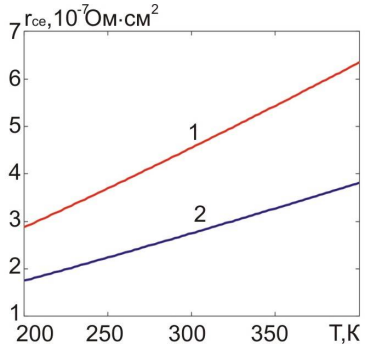

Fig.1. Temperature dependences of electrical contact resistance at transient layer thickness of 20 μm: 1 – A=0; 2 – A=1.

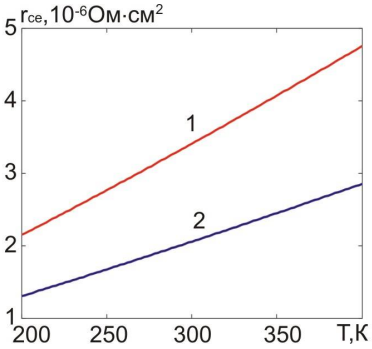

Fig.2. Temperature dependences of electrical contact resistance at transient layer thickness of 150 μm: 1 – A=0; 2 – A=1.

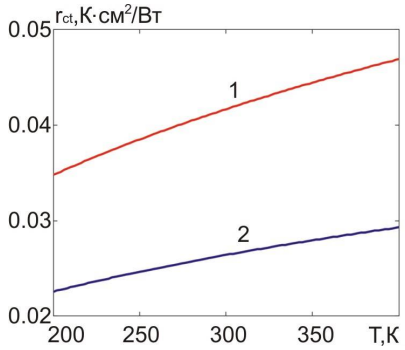

Fig.3. Temperature dependences of thermal contact resistance at transient layer thickness of 20 μm: 1 – A=0; 2 – A=1.

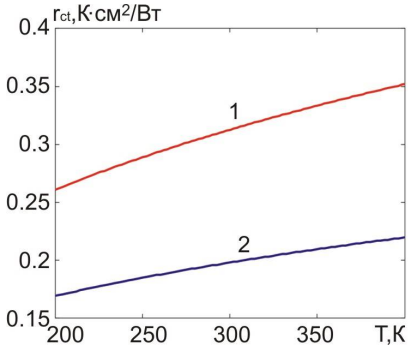

Fig.4. Temperature dependences of thermal contact resistance at transient layer thickness of 150 μm: 1 – A=0; 2 – A=1.

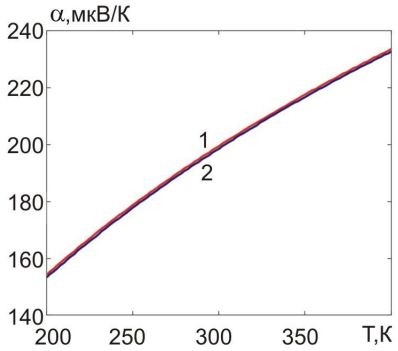

Fig.5. Temperature dependences of transient layer thermoEMF: 1 – A=0; 2 – A=1.

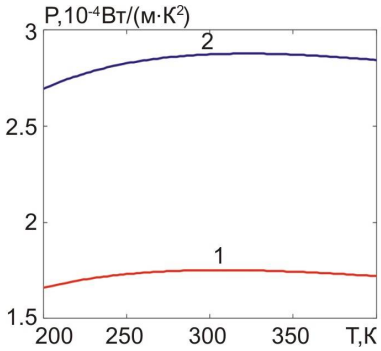

Fig.6. Temperature dependences of transient layer power factor: 1 – A=0; 2 – A=1.

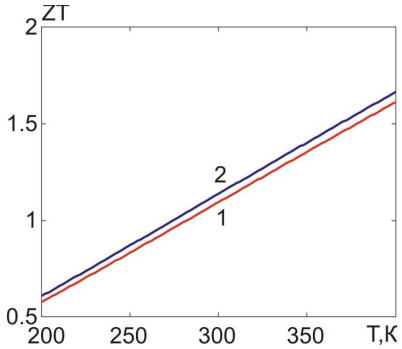

Fig.7. Temperature dependences of transient layer dimensionless thermoelectric figure of merit: 1 – A=0; 2 – A=1.

When plotting, the following material parameters for 300K were taken: σ_m=1.25·10^5 S/cm, σ_s=800 S/cm, κ_m=92 W /(m·K), κ_s=1.4 W /(m·K), α_m= – 23 μV/K, α_s= 200 μV/K, and, besides, A_m=58.5, A_s=801, ρ_m=9100 kg/m^3, ρ_s=7700 kg/m^3. It can be seen from the figures that in the temperature range studied, the electrical and thermal contact resistances, the thermoEMF, and the dimensionless thermoelectric figure of merit of transient layer increase, and the power factor has a maximum in the range of 300–350 K. Such temperature dependences can be explained by an increase in the resistivities of metal and semiconductor, a decrease in their thermal conductivity, and an increase in the thermoEMF of semiconductor with a rise in temperature. With an increase in the thickness of transient layer, the electrical and thermal contact resistances increase in proportion to this thickness. The presence of a maximum in the temperature dependence of power factor is explained by two competing processes: an increase in the thermoEMF and a decrease in TEM electrical conductivity with a rise in temperature. It should be noted that the thermoEMF of transient layer is mainly determined by the semiconductor due to the fact that thermal conductivity of metal is significantly greater than thermal conductivity of semiconductor.

In addition, it can be seen from the figures that with increasing parameter A, that is, the intensity of metal atoms entering transient layer, the thermal and electrical contact resistances, as well as the thermoEMF decrease, and the power factor and the dimensionless thermoelectric figure of merit increase. On the whole, in the studied ranges of temperature, the intensity of metal entering transient layer, and the transient layer thickness, the electrical contact resistance varies from 1.8·10^{-7} to 4.8·10^{-6} Ohm·cm^2, and the thermal contact resistance varies from 0.022 to 0.35 K·cm^2/W, the thermoEMF - from 155 to 235 μV/K, the power factor - from 1.6·10^{-4} до 2.9·10^{-4} W/(m·K^2), the dimensionless thermoelectric figure of merit - from 0.55 to 1.7.

4. Effect of levelling of metal concentration in transient layer on the temperature dependences of its thermoelectric characteristics

The above results were obtained on the assumption that the distribution of the volume fraction of metal in transient layer is subject to relation (4). However, the most intense supply of metal atoms into transient layer occurs directly during contact. Further, especially at low temperatures, this intensity decreases significantly and the uneven distribution of metal in transient layer is levelled. Therefore, it is worthwhile to study the effect of this levelling on the temperature dependences of thermoelectric characteristics of transient layer. After levelling, the average steady volume fraction of metal in transient layer will be determined as follows:

$$v_{ma} = \int_0^1 \frac{(A_m/\gamma_m)\left[1-(1-A)y-Ay^2\right]}{(A_m/\gamma_m)\left[1-(1-A)y-Ay^2\right]+(A_s/\gamma_s)\left[(1-A)y+Ay^2\right]}dy, \qquad (19)$$

So, the steady electrical conductivity of transient layer without regard to percolation theory will be determined as:

$$\sigma_a = \sigma_s + (\sigma_m - \sigma_s)v_{ma}, \tag{20}$$

and its electrical contact resistance as:

$$r_{ce} = h/\sigma_a . \tag{21}$$

The steady thermal conductivity of transient layer will be determined as:

$$\kappa_a = \kappa_s + (\kappa_m - \kappa_s)v_{ma}, \tag{22}$$

and its thermal contact resistance as:

$$r_{ce} = h/\kappa_a . \tag{23}$$

For the thermoEMF of transient layer the following relation is valid:

$$\alpha_l = \frac{(\alpha_m/\kappa_m)v_m + (\alpha_s/\kappa_s)(1-v_m)}{v_m/\kappa_m + (1-v_m)/\kappa_s}. \tag{24}$$

The results of calculations of the temperature dependences of thermoelectric characteristics of transient layer obtained in case of uniform distribution of metal concentration therein are presented in Figs.8–14.

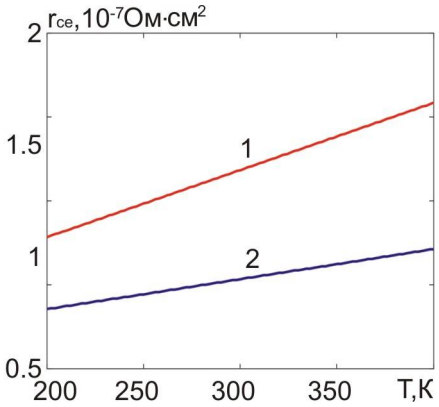

Fig.8. Temperature dependences of electrical contact resistance after levelling of metal concentration at transient layer thickness of 20 μm: 1 – A=0; 2 – A=1.

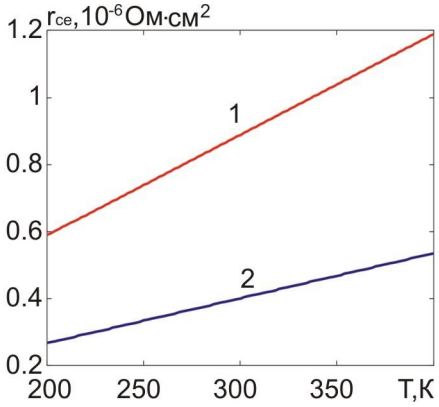

Fig.9. Temperature dependences of electrical contact resistance after levelling of metal concentration at transient layer thickness of 150 μm: 1 – A=0; 2 – A=1.

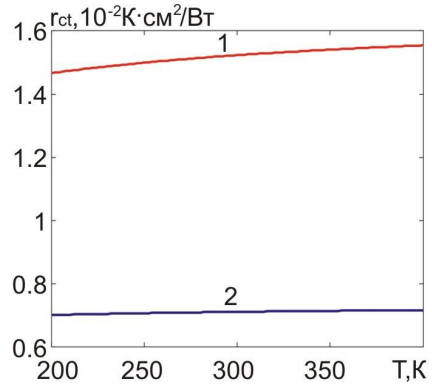

Fig.10. Temperature dependences of thermal contact resistance after levelling of metal concentration at transient layer thickness of 20 μm: 1 – A=0; 2 – A=1.

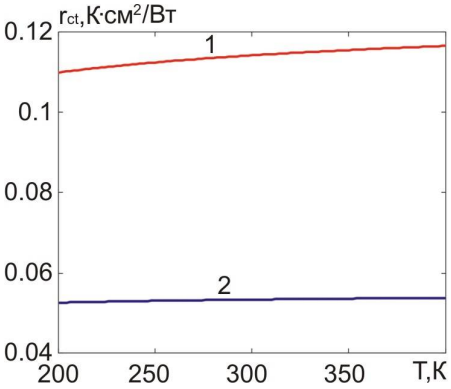

Fig.11. Temperature dependences of thermal contact resistance after levelling of metal concentration at transient layer thickness of 150 μm: 1 – A=0; 2 – A=1.

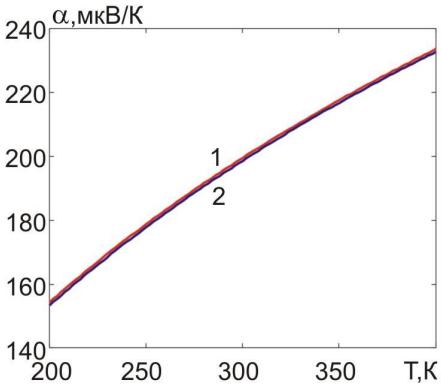

Fig.12. Temperature dependences of transient layer thermoEMF after levelling of metal concentration: 1 – A=0; 2 – A=1.

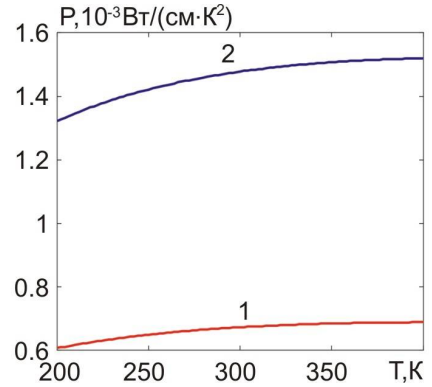

Fig.13. Temperature dependences of transient layer power factor after levelling of metal concentration: 1 – A=0; 2 – A=1.

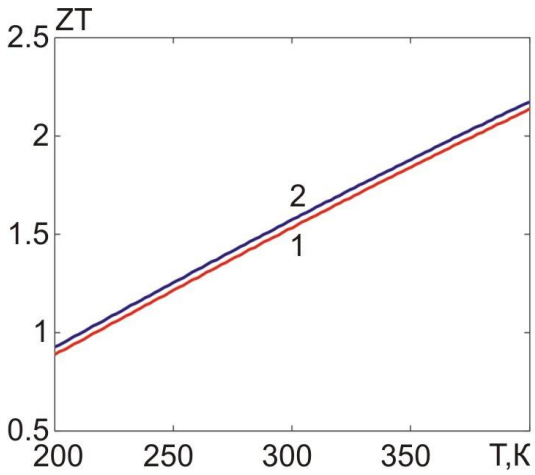

Fig.14. Temperature dependences of transient layer dimensionless thermoelectric figure of merit after levelling of metal concentration: 1 – A=0; 2 – A=1.

It can be seen from the figures that after levelling of metal concentration in the bulk of transient layer, the electrical and thermal contact resistances at all temperatures essentially decrease, the thermoEMF power practically does not change, and the power factor and thermoelectric figure of merit essentially increase. In contrast to the case of an uneven distribution of concentration, after its levelling in the studied temperature range, the power factor does not have a maximum, but is a growing function of temperature.

As regards the effect of parameter A, that is, the intensity of metal entering transient layer, on the thermoelectric properties of transient layer, after the concentration is levelled, the same tendency remains as with its uneven distribution.

In general, in the studied ranges of temperature, the intensity of metal entering transient layer and the thickness of transient layer after levelling metal concentration the electrical contact resistance varies from $8\cdot10^{-8}$ to $1.2\cdot10^{-6}$ Ohm·cm^2, the thermal contact resistance – from $7\cdot10^{-3}$ to 0.12 K·cm^2/W, the thermoEMF – from 155 to 235 V/K, the power factor – from $6\cdot10^{-4}$ to 1.5 $5\cdot10^{-3}$ W/(m·K^2), the dimensionless thermoelectric figure of merit – from 0.8 to 2.2. Thus, after the concentration is levelled, the electrical contact resistance drops by a factor of 2.25 – 4, the thermal contact resistance drops by a factor of 3, the thermoEMF is practically unvaried, the power factor grows by a factor of 3.75 – 5.3, the thermoelectric figure of merit increases 1.5 times.

Note that when designing thermoelectric energy converters, such parameters of transient contact layers as power factor and thermoelectric figure of merit do not have self-importance, but they may be of some interest for the integral evaluation of the contact structures.

It is clear that the results obtained can be considered valid only when nickel does not form bismuth telluride intermetallic compounds. But according to the data of [23], this is basically true.

Effect of contact resistance on the efficiency of thermoelectric generator module

The above temperature dependences of the electrical and thermal contact resistances were used to calculate the efficiency of thermoelectric generator modules with the height of thermoelectric legs 3 and 1.5 mm, respectively. The calculations were performed by methods of object-oriented simulation in Comsol Multiphysics software environment.

For this purpose a physical model of thermoelectric generator module was considered which is shown in Fig.15.

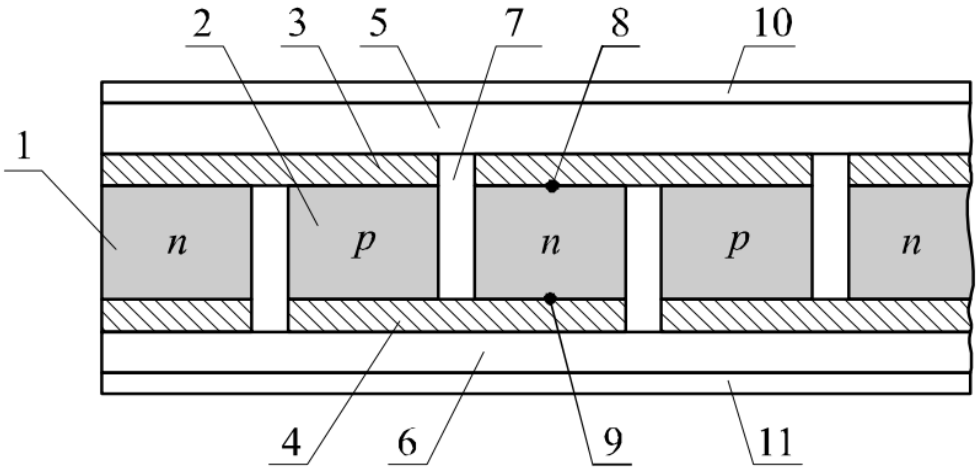

Fig. 15. Physical model of thermoelectric generator module. 1 – n-type leg; 2 – p-type leg; 3, 4 – electrical interconnects; 5, 6 – ceramic plates; 7 – gas; 8, 9 – electrical contacts between legs and interconnect plates; 10 – thermal contact between ceramic plate and hot thermostat; 11 – thermal contact between ceramic plate and cold thermostat.

The distribution of temperature and electrical potential in the module was found from the system of differential equations with respect to temperature T and electrochemical potential U. These equations were obtained on the basis of the law of energy conservation which is given by the following two equations:

$$\nabla \vec{w} = 0\,, \tag{25}$$

$$\vec{w} = \vec{q} + U\vec{j}\,. \tag{26}$$

In formulae (25) and (26), $\vec{j}$ – electric current density, $\vec{q}$ – heat flux density:

$$\vec{q} = -\kappa \nabla T + \Pi \vec{j}\,, \tag{27}$$

where Π is the Peltier coefficient, κ is thermal conductivity.

$$\Pi = \alpha T, \tag{28}$$

where α is the Seebeck coefficient, T is temperature.

The electric current density is found from the equation

$$\vec{j} = -\sigma \nabla U - \sigma \alpha \nabla T\,, \tag{29}$$

where σ is the electrical conductivity.

Substituting (26), (27) into (25), we obtain

$$-\nabla\left(\kappa \nabla T\right) + \left(\nabla \Pi + \nabla U\right)\vec{j} = 0\,. \tag{30}$$

From expression (30), using (28) and (29), we obtain the following equation to find the distributions of temperature and potential:

$$-\nabla\left[\left(\sigma\alpha^2T+\kappa\right)\nabla T\right]-\nabla\left(\sigma\alpha T\nabla U\right)-\sigma\left[\left(\nabla U\right)^2+\alpha\nabla T\nabla U\right]=0. \quad (31)$$

To obtain the second equation, we will use the law of conservation of electrical charge:

$$\nabla\vec{j}=0. \quad (32)$$

Substituting (29) into (32), we obtain the following equation:

$$\nabla\left(\sigma\alpha\nabla T\right)+\nabla\left(\sigma\nabla U\right)=0. \quad (33)$$

System (31), (33) is a system of differential equations with variable second-order partial differential coefficients, which describes the distribution of temperature and potential in an inhomogeneous thermoelectric medium. A feature of the system of equations (31), (33) is that the parameters α, σ, κ depend on the spatial coordinates x, y, z both directly and implicitly through the temperature T (x, y, z). This leads to the fact that it becomes inevitable to use numerous computer methods to solve equations of this kind.

In a computer model, the thermoelectric field is described by a two-element column matrix in the functional space of twice differentiable functions, namely, the coordinate dependences of temperature and potential:

$$M=\begin{pmatrix}T(x,y,z)\\U(x,y,z)\end{pmatrix}. \quad (34)$$

Matrix M satisfies one matrix differential equation

$$\nabla\left(c\nabla M\right)=f, \quad (35)$$

whose components are equations (31) and (33) if the matrix nonlinear coefficients of equation (35) have the form

$$c=\begin{pmatrix}\sigma\alpha^2T+\kappa & \sigma\alpha T\\ \alpha\sigma & \sigma\end{pmatrix}, f=\begin{pmatrix}\sigma\left[\left(\nabla U\right)^2+\nabla T\nabla U\right]\\ 0\end{pmatrix}. \quad (36)$$

A system of equations of the form (35) with allowance for (36) is solved for each of the layers that make up the thermoelectric module. For this, we additionally introduce the boundary conditions for the continuity of temperature, electric potential, heat flux, and electric current density at the boundaries of the layers. In addition, for reasons of optimality of the conditions under which the thermoelement operates, and which are determined from the requirement to achieve the maximum value of the efficiency, the potentials on the switching electrodes and the temperatures of the "hot" and "cold" thermostats are set. Therefore, the potentials on the switching electrodes of one of the legs are 0 and 0.0573 V, on the second - 0.0573 and 0.1146 V, and the temperatures of the "cold" and "hot" thermostats are 273 and 573 K, respectively.

The impact of the electrical and thermal contact resistances is taken into account in the physical model in the framework of two approaches. The first is that the contact layer is not explicitly introduced into the physical model, but its electrical conductivity and thermal conductivity are considered to be known from experiment or, in this case, temperature functions preliminarily calculated by calculation. Then, the proportionality of the electrical and thermal contact resistances to the layer thickness is taken into account. The second approach is that a contact layer with temperature-dependent thermal conductivity and electrical conductivity, taking into account its thickness, is explicitly introduced into the physical model. The thermoEMF of the contact layer at this stage of research is not taken into account.

Such mathematical description allows solving the above described system of equations for temperature and potential in Comsol Multiphysics simulation environment. The results of solving Eq.(11)

are three-dimensional temperature and electrical fields in given geometry of thermoelectric module. Their examples for one thermoelement which is part of the module with the height of leg 3 mm are shown in Figs. 16, 17. Knowing these fields, it is easy to calculate the basic energy characteristics of the module.

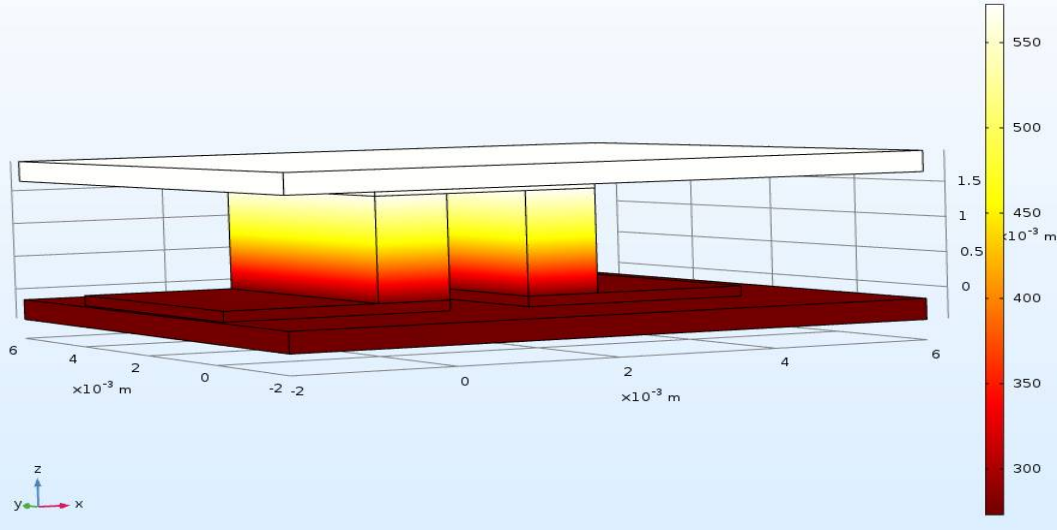

Fig.16. Temperature field in thermoelement

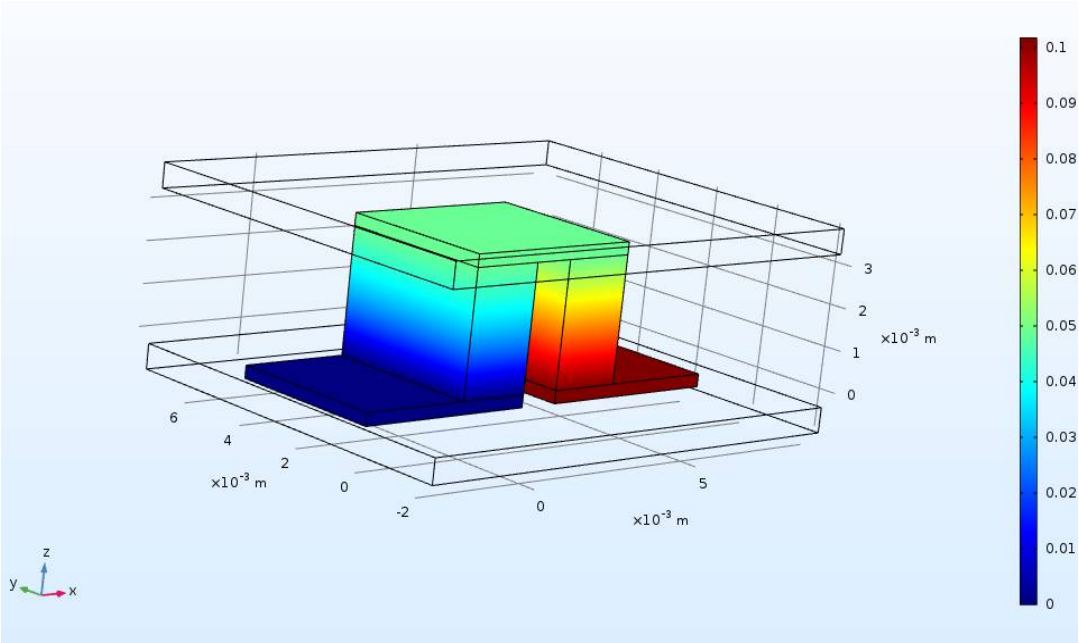

Fig.17.Electrical potential distribution in thermoelement

The results of these calculations are presented in Figs.18 – 21.

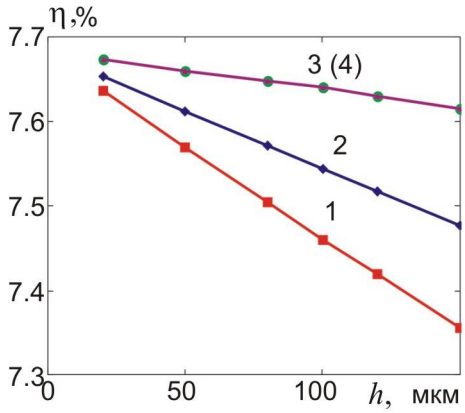

Fig.18.Dependence of generator module efficiency with the height of leg 3 mm on transient layer thickness for the case when contact resistance is considered to be a lumped parameter:1 – A=0, the distribution of metal atoms in transient layer is uneven; 2 – A=1, the distribution of metal atoms in transient layer is uneven; 3 – A=0, the distribution of metal atoms in transient layer is uniform;4 – A=1, the distribution of metal atoms in transient layer is uniform.

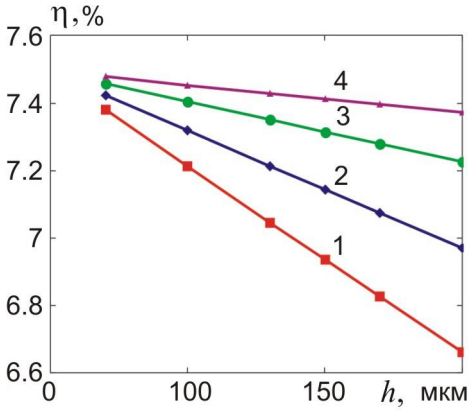

Fig.19.Dependence of generator module efficiency with the height of leg 1.5 mm on transient layer thickness for the case when contact resistance is considered to be a lumped parameter:1 – A=0, the distribution of metal atoms in transient layer is uneven; 2 – A=1, the distribution of metal atoms in transient layer is uneven; 3 – A=0, the distribution of metal atoms in transient layer is uniform;4 – A=1, the distribution of metal atoms in transient layer is uniform.

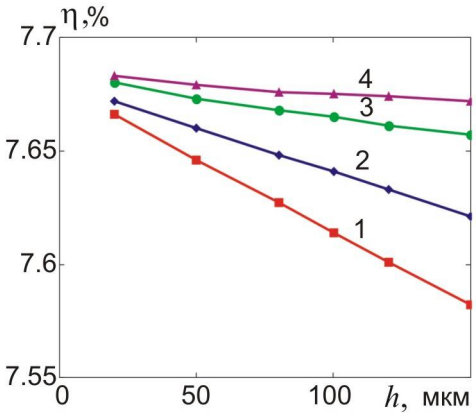

Fig.20.Dependence of generator module efficiency with the height of leg 3 mm on transient layer thickness for the case when transient layer is explicitly introduced into model:1 – A=0, the distribution of metal atoms in transient layer is uneven; 2 – A=1, the distribution of metal atoms in transient layer is uneven; 3 – A=0, the distribution of metal atoms in transient layer is uniform;4 – A=1, the distribution of metal atoms in transient layer is uniform.

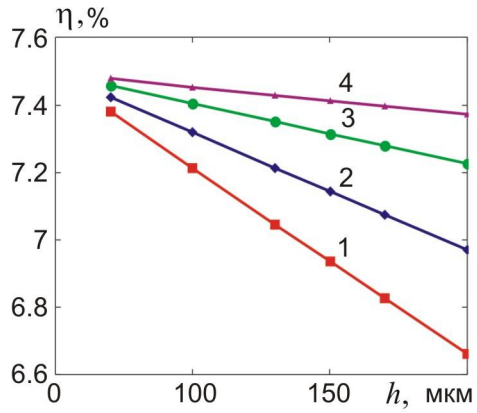

Fig.21.Dependence of generator module efficiency with the height of leg 1.5 mm on transient layer thickness for the case when transient layer is explicitly introduced into model:1 – A=0, the distribution of metal atoms in transient layer is uneven; 2 – A=1, the distribution of metal atoms in transient layer is uneven; 3 – A=0, the distribution of metal atoms in transient layer is uniform;4 – A=1, the distribution of metal atoms in transient layer is even.

Note that in this case, the thermoEMF of transient layer was considered to be zero.

It can be seen from the figures that the efficiency of the thermoelement in the mode of electric energy generation is maximum when the distribution of metal atoms in transient layer is uniform. In addition, other things being equal, it is the greater, the greater the intensity of the source from which the metal enters transient layer. In the case of uneven distribution of metal atoms in transient layer, the efficiency decreases with increasing transient layer thickness the more, the smaller the height of the thermoelectric leg. In general, in the considered range of thermoelectric leg heights and layer thicknesses, the efficiency changes from 6.4 to 7.7% when the contact layer is explicitly introduced into the model, and from 6.6 to 7.7% when the contact resistance is considered to be a lumped parameter. In the case when transient layer is introduced into model, the efficiency after levelling the distribution of metal atoms in transient layer depends only slightly on the intensity of the source from which a steady-state diffusion of metal to TEM occurs.

Conclusions

1. Without taking into account the formation of clusters in transient layer, the temperature dependences of the electrical and thermal contact resistances, the thermoEMF, the power factor and the thermoelectric figure of merit of bismuth telluride-nickel transient contact layers were calculated on the assumption that carrier scattering in semiconductor and metal occurs on the deformation potential of acoustic phonons, the thermal conductivity of metal is determined by electron gas, and the lattice thermal conductivity of semiconductor – by phonon-phonon scattering with umklapp. In this case it was believed that nickel does not form new phases with bismuth telluride.
2. It is shown that both with uneven and uniform distribution of metal atoms in transient layer, the electrical and thermal contact resistances, the thermoEMF and the dimensionless thermoelectric figure of merit of transient layer are growing functions of temperature and the intensity of metal atoms entering transient layer during contact creation.
3. Power factor in the temperature range under study is a growing function of the intensity of metal atoms entering transient layer, and at the same time has a maximum on the temperature dependence in case of uneven distribution of metal atoms in transient layer. However, it becomes a monotonically growing function of temperature in case of levelling the concentration of metal atoms in transient layer.
4. In the case of uneven distribution of metal atoms in the temperature range of 200 – 400 K, the intensity

of metal atoms entering transient layer, which corresponds to a change in parameter *A* from 0 to 1 and the thickness range of transient layer from 20 to 150 μm, the electrical contact resistance changes from $1.8 \cdot 10^{-7}$ to $4.8 \cdot 10^{-6}$ Ohm·cm^2, the thermal contact resistance – from 0.022 to 0.35 K·cm^2/W, the thermoEMF – from 155 to 235 μV/K, the power factor – from $1.6 \cdot 10^{-4}$ to $2.9 \cdot 10^{-4}$ W/(m·K^2), the dimensionless thermoelectric figure of merit – from 0.55 to 1.7.

5. In the case of levelling the distribution of metal atoms in transient layer, the electrical contact resistance decreases by a factor of 2.25 – 4, the thermal contact resistance decreases by a factor of 3, the thermoEMF is practically unvaried, the power factor increases by a factor of 3.75 – 5.3, the thermoelectric figure of merit grows by a factor of 1.5 as compared to the case of uneven distribution.
6. Studies of the effect of transient contact layer without clusters on the efficiency of thermoelement in generation mode have shown that, all other things being equal, if the influence of the thermoEMF of transient layer is ignored, in the considered range of thermoelectric leg heights and layer thicknesses in the case when a contact layer is explicitly introduced into the model, the efficiency varies from 6.4 to 7.7%. However, if contact resistance is considered to be a lumped parameter, the efficiency changes from 6.6 to 7.7%. In the case when transient layer is introduced into the model, the efficiency after levelling the distribution of metal atoms in transient layer depends only slightly on the intensity of the source from which steady diffusion of metal into TEM occurs, whereas in the case when contact resistance is considered to be a lumped parameter, this dependence is much stronger.

References

1. Aswal D.K., Basu R., Singh A. (2016). Key issues in development of thermoelectric power generators: high figure-of-merit materials and their highly conducting interfaces with metallic interconnects. *Energy Convers. Manag.,* 114, 50-67. http://refhub.elsevier.com/S2468-6069(18)30133-3/sref1
2. Anatychuk L.I., Kuz R.V. (2012). The energy and economic parameters of *Bi-Te* based thermoelectric generator modules for waster heat recovery. *J.Thermoelectricity*, 4, 75-82.
3. Drabkin I.A., Osvensky V.B., Sorokin A.I., Panchenko V.P., Narozhnaya O.E. (2017). Contact resistance in composite thermoelectric legs. *Semiconductors,* 51(8), 1038-1040.
4. Anatychuk L.I. (2003). *Termoelektrichestvo. Tom 2. Termoelektricheskiie preobrazovateli energii [Thermoelectricity. Vol.2. Thermoelectric power converters]*. Kyiv, Chernivtsi: Institute of Thermoelectricity [in Russian].
5. Semenyuk V. (2001). Thermoelectric micro modules for spot cooling of high density heat sources. *Proc. of 20th International Conference on Thermoelectrics*, 391-396.
6. Semenyuk V.A. (2006). Thermoelectric cooling of electro-optic components. *Thermoelectrics Handbook: Macro to Nano, 58-1 – 58-20. D.M. Rowe (Ed.).* CRC Taylor&Francis.
7. Fleurial J.-P., Snyder G.J., Patel J., et al. (2001). Solid-state power generation and cooling microdevices for distributed system architectures. *Proc of 20th International Conference on Thermoelectrics*, 24-29.
8. Bottner Harald, Nurnus Joachim, Schubert Axel (2006). Miniaturized thermoelectric converters. *Thermoelectrics Handbook, Macro to Nano. D.M. Rowe (Ed.).* CRC Taylor&Francis, 46-1 – 46-18.
9. Crane N. B., Misra P., Murray Jr. J.L., Nolas G.S. (2009). Self-assembly for integration of microscale thermoelectric coolers. *Journal of Electronic Materials*, 38 (7), 1252-1256.
10. I-Yu Huang, Jr-Ching Linb, Kun-Dian She (2008). Development of low-cost micro-thermoelectric coolers utilizing MEMS technology. *Sensors and Actuators*, A 148, 176–185.

11. Navone C., Soulier M., Plissonnier M., Seiler A.L. (2010). Development of $(Bi,Sb)_2(Te,Se)_3$-based thermoelectric modules by a screen-printing process. *Journal of Electronic Materials*, 39 (9), 1755-1759.
12. Goncalves L.M., Couto C., Alpuim P., Correia J.H. (2008). Thermoelectric micro converters for cooling and energy-scavenging systems. *J. Micromech. Microeng.*, 18, 064008, 1-5.
13. Misra P., Nagaraju J. (2004). Test facility for simultaneous measurement of electrical and thermal contact resistance. *Rev. Sci. Instr*., 75, 2625-2630 (doi 10.1063/1.1775316).
14. Maheshappa H.D., Nagaraju J., KrishnaMurthu N.V. (1998). A facility for electrical contact resistance measurement. *Rev. Sci. Instr*., 69, 534-1539 (doi 10.1063/1.1148810).
15. Deepak, Krishna H. (2007). Measurement of small specific contact resistance of metals with resistive semiconductors. *J. El. Mat*., 36, 598-605 (doi 10.1007/s11664-007-0091-y).
16. Gupta R.P., McCarty R., Sharp J. (2014). Practical contact resistance measurement method for bulk Bi_2Te_3 based thermoelectric devices. *J. El. Mat*., 43 (6), 1608-1612.
17. Kim Y., Yoon G., Park S.H. (2016). Direct contact resistance evaluation of thermoelectric legs. *Experimental Mechanics*, 56 (5), 861-869. https://doi.org/10.1007/s11340-016-0131-8-
18. Alieva T.D., Barkhalov B.Sh., Abdinov D.Sh. (1995). Struktura i elektricheskiie svoistva granits razdela kristallov $Bi_{0.5}Sb_{1.5}Te_3$ i $Bi_2Te_{2.7}Se_3$ s nekotorymi splavami [Structure and electrical properties of interfaces between $Bi_{0.5}Sb_{1.5}Te_3$ and $Bi_2Te_{2.7}Se_3$ crystals with certain alloys]. *Neorganicheskiie Materialy – Inorganic Materials*, 31 (2), 194-198.
19. Dzhamalov N.A., Barkhalov B.Sh., Salaiev E.Yu., Gasanov N.A., Abdinov D.Sh.(1983). *Neorganicheskiie Materialy – Inorganic Materials*, 19(4), 593-595.
20. Alieva T.D., Akhundova N.M., Dzhamalov N.A., et al. (1985). *Reports of the Academy of Sciences of Azerbaijan SSR,* 41(12), 18-20.
21. Kuznetsov G.D., Polystanskiy Y.G., Evseev V.A. (1995). The metallization of the thermoelement branches by ionic sputtering of the nickel and cobalt. *Proc of the XIV International Conference on Thermoelectrics (St.Petersburg, June 27-30, 1995)* (p.166-167).
22. Astakhov M.V., Bublik V.T., Karataiev V.V., et al. (2004). Vliianiie protsessa nikelirovaniia na strukturu i adhesionnyie svoistva poverkhnostnykh sloiov termoelektricheskogo materiala na osnove khalkogenidov Bi i Sb. [The influence of nickel plating process on the structure and adhesion properties of surface layers of thermoelectric material based on Bu and Sb charlcogenides]. In: *"Thermoelectrics and their Application" (Saint-Petersburg, 2004)* (p.243-248).
23. Bublik V.T., Voronin A.I., Ponomarev V.F., Tabachkova N.Yu. (2012). Izmeneniie struktury prikontaknoi oblasti termoelektricheskikh materialov na osnove telluride vismuta pri povyshennykh temperaturakh [Change in the structure of near-contact area of thermoelectric materials based on bismuth telluride at elevated temperatures]. *Izvestiia vysshykh uchebnykh zavedenii.* Materaily Elektronnoi Tekhniki - *News of Higher Educational Institutions.* Materials of Electronic Technique, 2, 17-20 [in Russian].
24. Belonogov E.A., Dybov V.A., Kostiuchenko A.V., et al. Kondensirovannyie sredy i mezhfaznyie granitsy [Condensed media and interphase boundaries], Vol.19, №4, p.479-488.
25. Gupta Rahul P., Xiong K., White J.B., Cho Kyeongjae, Alshareef H.N., Gnade B.E. (2010). Low resistance ohmic contacts to Bi2Te3 using Ni and Co metallization. *Journal of the Electrochemical Society,* 157 (6), H666-H670, 2010. DOI: 10.1149/1.3385154
26. Ngan Hoang Pham, Nader Farahi, Hasbuna Kamila, Aryan Sankhla, Sahar Ayachi, Eckhard Müller, Johannes de Boor (2019). Ni and Ag electrodes for magnesium silicide based thermoelectric generators. *Materials Today Energy*, 11 97e105. https://doi.org/10.1016/j.mtener.2018.10.016.

27. Nikirsa D.D. (1987). Fizicheskiie osobennosti mikrominiaturizatsii polyprovodnikovykh okhlazhdaiushchikh termoelementov [Physical features of microminiaturization of semiconductor cooling thermoelements]. Candidate's thesis (Tech.sciences). Chernivtsi [in Russian].
28. Bartkowiak M., Mahan G.D. (2001). Heat and electricity transport through interfaces, in: *Recent Trends in Thermoelectric Materials, vol. II, Semiconductors and Semimetals*, vol. 70. New York: Academic Press.
29. Sze S.M. (1985). *Semiconductor Devices - Physics and Technology*, John Wiley & Sons.
30. Goldberg Yu.A. (1994). Ohmic contact metal-semiconductor AIIIBV: creation methods and properties. *Semiconductors*, 28(10), 1681-1698.
31. Da Silva L.W., Kaviany M. (2004). Microthermoelectric cooler: interfacial effects on thermal and electrical transport. *International Journal of Heat and Mass Transfer*, 47(10-11), 2417–2435.
32. Anatychuk L.I., Dugaev V.K., Litvinov V.I., Volkov V.L. (1994). Contact resistance between metal and thermoelectric material. *J. Thermoelectricity*, 1, 70-77.
33. Goltsman B.M., Kudinov I.A., Smirnov I.A. (1972). *Poluprovodnikovyie termoelektricheskiie materaily na osnove Bi_2Te_3 [Semiconductor thermoelectric materials based on Bi_2Te_3]*. Moscow: Nauka [in Russian].
34. Lifshits E.M., Pitaevskii L.P. (1979). *Fizicheskaia kinetika [Physical kinetics]*. Moscow: Nauka [in Russian].

Submitted 17.04.2019

Горський П.В. *док. фіз.-мат. наук*[1,2]
Мицканюк Н.В.[1,2]

[1]Інститут термоелектрики НАН і МОН України,
вул. Науки, 1, Чернівці, 58029, Україна;
e-mail: anatych@gmail.com;
[2]Чернівецький національний університет
ім. Юрія Федьковича, вул. Коцюбинського 2,
Чернівці, 58000, Україна

ПРО ТЕМПЕРАТУРНІ ЗАЛЕЖНОСТІ ТЕРМОЕЛЕКТРИЧНИХ ХАРАКТЕРИСТИК ПЕРЕХІДНОГО ШАРУ ТЕРМОЕЛЕКТРИЧНИЙ МАТЕРІАЛ-МЕТАЛ БЕЗ УРАХУВАННЯ ЯВИЩА ПЕРКОЛЯЦІЇ

Розрахунковим шляхом отримано основні співвідношення, які визначають температурні залежності термоелектричних характеристик перехідних контактних шарів термоелектричний матеріал-метал без урахування теорії протікання. Конкретні кількісні результати та графіки температурних залежностей електричного та теплового контактних опорів, термоЕРС, фактору потужності та безрозмірної термоелектричної ефективності наведено для контактної пари телурид вісмуту – нікель. Встановлено, що разі нерівномірного розподілу атомів металу в інтервалі температур 200 – 400 К, інтенсивності надходження атомів металу у перехідний шар, яка відповідає зміні розподілу атомів металу за товщиною перехідного шару від лінійного до квадратичного та інтервалі товщин перехідного шару від 20 до 150 мкм електричний контактний опір змінюється від $1.8\cdot10^{-7}$ до $4.8\cdot10^{-6}$ Ом·см^2, тепловий контактний опір – від 0.022 до 0.35 К·см^2/Вт, термоЕРС – від 155 до 235 мкВ/К, фактор потужності – від $1.6\cdot10^{-4}$ до $2.9\cdot10^{-4}$ Вт/(м·К^2), безрозмірна термоелектрична ефективність – від 0.55 до 1.7. Бібл. 34, рис. 21.

Ключові слова: контакт термоелектричний матеріал – метал, приконтактний перехідний шар, електричний контактний опір, тепловий контактний опір, термоЕРС, фактор потужності, безрозмірна термоелектрична ефективність, температурні залежності.

Горский П.В., *док. физ-мат. наук*[1,2]
Мыцканюк Н.В.[1,2]

[1]Институт термоэлектричества НАН и МОН Украины, ул. Науки, 1,
Черновцы, 58029, Украина, *e–mail: anatych@gmail.com;*
[2]Черновицкий национальный университет
им. Юрия Федьковича, ул. Коцюбинского, 2,
Черновцы, 58012, Украина

О ТЕМПЕРАТУРНЫХ ЗАВИСИМОСТЯХ ТЕРМОЭЛЕКТРИЧЕСКИХ ХАРАКТЕРИСТИК ПЕРЕХОДНОГО СЛОЯ ТЕРМОЭЛЕКТРИЧЕСКИЙ МАТЕРИАЛ-МЕТАЛЛ БЕЗ УЧЕТА ЯВЛЕНИЯ ПЕРКОЛЯЦИИ

Расчетным путем получены основные соотношения, определяющие температурные зависимости термоэлектрических характеристик переходных контактных слоев термоэлектрический материал-металл без учета теории протекания. Конкретные количественные результаты и графики температурных зависимостей электрического и теплового контактных сопротивлений, термоЭДС, фактора мощности и безразмерной термоэлектрической эффективности приведены для контактной пары телурид висмута - никель. Установлено, что в случае неравномерного распределения атомов металла в интервале температур 200 - 400 К, интенсивности поступления атомов металла в переходной слой, которая отвечает изменению распределения атомов металла по толщине переходного слоя от линейного к квадратичному в интервале толщин переходного слоя от 20 до 150 мкм электрическое контактное сопротивление изменяется от 1.8· 10^{-7} до 4.8 10^{-6} Ом·см^2, тепловое контактное сопротивление - от 0.022 до 0.35 К·см^2/Вт, термоЭДС - от 155 до 235 мкВ/К, фактор мощности - от 1.6 10^{-4} до 2.9 10^{-4} Вт/(м·К^2), безразмерная термоэлектрическая эффективность - от 0.55 до 1.7. Библ. 34, рис. 20.

Ключевые слова: контакт термоэлектрический материал - металл, приконтактный переходный слой, электрическое контактное сопротивление, тепловое контактное сопротивление, термоЭДС, фактор мощности, безразмерная термоэлектрическая эффективность, температурные зависимости.

References

1. Aswal D.K., Basu R., Singh A. (2016). Key issues in development of thermoelectric power generators: high figure-of-merit materials and their highly conducting interfaces with metallic interconnects. *Energy Convers. Manag.,* 114, 50-67. http://refhub.elsevier.com/S2468-6069(18)30133-3/sref1
2. Anatychuk L.I., Kuz R.V. (2012). The energy and economic parameters of *Bi-Te* based thermoelectric generator modules for waster heat recovery. *J.Thermoelectricity*, 4, 75-82.
3. Drabkin I.A., Osvensky V.B., Sorokin A.I., Panchenko V.P., Narozhnaya O.E. (2017). Contact resistance in composite thermoelectric legs. *Semiconductors,* 51(8), 1038-1040.

4. Anatychuk L.I. (2003). *Termoelektrichestvo. Tom 2. Termoelektricheskiie preobrazovateli energii [Thermoelectricity. Vol.2. Thermoelectric power converters]*. Kyiv, Chernivtsi: Institute of Thermoelectricity [in Russian].
5. Semenyuk V. (2001). Thermoelectric micro modules for spot cooling of high density heat sources. *Proc. of 20th International Conference on Thermoelectrics*, 391-396.
6. Semenyuk V.A. (2006). Thermoelectric cooling of electro-optic components. *Thermoelectrics Handbook: Macro to Nano, 58-1 – 58-20. D.M. Rowe (Ed.).* CRC Taylor&Francis.
7. Fleurial J.-P., Snyder G.J., Patel J., et al. (2001). Solid-state power generation and cooling microdevices for distributed system architectures. *Proc of 20th International Conference on Thermoelectrics*, 24-29.
8. Bottner Harald, Nurnus Joachim, Schubert Axel (2006). Miniaturized thermoelectric converters. *Thermoelectrics Handbook, Macro to Nano. D.M. Rowe (Ed.).* CRC Taylor&Francis, 46-1 – 46-18.
9. Crane N. B., Misra P., Murray Jr. J.L., Nolas G.S. (2009). Self-assembly for integration of microscale thermoelectric coolers. *Journal of Electronic Materials*, 38 (7), 1252-1256.
10. I-Yu Huang, Jr-Ching Linb, Kun-Dian She (2008). Development of low-cost micro-thermoelectric coolers utilizing MEMS technology. *Sensors and Actuators*, A 148, 176–185.
11. Navone C., Soulier M., Plissonnier M., Seiler A.L. (2010). Development of $(Bi,Sb)_2(Te,Se)_3$-based thermoelectric modules by a screen-printing process. *Journal of Electronic Materials*, 39 (9), 1755-1759.
12. Goncalves L.M., Couto C., Alpuim P., Correia J.H. (2008). Thermoelectric micro converters for cooling and energy-scavenging systems. *J. Micromech. Microeng.*, 18, 064008, 1-5.
13. Misra P., Nagaraju J. (2004). Test facility for simultaneous measurement of electrical and thermal contact resistance. *Rev. Sci. Instr*., 75, 2625-2630 (doi 10.1063/1.1775316).
14. Maheshappa H.D., Nagaraju J., KrishnaMurthu N.V. (1998). A facility for electrical contact resistance measurement. *Rev. Sci. Instr*., 69, 534-1539 (doi 10.1063/1.1148810).
15. Deepak, Krishna H. (2007). Measurement of small specific contact resistance of metals with resistive semiconductors. *J. El. Mat*., 36, 598-605 (doi 10.1007/s11664-007-0091-y).
16. Gupta R.P., McCarty R., Sharp J. (2014). Practical contact resistance measurement method for bulk Bi_2Te_3 based thermoelectric devices. *J. El. Mat*., 43 (6), 1608-1612.
17. Kim Y., Yoon G., Park S.H. (2016). Direct contact resistance evaluation of thermoelectric legs. *Experimental Mechanics*, 56 (5), 861-869. https://doi.org/10.1007/s11340-016-0131-8-
18. Alieva T.D., Barkhalov B.Sh., Abdinov D.Sh. (1995). Struktura i elektricheskiie svoistva granits razdela kristallov $Bi_{0.5}Sb_{1.5}Te_3$ i $Bi_2Te_{2.7}Se_3$ s nekotorymi splavami [Structure and electrical properties of interfaces between $Bi_{0.5}Sb_{1.5}Te_3$ and $Bi_2Te_{2.7}Se_3$ crystals with certain alloys]. *Neorganicheskiie Materialy – Inorganic Materials*, 31 (2), 194-198.
19. Dzhamalov N.A., Barkhalov B.Sh., Salaiev E.Yu., Gasanov N.A., Abdinov D.Sh.(1983). *Neorganicheskiie Materialy – Inorganic Materials*, 19(4), 593-595.
20. Alieva T.D., Akhundova N.M., Dzhamalov N.A., et al. (1985). *Reports of the Academy of Sciences of Azerbaijan SSR,* 41(12), 18-20.
21. Kuznetsov G.D., Polystanskiy Y.G., Evseev V.A. (1995). The metallization of the thermoelement branches by ionic sputtering of the nickel and cobalt. *Proc of the XIV International Conference on Thermoelectrics (St.Petersburg, June 27-30, 1995)* (p.166-167).
22. Astakhov M.V., Bublik V.T., Karataiev V.V., et al. (2004). Vliianiie protsessa nikelirovaniia na strukturu i adhesionnyie svoistva poverkhnostnykh sloiov termoelektricheskogo materiala na osnove khalkogenidov Bi i Sb. [The influence of nickel plating process on the structure and adhesion properties

of surface layers of thermoelectric material based on Bu and Sb charlcogenides]. In: *"Thermoelectrics and their Application" (Saint-Petersburg, 2004)* (p.243-248).

23. Bublik V.T., Voronin A.I., Ponomarev V.F., Tabachkova N.Yu. (2012). Izmeneniie struktury prikontaknoi oblasti termoelektricheskikh materialov na osnove telluride vismuta pri povyshennykh temperaturakh [Change in the structure of near-contact area of thermoelectric materials based on bismuth telluride at elevated temperatures]. *Izvestiia vysshykh uchebnykh zavedenii.* Materaily Elektronnoi Tekhniki - *News of Higher Educational Institutions.* Materials of Electronic Technique, 2, 17-20 [in Russian].
24. Belonogov E.A., Dybov V.A., Kostiuchenko A.V., et al. Kondensirovannyie sredy i mezhfaznyie granitsy [Condensed media and interphase boundaries], Vol.19, №4, p.479-488.
25. Gupta Rahul P., Xiong K., White J.B., Cho Kyeongjae, Alshareef H.N., Gnade B.E. (2010). Low resistance ohmic contacts to Bi2Te3 using Ni and Co metallization. *Journal of the Electrochemical Society,* 157 (6), H666-H670, 2010. DOI: 10.1149/1.3385154
26. Ngan Hoang Pham, Nader Farahi, Hasbuna Kamila, Aryan Sankhla, Sahar Ayachi, Eckhard Müller, Johannes de Boor (2019). Ni and Ag electrodes for magnesium silicide based thermoelectric generators. *Materials Today Energy*, 11 97e105. https://doi.org/10.1016/j.mtener.2018.10.016.
27. Nikirsa D.D. (1987). Fizicheskiie osobennosti mikrominiaturizatsii polyprovodnikovykh okhlazhdaiushchikh termoelementov [Physical features of microminiaturization of semiconductor cooling thermoelements]. Candidate's thesis (Tech.sciences). Chernivtsi [in Russian].
28. Bartkowiak M., Mahan G.D. (2001). Heat and electricity transport through interfaces, in: *Recent Trends in Thermoelectric Materials, vol. II, Semiconductors and Semimetals*, vol. 70. New York: Academic Press.
29. Sze S.M. (1985). *Semiconductor Devices - Physics and Technology*, John Wiley & Sons.
30. Goldberg Yu.A. (1994). Ohmic contact metal-semiconductor AIIIBV: creation methods and properties. *Semiconductors*, 28(10), 1681-1698.
31. Da Silva L.W., Kaviany M. (2004). Microthermoelectric cooler: interfacial effects on thermal and electrical transport. *International Journal of Heat and Mass Transfer*, 47(10-11), 2417–2435.
32. Anatychuk L.I., Dugaev V.K., Litvinov V.I., Volkov V.L. (1994). Contact resistance between metal and thermoelectric material. *J. Thermoelectricity*, 1, 70-77.
33. Goltsman B.M., Kudinov I.A., Smirnov I.A. (1972). *Poluprovodnikovyie termoelektricheskiie materaily na osnove Bi_2Te_3 [Semiconductor thermoelectric materials based on Bi_2Te_3]*. Moscow: Nauka [in Russian].
34. Lifshits E.M., Pitaevskii L.P. (1979). *Fizicheskaia kinetika [Physical kinetics]*. Moscow: Nauka [in Russian].

Submitted 17.04.2019

V.V. Lysko, *cand. phys.– math. Sciences*[1,2]
Tudoroi P.F.[1,2]

[1]Institute of Thermoelectricity of the NAS and MES of Ukraine,
1, Nauky str, Chernivtsi, 58029, Ukraine;
e-mail: anatych@gmail.com
[2]Yu.Fedkovych Chernivtsi National University,
2, Kotsiubynskyi str., Chernivtsi, 58000, Ukraine

COMPUTER SIMULATION OF EXTRUSION PROCESS OF Bi_2Te_3 BASED TAPE THERMOELECTRIC MATERIALS

As long as in the process of hot extrusion of thermoelectric materials in the form of tape structures, billets of material are deformed under practically perfect plastic conditions, when optimizing equipment to obtain such materials, viscous fluid approximation may be used. This allows a computer simulation of the extrusion process using the hydrodynamic theory, where material is regarded as a fluid with a very high viscosity, which is a function of velocity and temperature. This paper presents the results of an object-oriented computer simulation of the process of hot extrusion of Bi_2Te_3 based thermoelectric material. Cases of producing thermoelectric materials in the form of tape structures for various matrix configurations are considered. The distributions of temperature and flow velocity of material in the matrix are obtained, as well as material velocity fields at the exit from the matrix which directly affect the structure of resulting material and its thermoelectric properties. Bibl. 6, Fig. 5, Tabl. 1.
Key words: simulationo, extrusion, tape thermoelectric material.

Introduction

At present, alongside with single-crystal *Bi-Te* based thermoelectric materials, extruded materials are also used for the production of thermoelectric products. The main advantage of the extrusion method is associated with improved material strength. Moreover, their thermoelectric properties may remain at the level of properties obtained by crystallization from the melt.

Generally, extruded thermoelectric materials are made in the form of cylindrical samples up to 25-30 mm in diameter. The use of extruded thermoelectric materials in the form of tape structures for the production of standard modules can reduce their cost by significantly reducing material losses.

At the same time, when creating equipment for producing extruded materials in the form of tape structures, the design and optimization of its structure are necessary.

One of effective ways to study the effect of conditions for producing material on its structure is mathematical simulation of the extrusion process in combination with the experimental results of structural studies [4, 5].

The purpose of this work is to create a computer model of the hot extrusion process of Bi_2Te_3 based thermoelectric material to study the distributions of temperature and material flow velocity in a rectangular-shaped matrix, which can be the basis for optimization of equipment for producing extruded thermoelectric material.

Physical, mathematical and computer extrusion models

To build a computer model of the hot extrusion process of tape thermoelectric material, the viscous fluid approximation and the application package of object-oriented simulation Comsol Multiphysics were

used [5]. The model employs the hydrodynamic theory, where a material is regarded as a fluid of high viscosity which is a function of velocity and temperature. The internal friction of the moving layers of material serves as a heat source. The developed computer model allows one to determine mechanical stress distribution in the matrix due to external pressure and thermal loads.

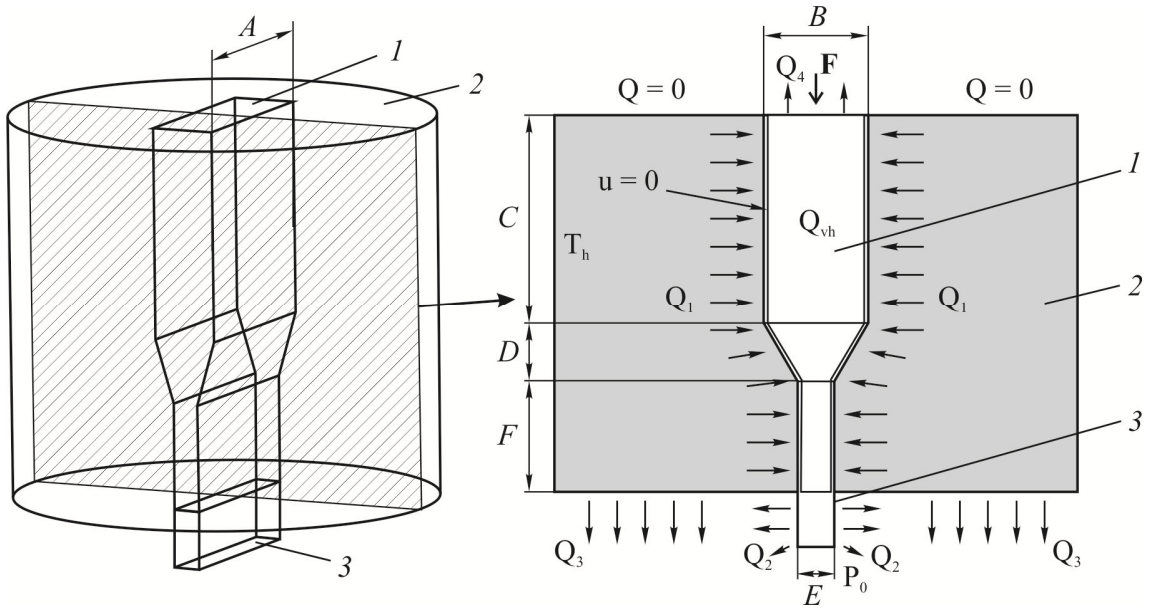

Fig. 1. Physical model of the extrusion process of tape thermoelectric material.
1 – thermoelectric material billet; 2 – matrix; 3 – tape thermoelectric material after leaving the matrix.

The employed physical model of the extrusion process of tape material is shown in Fig. 1. The model considers a stationary case of flowing through matrix 2 of material billet 1 obtained by cold pressing. The geometrical dimensions: *A*, *B* and *C* are width, thickness and length of matrix inlet (thermoelectric material billet); *D* is the length of the beveled part of the matrix; *E*, *F* are the thickness and length of matrix outlet whose width is *A*.

To find the distributions of velocities and temperatures, one should solve the following system of equations [5]

$$\rho(\boldsymbol{u}\cdot\nabla\boldsymbol{u}) = \nabla\left[-p\boldsymbol{I} + \eta(\nabla\boldsymbol{u} + (\nabla\boldsymbol{u})^T) - \frac{2}{3}\eta(\nabla\cdot\boldsymbol{u})\boldsymbol{I}\right] + \boldsymbol{F};$$

$$\nabla\cdot(\rho\boldsymbol{u}) = 0; \qquad (1)$$

$$\rho C_p\boldsymbol{u}\cdot\nabla\boldsymbol{T} = \nabla\cdot(\kappa\nabla T) + Q_{vh};$$

$$Q_{vh} = \eta(\nabla\boldsymbol{u} + (\nabla\boldsymbol{u})^T - \frac{2}{3}(\nabla\cdot\boldsymbol{u})\boldsymbol{I}) : \nabla\boldsymbol{u}$$

with the corresponding boundary conditions:

- thermostated lateral surface of matrix: $T = T_h$,
- convective heat exchange of the lateral surface of sample after leaving the matrix:

$$-\boldsymbol{n}\cdot(-\kappa\nabla T) = h_2(T - T_0),$$

- heat removal by structural members, not shown in Fig.1, from lower matrix part and upper part of

thermoelectric material billet:

$$-\boldsymbol{n}\cdot(-\kappa\nabla T) = h_3(T - T_0),\ -\boldsymbol{n}\cdot(-\kappa\nabla T) = h_4(T - T_0),$$

– thermal insulation of upper matrix part:

$$-\boldsymbol{n}\cdot(-\kappa\nabla T) = 0,$$

– input pressure on the billet: $p = p_1$,
– atmospheric pressure at sample exit from the matrix: $p = p_0 = 1$ atm.,
– equality to zero of fluid velocity at the boundary of contact with the matrix $\mathbf{u} = 0$,
– equality to zero of fluid velocity component perpendicular to the lateral side of the sample after leaving the matrix $\mathbf{u_n} = 0$,

where: $\boldsymbol{u}$ is velocity field, ρ is density, p is pressure, η is dynamic viscosity factor, κ is thermal conductivity, $\boldsymbol{F}$ is vector field of forces, Qvh is volumetric heat source due to internal friction, $\boldsymbol{I}$ is unit matrix, h_2 - h_4 are heat exchange coefficients, T_0 is ambient temperature.

Heating due to internal friction and contact thermal resistance at the boundary of contact between material and matrix are taken into account. The properties of thermoelectric material and matrix material used in simulation are given in Table 1.

Table 1.

Material properties

1.	Thermoelectric material	Thermal conductivity, W/(m*K)	4
		Density, kg/ m^3	7600
		Heat capacity, J/(kg*K)	150
2.	Steel (matrix)	Thermal conductivity, W/(m*K)	24.3
		Density, kg/ m^3	7850
		Heat capacity, J/(kg*K)	500

Equivalent viscosity of test fluid and other parameters necessary for computer model are calculated by the formulae given in [6].

Fig. 2 shows a mesh of finite element method which is used in Comsol Multiphysics for matrix configuration under study.

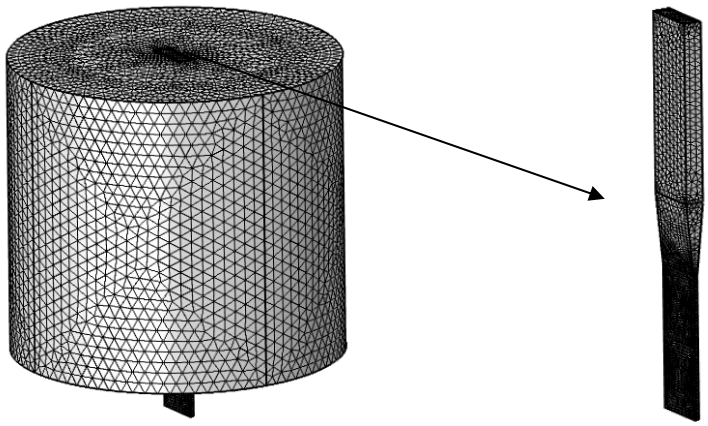

Fig. 2.Finite element method mesh built for matrix configuration shown in Fig. 1.

Computer simulation results

Typical velocity fields and temperature distributions in the matrix and thermoelectric material obtained by computer simulation are shown in Figs. 3, 4. The velocity in mm/min and temperature in degrees Celsius are marked in colour.

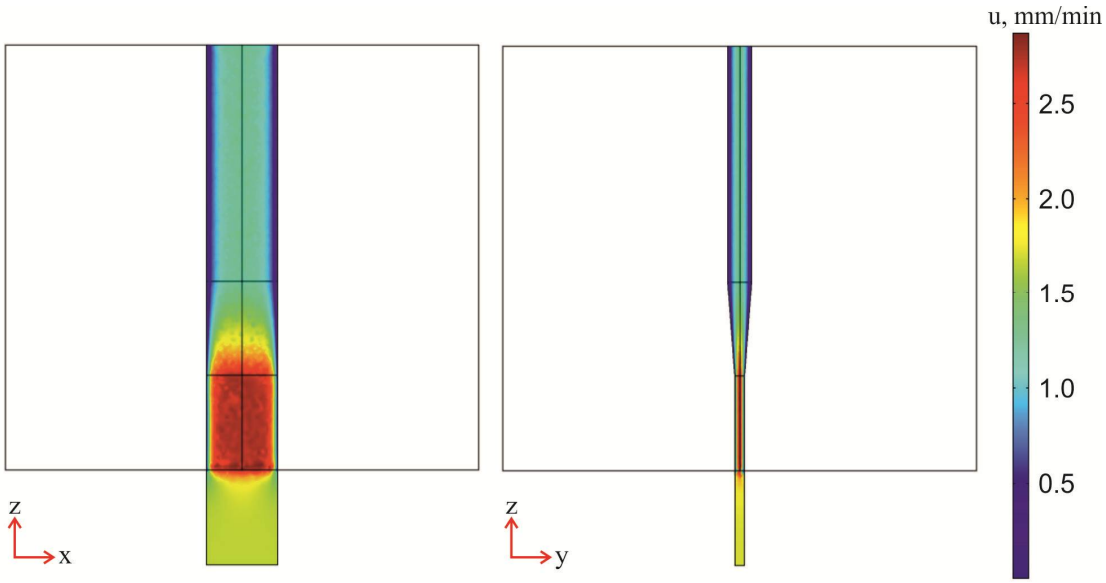

Fig. 3.Velocity field of thermoelectric material inside the matrix and after leaving it (for matrix with dimensions: A = 15mm; B = 5 mm; C = 50 mm; D = 20 mm; E = 2 mm; F = 20 mm).

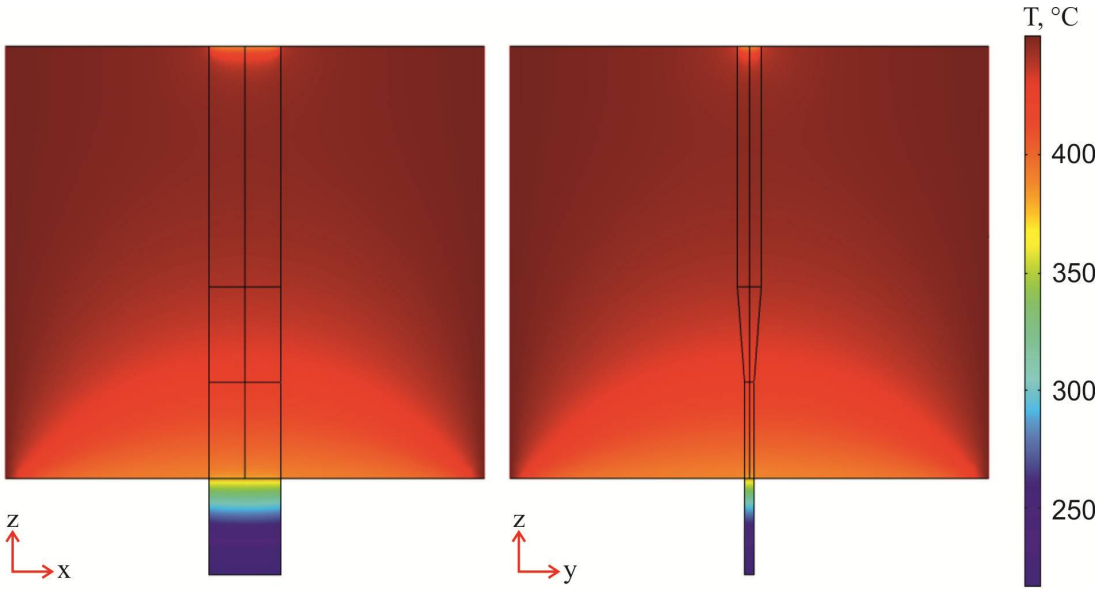

Fig. 3.Temperature distributions in thermoelectric material and matrix (for matrix with dimensions: A = 15mm; B = 5 mm; C = 50 mm; D = 20 mm; E = 2 mm; F = 20 mm).

Fig. 4 shows velocity fields in thermoelectric material at the exit from matrix obtained for various matrix configurations – its inlet and outlet dimensions (indicated in the figure in mm).

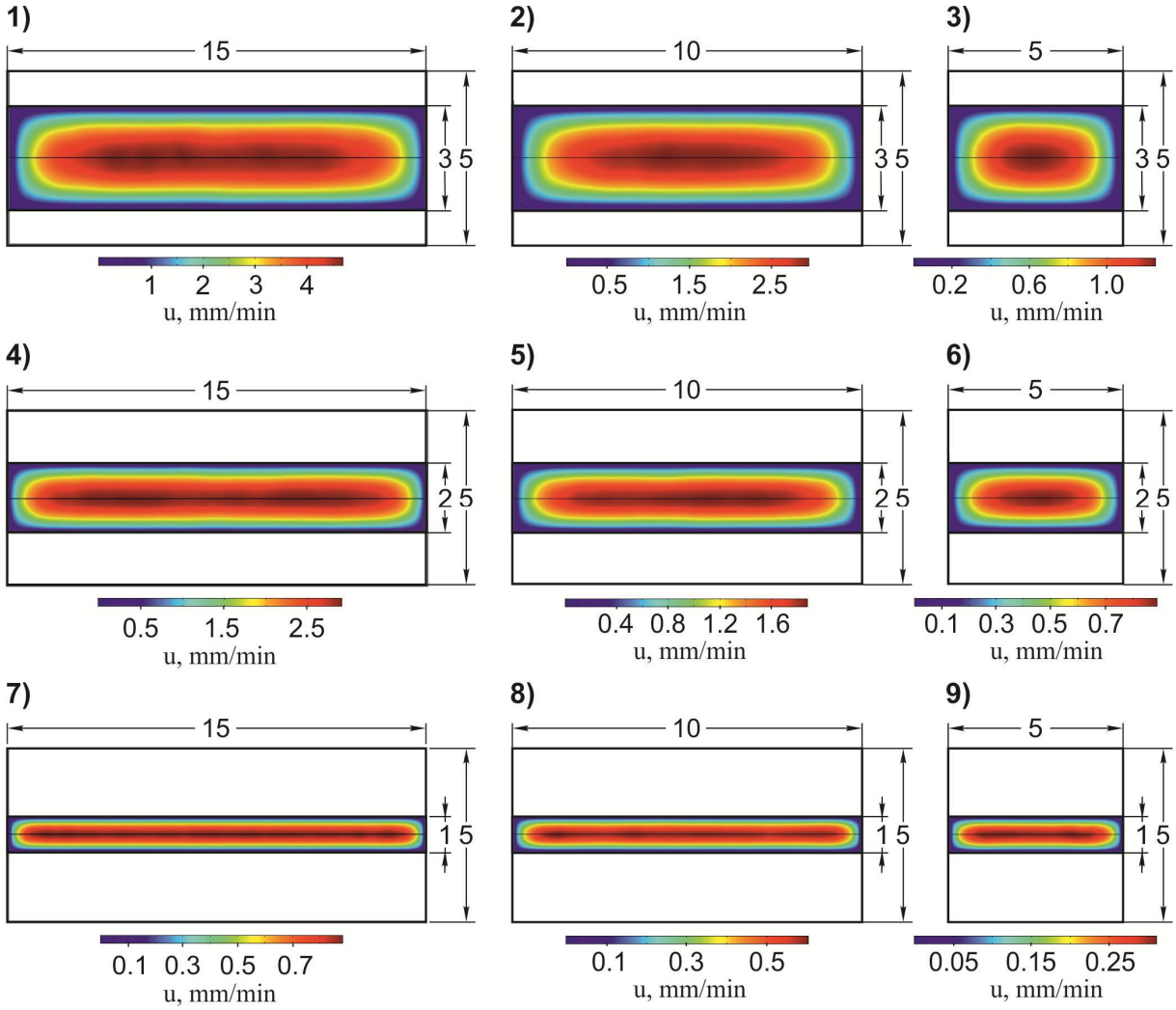

Fig. 4.Velocity fields in thermoelectric material at the exit from matrix obtained for various matrix configurations.
1 – A = 15 mm, B = 5 mm,, E = 3 mm, 2 – A = 10 mm,, B = 5 mm,, E = 3 mm,;
3 – A = 5 mm,, B = 5 mm,, E = 3 mm,; 4 – A = 15 mm,, B = 5 mm,, E = 2 mm,;
5 – A = 10 mm, B = 5 mm, E = 2 mm,; 6 – A = 5 mm,, B = 5 mm,, E = 2 mm,;
7 – A = 15 mm, B = 5 mm, E = 1 mm; 8 – A = 10 mm, B = 5 mm, E = 1 mm;
9 – A = 5 mm, B = 5 mm, E = 1 mm.

Fig. 5 shows velocity distributions along the width of the output tape thermoelectric material (1 mm after leaving the matrix). In the percentage ratio, the smallest velocity spread is typical for cases with the largest thickness ratio of matrix inlet and outlet.

Since extrusion conditions, i.e. die shape, temperature and strain rate, etc., directly affect the final structure and properties of the extruded material, the information obtained is useful for optimizing the design of equipment for extrusion of *Bi-Te* based tape materials. The computer model developed can also, if necessary, reproduce these results for other materials and extrusion conditions.

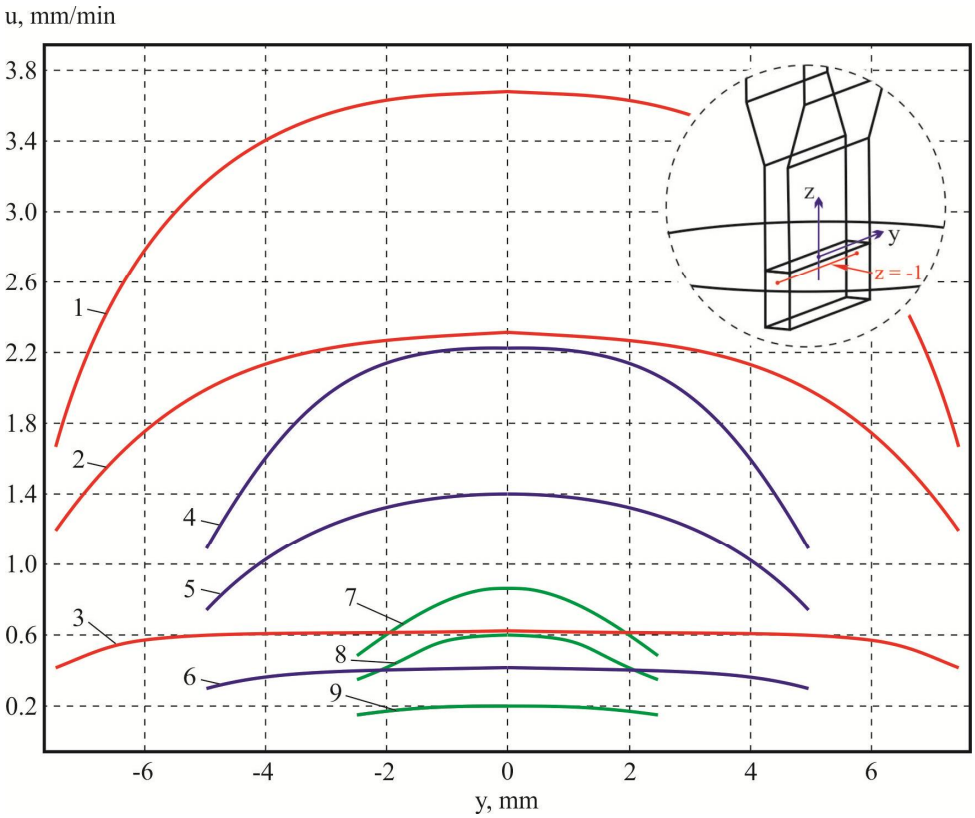

Fig. 5. Velocity distributions along the width of the output tape thermoelectric material (1 mm after leaving the matrix) for various matrix geometry:1 – A = 15 mm, B = 5 mm, E = 3 mm; 2 – A = 15 mm, B = 5 mm, E = 2 mm; 3 – A = 15 mm, B = 5 mm, E = 1 mm; 4 – A = 10 mm, B = 5 mm, E = 3 mm; 5 – A = 10 mm, B = 5 mm, E = 2 mm; 6 – A = 10 mm, B = 5 mm, E = 1 mm; 7 – A = 5 mm, B = 5 mm, E = 3 mm; 8 – A = 5 mm, B = 5 mm, E = 2 mm; 9 – A = 5 mm, B = 5 mm, E = 1 mm.

Conclusions

1. A computer model of the hot extrusion process of Bi_2Te_3 based thermoelectric material was created which can be used to study the distributions of temperature and material flow velocity in the matrix, as well as mechanical stress distribution in the matrix due to external pressure and thermal loads.
2. The temperature and material flow velocity distributions in the matrix were obtained depending on matrix configuration for the case of thermoelectric material extrusion in the form of tape structures.
3. Dependences of velocity distribution of tape thermoelectric material after leaving the matrix were obtained versus size ratio of matrix inlet and outlet. Conditions for approximation of this distribution to the one-dimensional were determined.

References

1. Bulat L.P. (2002). *Thermoelectric cooling*. St.-Petersburg: St.-Petersburg State Academy of Cool and Food Technologies.
2. Sabo E.P. (2006). Technology of chalcogenide thermoelements. Physical fundamentals. *J.Thermoelectricity*, 1, 45-66.
3. *Patent of RF 2475333 C1* (2011). Sorokin A.I., Parkhomenko Yu.N., Osvenskyi V.B., Lavrentiev M.G., Karataiev V.V., Drabkin I.A. Extrusion process of thermoelectric material based on bismuth and antimony chalcogenides [in Russian]. .

4. Lavrentiev M.G., Osvenskyi V.B., Mezhennyi M.V., Prostomolotov A.I., Bublik V.T., Tabachkova N,Yu. (2012). Teoreticheskoie i eksperimentalnoie issledovaniie formirovaniia struktyry termoelektricheskogo materiala na osnove tverdykh rastvorov (Bi, $Sb)_2Te_3$ poluchennogo metodom goriachei ekstruzii [Theortical and experimental research on the formation of structure of thermoelectric material based on (Bi, $Sb)_2Te_3$ solid solutions obtained by hot extrusion method. XIII Interstate Workshop "Thermoelectrics and Their Applications" (St.Petersburg, Russia, 2012).
5. Lysko V.V. (2019). Viscous fluid approximation when simulating Bi_2Te_3 based thermoelectric material extrusion process.
6. Fluid-structure interaction in aluminum extrusion (2008). *Structural Mechanics Module Model Library.* COMSOL AB, p. 301-316.

Submitted 24.04.2019

Лисько В.В. *канд. фіз.-мат. наук* [1,2]
Тудорой П.О.

[1]Інститут термоелектрики НАН і МОН України,
вул. Науки, 1, Чернівці, 58029, Україна, *e-mail: anatych@gmail.com*;
[2]Чернівецький національний університет імені Юрія Федьковича,
вул. Коцюбинського 2, Чернівці, 58012, Україна

КОМП'ЮТЕРНЕ МОДЕЛЮВАННЯ ПРОЦЕСУ ЕКСТРУЗІЇ СТРІЧКОВИХ ТЕРМОЕЛЕКТРИЧНИХ МАТЕРІАЛІВ НА ОСНОВІ Bi_2Te_3

Оскільки в процесі гарячої екструзії термоелектричних матеріалів у вигляді стрічкових структур заготовки матеріалу деформуються в практично ідеальних пластичних умовах, при оптимізації обладнання для отримання таких матеріалів може бути використано наближення в'язкої рідини. Це дозволяє проводити комп'ютерне моделювання процесу екструзії з використанням теорії гідродинаміки, де матеріал розглядається як рідина з дуже високою в'язкістю, яка залежить від швидкості і температури. У роботі наведено результати об'єктно-орієнтованого комп'ютерного моделювання процесу гарячої екструзії термоелектричного матеріалу на основі Bi_2Te_3. Розглянуті випадки отримання термоелектричних матеріалів у вигляді стрічкових структур для різних конфігурацій матриці. Отримано розподіли температури та швидкості протікання матеріалу у матриці, а також поля швидкостей матеріалу на виході з матриці, які безпосередньо впливають на структуру отриманого матеріалу та його термоелектричні властивості. Бібл. 6, рис. 5, табл. 1.
Ключові слова: моделювання, екструзія, стрічковий термоелектричний матеріал.

Лысько В.В., *канд. физ – мат. наук,* [1,2]
Тудорой П.Ф. [1,2]

[1]Институт термоэлектричества НАН и МОН Украины,
вул. Науки, 1, Черновцы, 58029, Украина;
[2]Чернивецький национальный университет имени. Юрия Федьковича,
ул. Коцюбинского 2, Черновцы, 58000, Украина, *e-mail: anatych@gmail.com*

КОМПЬЮТЕРНОЕ МОДЕЛИРОВАНИЕ ПРОЦЕССА ЭКСТРУЗИИ ЛЕНТОЧНЫХ ТЕРМОЭЛЕКТРИЧЕСКИХ МАТЕРИАЛОВ НА ОСНОВЕ Bi_2Te_3

Поскольку в процессе горячей экструзии термоэлектрических материалов в виде ленточных структур заготовки материала деформируются в практически идеально пластических условиях, при оптимизации оборудования для получения таких материалов может быть использовано приближение вязкой жидкости. Это позволяет проводить компьютерное моделирование процесса экструзии с использованием теории гидродинамики, где материал рассматривается как жидкость с очень высокой вязкостью, которая зависит от скорости и температуры. В работе приведены результаты объектно-ориентированного компьютерного моделирования процесса горячей экструзии термоэлектрического материала на основе Bi_2Te_3. Рассмотренные случаи получения термоэлектрических материалов в виде ленточных структур для разных конфигураций матрицы. Получены распределения температуры и скорости протекания материала в матрицы, а также поля скоростей материала на выходе из матрицы, которые непосредственно влияют на структуру полученного материала и его термоэлектрические свойства. Библ. 6, рис. 5, табл. 1.

Ключевые слова: моделирование, экструзия, ленточный термоэлектрический материал.

References

1. Bulat L.P. (2002). *Thermoelectric cooling*. St.-Petersburg: St.-Petersburg State Academy of Cool and Food Technologies.
2. Sabo E.P. (2006). Technology of chalcogenide thermoelements. Physical fundamentals. *J.Thermoelectricity*, 1, 45-66.
3. *Patent of RF 2475333 C1* (2011). Sorokin A.I., Parkhomenko Yu.N., Osvenskyi V.B., Lavrentiev M.G., Karataiev V.V., Drabkin I.A. Extrusion process of thermoelectric material based on bismuth and antimony chalcogenides [in Russian]. .
4. Lavrentiev M.G., Osvenskyi V.B., Mezhennyi M.V., Prostomolotov A.I., Bublik V.T., Tabachkova N,Yu. (2012). Teoreticheskoie i eksperimentalnoie issledovaniie formirovaniia struktyry termoelektricheskogo materiala na osnove tverdykh rastvorov (Bi, $Sb)_2Te_3$ poluchennogo metodom goriachei ekstruzii [Theortical and experimental research on the formation of structure of thermoelectric material based on (Bi, $Sb)_2Te_3$ solid solutions obtained by hot extrusion method. XIII Interstate Workshop “Thermoelectrics and Their Applications” (St.Petersburg, Russia, 2012).
5. Lysko V.V. (2019). Viscous fluid approximation when simulating Bi_2Te_3 based thermoelectric material extrusion process.
6. Fluid-structure interaction in aluminum extrusion (2008). *Structural Mechanics Module Model Library.* COMSOL AB, p. 301-316.

Submitted 24.04.2019

L.I. Anatychuk, *acad. of the NAS of Ukraine*[1,2],
O.V. Nitsovych *cand. phys.– math. sciences*[1,2]


L.I. Anatychuk

[1]Institute of Thermoelectricity of the NAS and MES of Ukraine,
1 Nauky str., Chernivtsi, 58029, Ukraine;
e-mail: anatych@gmail.com
[2]Yuriy Fedkovych Chernivtsi National University,
2 Kotsiubynsky str., Chernivtsi, 58012, Ukraine;


O.V. Nitsovych

COMPUTER RESEARCH ON THE INFLUENCE OF THE PELTIER EFFECT ON THE CRYSTALLIZATION PROCESS OF Bi_2Te_3 BASED THERMOELECTRIC MATERIALS

The article presents the results of computer simulation of the process of growing Bi_2Te_3 based thermoelectric materials by the vertical zone melting method with regard to the Peltier effect occurring at the interface between solid and liquid phases of the grown material when electric current is passed through an ingot. Bibl. 7, Fig. 6, Tabl. 1.
Key words: simulation, vertical zone melting, thermoelectric material, growing in electric field.

Introduction

Bismuth telluride-based solid solutions are unique commercially available thermoelectric materials (TEM) for solid-state cooling and generation of electrical energy. Therefore, much attention is paid to the improvement of Bi_2Te_3 based TEM production methods.

Zone melting is one of the most used methods for the production of semiconductor materials, in particular thermoelectric. However, the production of thermoelectric materials with the necessary properties is possible only under the conditions of a controlled crystallization process, since when TEM is obtained by this method, the crystallization front curvature, the temperature gradient at the interface between the solid and liquid phases, the melt zone geometry, and the velocity have a great influence on the single crystal growth stability and homogeneity.

In [1-3], the possibility of growing single crystals of thermoelectric materials by the method of vertical zone melting in the presence of electric current passing through an ingot was considered. It is known that when passing an electric current, at the interface between the solid and liquid phases of the same semiconductor, just as at the interface between two different materials, the Peltier heat will be released or absorbed. This amount of heat is sufficient to affect the course of crystallization. However, studies of temperature distributions and geometry of the crystallization front cause considerable experimental difficulties, so simulation of the TEM growth process is relevant, which makes it possible to optimize the choice of technological parameters of the setup and the modes of material growth.

So, *the purpose of this work* is computer research on the influence of the Peltier effect that occurs at the interface between the solid and liquid phases when growing Bi_2Te_3 based thermoelectric materials by the vertical zone melting when passing electric current through the molten zone, on growing process, specifically, on the shape of crystallization front and temperature gradients.

Physical model of vertical zone melting process with current

The physical model of the process of growing single crystals based on Bi_2Te_3 by the method of vertical zone melting is shown in Fig.1.

The figure shows an ingot fragment, including polycrystalline material 2, molten zone 6 and single crystal 3. The ingot is placed in quartz ampoule 1. With the help of heater 7 and cooler system 8, molten zone 6 is formed, which, moving with the heater along the sample, provides melting of polycrystal and melt crystallization below boundary 5, which is called the crystallization front.

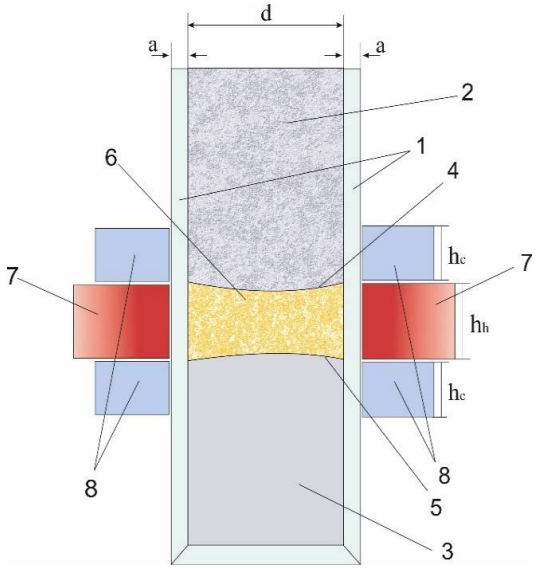

Fig.1. Physical model of installation for growing TEM by vertical zone melting method:
1 – quartz ampoule, 2 – material in solid phase (polycrystal), 3 – material n solid phase (single crystal),
4 – melt front boundary, 5 – crystallization front boundary, 6 – material in liquid phase (melt zone),
7 – heater, 8 – coolers.

When simulating zone growth, the stationary mode was considered, that is, the movement of the heat unit, including heater 7 and coolers 8, was not taken into account. It is known that crystals based on bismuth telluride are grown at a velocity of 1.5-2.5 cm/h. Estimating the time required for the system to achieve thermal equilibrium, which, even with rough calculations, was 40 s, it was determined that during this time the furnace will only move 0.2 mm. The heat loss in this area will be two orders of magnitude less than the heat that is transferred from the thermal unit to the ampoule. Thus, these losses can be neglected in computer simulation, since they will have little effect on the overall temperature distribution.

Mathematical model of TEM growing process by vertical zine melting method with current

When simulating the heat conduction process in a homogeneous medium with a phase transition in the COMSOL Multiphysics software package, the classical system of nonstationary differential heat conduction equations is solved, supplemented by the dependences of the physical properties of the solid under study as a function of the phase state at a given point at a specified temperature with regard to the Joule-Lenz heat and thermoelectric effects:

$$\rho C_p \frac{\partial T}{\partial t} + \rho C_p u \nabla T + \nabla q = Q + Q_e \quad (1)$$

$$q = -\kappa \nabla T + Pj, \quad (2)$$

$$Q_e = jE \tag{3}$$

here

$$j = \sigma E + j_e, \tag{4}$$

$$j_e = -\sigma\alpha\nabla T, \tag{5}$$

$$P = \alpha T, \tag{6}$$

$$E = -\nabla U, \tag{7}$$

$$\rho = \theta\rho_{phase1} + (1-\theta)\rho_{phase2}, \tag{8}$$

$$C_p = \frac{1}{2}\left(\theta\rho_{phase1}C_{p_{phase1}} + (1-\theta)\rho_{phase2}C_{p_{phase2}}\right) + L\frac{d\alpha_m}{dT}, \tag{9}$$

$$\alpha_m = \frac{1}{2}\cdot\frac{(1-\theta)\rho_{phase2} - \theta\rho_{phase1}}{\theta\rho_{phase1} + (1-\theta)\rho_{phase2}}, \tag{10}$$

$$\kappa = \theta\kappa_{phase1} + (1-\theta)\kappa_{phase2}. \tag{11}$$

де ρ is the density, kg/m^3; C_p is heat capacity of material at constant pressure, J/(kg·K); κ is thermal conductivity, W/(cm·K), u is medium velocity, m/s, in the investigated problem is zero; T is temperature, K; t is time, s; θ is the phase ratio at a given temperature; α_m is mass ratio between phases; L is the latent heat of phase transition, J/kg; Q is external heat flux, W. The indices phase1 and phase2 indicate to what phase the properties, solid phase or liquid, respectively, are related.

To simulate the effect of the electrical field on the growing process, the following boundary conditions are set at the upper and lower boundaries of the ingot:

$$U|_{z=0} = U_0\,,\; U|_{z=l} = 0. \tag{11}$$

The condition of thermal insulation was set on all external walls of the heater and coolers:

$$-n\cdot(-\kappa\nabla T) = 0. \tag{12}$$

On the outer wall of the quartz ampoule the boundary condition is set as a function of:

$$-n(-\kappa\nabla T) = h(T_{ext} - T) + \varepsilon\sigma_b(T_{ext}^4 - T^4), \tag{13}$$

where T_{ext} is the ambient temperature, K; T is the temperature of the wall of the quartz ampoule, K; n is vector directed along the normal to the surface of the cylinder (ampoule); ε is quartz emissivity; σ_b is Stephan-Boltzmann constant, Wт/(m^2·K^4); h is the heat transfer coefficient, W/(m^2·K), which is expressed by the formula [4]:

$$h = \begin{cases} \frac{k}{l}\left(0{,}68 + \frac{0{,}67\,Ra_l^{1/4}}{\left(1+\left(\frac{0{,}492\,k}{\mu C_p}\right)^{9/16}\right)^{4/9}}\right), \text{якщо } Ra_l \le 10^9 \\ \frac{k}{l}\left(0{,}825 + \frac{0{,}38\,Ra_l^{1/6}}{\left(1+\left(\frac{0{,}492\,k}{\mu C_p}\right)^{9/16}\right)^{8/27}}\right), \text{якщо } Ra_l > 10^9 \end{cases},$$

here, Ra_l is the Raleigh number which is defined by the following expression:

$$Ra_l = \frac{g\alpha_p\rho^2 C_p(T-T_{ext})l^3}{\mu\kappa},$$

where g is the acceleration of gravity, m/s^2; α_p is the temperature coefficient of volumetric expansion, K^{-1}; l is the length of the air layer, m; μ is the dynamic viscosity, (Pa·S).

In order to take into account the features of phase transitions during heating – cooling of Bi_2Te_3, the thermoelectric properties of TEM are set depending on temperature, according to the data obtained in [5]. Convection and mass transfer of molten Bi_2Te_3 were not taken into account in this model.

Computer simulation results

Below are the results of computer simulation of the influence of the Peltier effect on the crystallization of bismuth telluride by vertical zone melting in the presence of electric current, in accordance with the physical model shown in Fig. 1. Table 1 shows some input parameters of the model.

Table 1.

Input data used in simulation

	T, °C	ε	C_p, J/(mole·K)	ρ, g/cm^3	*Liquidus and solidus*, °C
Bi_2Te_3	-	-	59.73-126.19	7.74	585-530
Quartz	-	0.9-0.41	-	-	-
Heater	700-820	0.8	-	7.0	-
Cooler	30	-	-	-	-

The diameter d of the grown crystal was taken to be 24 mm, the height of the heater was chosen optimal and, as noted in [6], should be equal to h_h=3d. The height of the coolers h_c=1/2d, the distance between the quartz tube, as well as between the heater and coolers was 2 mm. To simulate the effect of the electric field on the growing process, a potential difference was set at the upper and lower boundaries of the material.

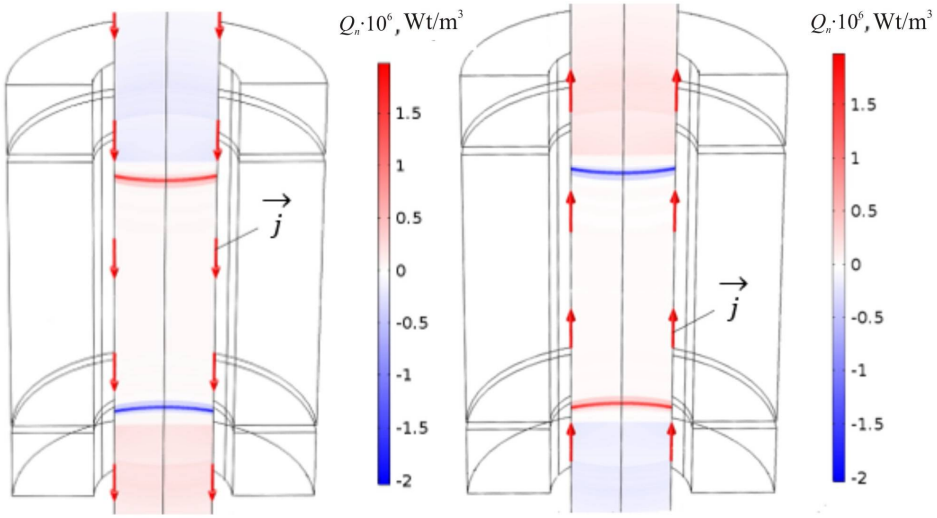

Fig.2. Release and absorption of the Peltier heat at the interfaces between solid and liquid phases depending on the direction of current passage

As can be seen from Fig. 2, the Peltier heat is a positive value, when current passes from the solid to liquid phase and, on the contrary, when current flows from the liquid to solid phase, the Peltier heat is absorbed.

The shape of the crystallization front, which can be concave, flat, or convex, is of great importance for the formation of a structurally homogeneous crystal during growth [6–7]. On a concave surface in the

melt, near the walls of the container, parasitic nuclei easily appear. This form of the front contributes to stresses, shrinkage shells and uneven distribution of impurities over the cross section of the grown crystal. The convex interface prevents the growth of random nuclei formed near the walls of the container, but the higher the growth rate, the more likely the formation of parasitic nuclei and the smaller the radius of curvature of the interface. A flat interface minimizes the occurrence of stresses in the crystal and promotes a uniform distribution of impurities over the cross section of the crystal. Therefore, it is important to create a flat crystallization front (Fig. 3, b).

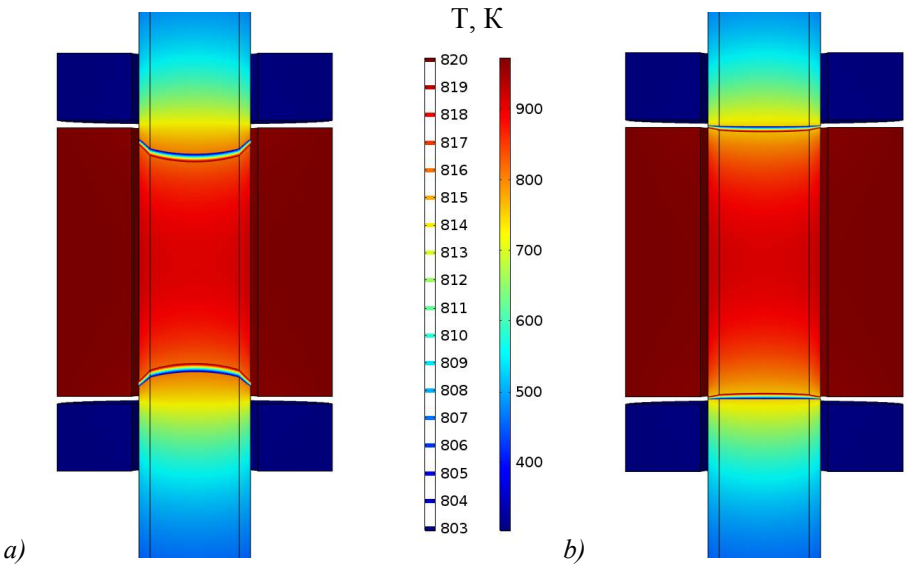

Fig.3. Crystallization front view for different heater temperatures at j=0.5·10^5: a) T_h=700°C; b) T_h=790°C

Fig.4 shows the dependence of the curvature value k of the crystallization front on the heater temperature at different densities of current passed through the molten zone. The curvature was calculated as $k = z_{max} - z_{min}$ along the front.

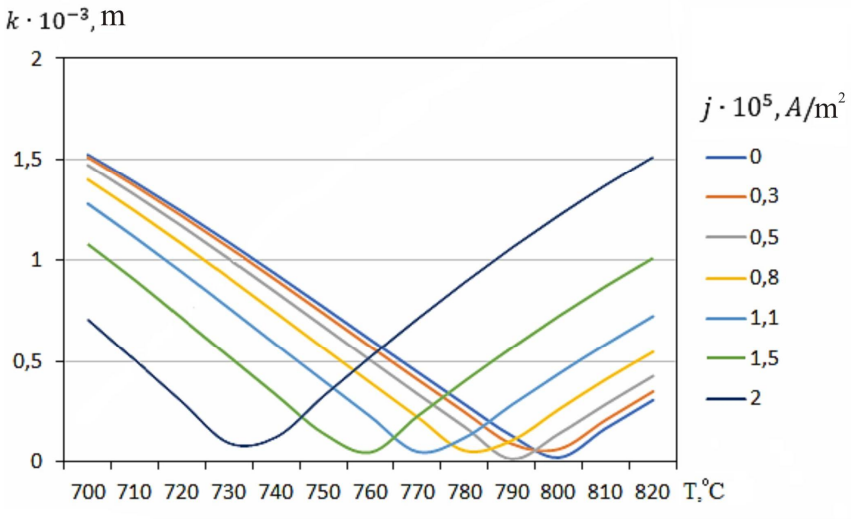

Fig.4. Dependence of the curvature value k of the crystallization front on the heater temperature at different densities of current

As can be seen from Fig. 4, for a given installation configuration, without passing an electric current, a flat crystallization front was achieved at temperatures of 790-800 ° C. By varying the current density from *0.3* до $2\cdot10^5$ *A/m*^{2}, a flat front can be achieved at lower heater temperatures.

The dependence of the temperature gradient along the crystallization front on the direction of current passage is shown in Fig.5. In this case the temperature of the heater is T_h=785°C, the current density j=0.5·10^5 A/m^2.

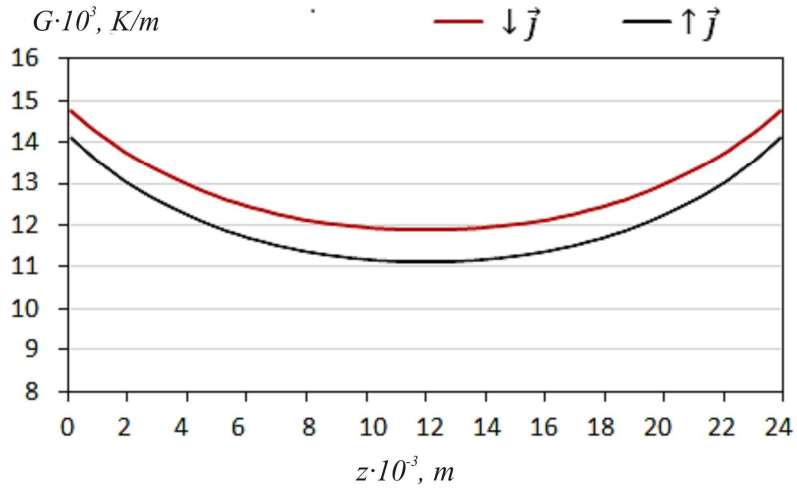

Fig.5. Dependence if the radial temperature gradient G on the direction of current passage

The use of the Peltier effect for zone growing with the passage of direct electric current is complicated by the fact that the Joule-Lenz heat is simultaneously released in the solid and liquid phases, which enhances the Peltier effect at the melt front and weakens it at the crystallization front.

Fig.6. shows the dependence of the radial temperature gradient G on the heater temperatures for different densities of current which is passed through the molten zone.

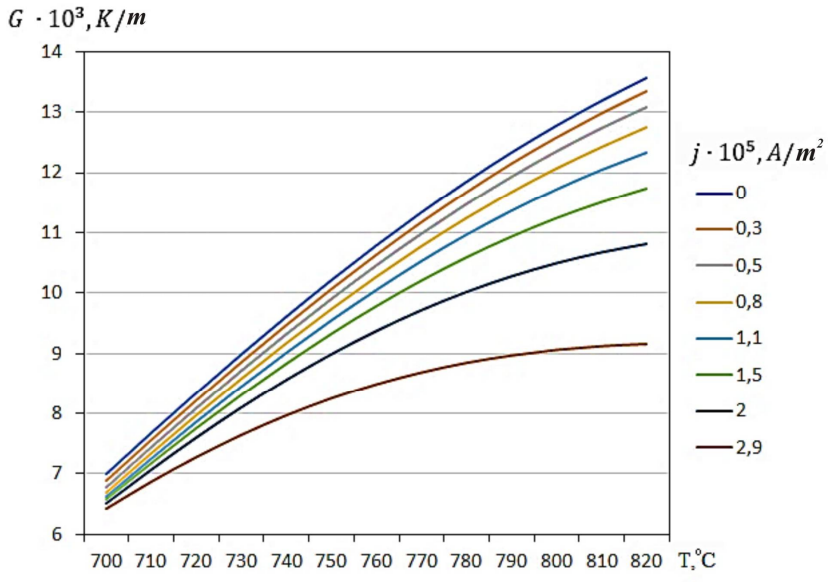

Fig.5. Dependence of the radial temperature gradient G on the heater temperatures for different current densities

From these results it follows that due to an increase in the Joule-Lenz heat, the temperature gradient at the crystallization front decreases with increasing current.

Conclusions

1. A technique was developed for computer simulation of the process of growing TEM based on Bi_2Te_3 by the method of vertical zone recrystallization with the passage of electric current through the sample.
2. The possibility of controlling the temperature distribution in the ingot during TEM growth by vertical zone melting method by passing electric current through the molten zone and the origination of the Peltier effect at the interface between the solid and liquid phases was confirmed.

The optimal values of the heater temperatures and current values were determined which ensure the formation of a flat crystallization front.

References

1. Pfan U.G. (1970). *Zonnaya plavka [Zone melting]*. V.N.Vigdorovich (Ed.). Moscow: Mir [in Russian].
2. Goltsman B.M., Liaschenok V.I., Strekopytova N.I. (1986). Kristallizatsiia v elektricheskom pole termoelektricheskikh materialov na osnove telluride vismuta [Crystallization in electrical field of thermoelectric materials based on bismuth telluride]. In: *Termoelektricheskiie istochniki toka: materaily, konstruktsiia, primeneniie. Tezisy dokladov vsesoiuznogo soveshchaniia - Thermoelectric current sources: materials, design, application. Abstracts of All-Union Conference reports. Ashgabad* [in Russian].
3. Liaschenok V.I., Strekopytova N.I. (1995). Influence of electric current flow during crystallization process on thermoelectric properties of materials. *Proc. of XIV International Conference of Thermoelectrics (1995),* 112-114.
4. Incropera F.P., DeWitt D.P., Bergman T.L., Lavine A.S. (2007). *Fundamentals of heat and mass transfer*. 6th Ed. New York: John Wiley & Sons Ltd.
5. Nitsovych O.V. (2018). Computer simulation of Bi_2Te_3 crystallization process in the presence of electric current. *J.Thermoelectricity*, 5, 12-21.
6. Nitsovych O.V. (2018). Research on the conditions of forming a flat crystallization front when growing Bi_2Te_3 based thermoelectric material by vertical zone melting method. *J.Thermoelectricity*, 3, 76-82.
7. Vilke K.T. (1977). *Metody vyrashchivaniia kristallov [Methods of crystal growth]*. Leningrad: Nedra [in Russian].

Submitted 01.05.2019

Анатичук Л.І. *акад. НАН Украини*[1,2]
О.В.Ніцович, *канд. фіз.-мат. наук*[1,2]

[1]Інститут термоелектрики НАН і МОН України,
вул. Науки, 1, Чернівці, 58029, Україна,
e-mail: anatych@gmail.com;
[2]Чернівецький національний університет
імені Юрія Федьковича, вул. Коцюбинського 2,
Чернівці, 58012, Україна

КОМП'ЮТЕРНЕ ДОСЛІДЖЕННЯ ВПЛИВУ ЕФЕКТУ ПЕЛЬТЬЄ НА ПРОЦЕС КРИСТАЛІЗАЦІЇ ТЕРМОЕЛЕКТРИЧНИХ МАТЕРІАЛІВ НА ОСНОВІ Bi_2Te_3

У статті наведено результати комп'ютерного моделювання процесу вирощування термоелектричних матеріалів на основі Bi2Te3 методом вертикальної зонної плавки з врахуванням ефекту Пельтьє, що виникає на межі розділу твердої та рідкої фаз вирощуваного матеріалу при пропусканні через злиток електричного струму. . Бібл. 7, рис. 5, табл. 1.
Ключові слова: моделювання, вертикальна зонна плавка, термоелектричний матеріал, вирощування в електричному полі.

Анатычук Л.И., *акад. НАН Украины*[1,2]
О.В.Ницович, *канд. физ.-мат. наук*[1,2]

[1]Институт термоэлектричества НАН и МОН Украины
ул. Науки, 1, Черновцы, 58029, Украина
e-mail: anatych@gmail.com;
[2]Черновицкий национальный университет
им. Ю.Федьковича, ул. Коцюбинского, 2,
Черновцы, 58012, Украина

КОМПЬЮТЕРНОЕ ИССЛЕДОВАНИЕ ВЛИЯНИЯ ЭФФЕКТА ПЕЛЬТЬЕ НА ПРОЦЕСС КРИСТАЛЛИЗАЦИИ ТЕРМОЭЛЕКТРИЧЕСКИХ МАТЕРИАЛОВ НА ОСНОВЕ Bi_2Te_3

В статье приведены результаты компьютерного моделирования процесса выращивания термоэлектрических материалов на основе Bi_2Te_3 методом вертикальной зонной плавки с учетом эффекта Пельтье, который возникает на границе раздела твердой и жидкой фаз выращиваемого материала при пропускании через слиток электрического тока. Библ. 7, рис. 6, табл. 1.
Ключевые слова: моделирование, вертикальная зонная плавка, термоэлектрический материал, выращивание в электрическом поле.

References

1. Pfan U.G. (1970). *Zonnaya plavka [Zone melting].* V.N.Vigdorovich (Ed.). Moscow: Mir [in Russian].
2. Goltsman B.M., Liaschenok V.I., Strekopytova N.I. (1986). Kristallizatsiia v elektricheskom pole termoelektricheskikh materialov na osnove telluride vismuta [Crystallization in electrical field of thermoelectric materials based on bismuth telluride]. In: *Termoelektricheskiie istochniki toka: materaily, konstruktsiia, primeneniie. Tezisy dokladov vsesoiuznogo soveshchaniia - Thermoelectric current sources: materials, design, application. Abstracts of All-Union Conference reports. Ashgabad*

[in Russian].

3. Liaschenok V.I., Strekopytova N.I. (1995). Influence of electric current flow during crystallization process on thermoelectric properties of materials. *Proc. of XIV International Conference of Thermoelectrics (1995),* 112-114.
4. Incropera F.P., DeWitt D.P., Bergman T.L., Lavine A.S. (2007). *Fundamentals of heat and mass transfer*. 6th Ed. New York: John Wiley & Sons Ltd.
5. Nitsovych O.V. (2018). Computer simulation of Bi_2Te_3 crystallization process in the presence of electric current. *J.Thermoelectricity*, 5, 12-21.
6. Nitsovych O.V. (2018). Research on the conditions of forming a flat crystallization front when growing Bi_2Te_3 based thermoelectric material by vertical zone melting method. *J.Thermoelectricity*, 3, 76-82.
7. Vilke K.T. (1977). *Metody vyrashchivaniia kristallov [Methods of crystal growth]*. Leningrad: Nedra [in Russian].

Submitted 01.05.2019

L.I. Anatychuk *acad. National Academy of sciences of Ukraine*[1,2]
P.D. Mykytiuk. *cand. phys.– math. sciences* [1,2],
O.Yu. Mykytiuk. *cand. phys.– math. sciences, assist. professor*[3]

[1]Institute of Thermoelectricity of the NAS and MES of Ukraine, 1, Nauky str, Chernivtsi, 58029, Ukraine;
e-mail: anatych@gmail.com;
[2]Yuriy Fedkovych Chernivtsi National University, 2, Kotsiubynsky str., Chernivtsi, 58012, Ukraine;
[3]Higher State Educational Institution of Ukraine "Bukovinian State Medical University", 2, Theatre Square, Chernivtsi, 58002, Ukraine

EXPERIMENTAL STUDIES OF A THERMOELECTRIC CURRENT SOURCE WITH AN ANNULAR THERMOPILE

The results of studies of a single-acting thermoelectric current source with an annular thermopile are presented. The research results confirmed the efficiency of current source breadboard models with an annular thermopile and the compliance of their electrical parameters with the requirements of the Performance Specification under Contract 3/2019. Bibl. 2, Fig. 6, Tabl. 1.
Key words: thermoelectric battery, current source, voltage, output power.

Introduction

In conformity with the Performance Specification under Contract 3/2019 of 16.04.2019, a thermoelectric current source with an annular thermopile shall be made and investigated. A thermoelectric converter for the current source shall be structurally made in the form of a toroidal ring with the outer and inner diameters of 50 and 39 mm, respectively, and a width of 16.5 mm. In this case, the current source shall provide an output power of not less than 20 W at a voltage of 5 V. The operating temperature difference ΔT, in this case, shall not exceed 300 K.

Studies of elementary thermopiles for an annular thermopile

At each stage of manufacturing a component part of an annular thermopile for current source, i.e. elementary single-row thermopiles, a step-by-step visual inspection of thermoelement legs was carried out with the rejection of defective elements according to geometric dimensions, and a sorting was carried out by the resistance of thermoelement legs.

Each thermopile assembled from those that passed step-by-step inspection (Fig. 1), which is a component part of an annular thermopile for current source, was tested and selected after measuring its main parameters at the "Altec-10002" installation specially created at the Institute of Thermoelectricity, the appearance of which is shown in Fig. 2.

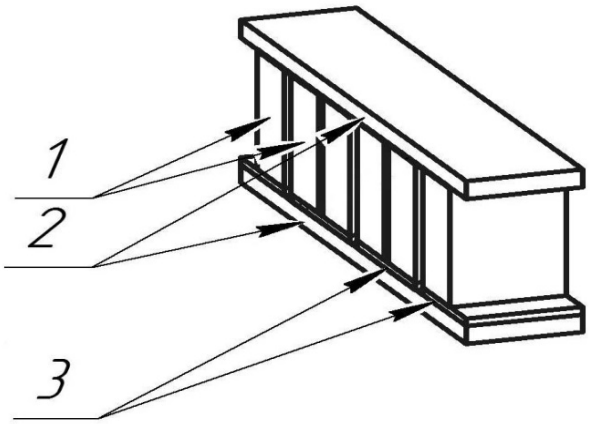

Fig. 1 – Appearance of elementary thermopiles.
1 – thermoelement legs of n- and p-type conductivity,
2 – ceramic plates, 3 – copper connecting plates.

This installation is intended for determination of the electrical and thermal parameters of thermoelectric modules working in generator mode.

Fig. 2 – Installation "Altec-10002".

The operating principle of the installation when used to measure thermopile lies in direct measurement of thermoEMF or voltage at given thermopile load. The thermopile is arranged between heat exchangers that create a regulated steady-state heat flux. The installation also makes it possible to measure current in the load circuit of thermopile, heat flux flowing through the thermopile and to determine its power and efficiency at the installed load.

In laboratory investigations, thermal conditions similar to those set in Performance Specification were reproduced on the measuring installation. The purpose of such investigations was exact assignment of operating ΔT on a thermopile intended for the assembly of annular thermopile breadboard models and determination of their initial characteristics.

Under the elementary thermopile, a heat meter is placed - a device for measuring the heat flux created by the temperature difference between the thermopile working surfaces. The heat meter is a collection of copper rods of the same length and cross-sectional area, in the lateral surfaces of which, at the same distance from the ends, differential thermocouples are mounted. To increase the sensitivity of the heat meter, these thermocouples are interconnected in series. The heat flux that runs along the rods creates a predetermined temperature difference ΔT at the locations of the thermocouples, which is proportional to the value of the heat flux. The proportionality coefficient for each size of the heat

meter is calculated and depends on the geometric dimensions and constants of the materials from which it is made. The ends of the rods on both sides are soldered into the heat-leveling copper plates, which are the basis of the heat meter. A junction of a measuring differential thermocouple is integrated on the upper base of the heat meter. The EMF of this thermocouple displays the cold side temperature of the thermopile. The fact that the heat meter is located on the cold side of the thermopile makes it possible to significantly increase the accuracy of heat flux measurement, since the heat loss from the heat meter is minimal.

The hot heat exchanger and heat meter are replaceable and chosen in conformity with the dimensions of thermopiles that are measured.

For more efficient heat transfer between the heat exchangers and thermopiles, the compression force between them must be reliable, optimized and controlled. This is achieved using a lever-weight device, the operation of which is clear from the test bench schematic. The compression force must be limited by the strength of the materials used to create thermopiles (for Bi_2Te_3, the least durable material from which the legs of the module are made, the force should not exceed 20 kg/cm^2).

In the process of measurement, to determine the magnitude of the current, the thermopile should be loaded with external resistance. For this, a rheostat with linear conductors of high resistivity is used in the installation. This form of rheostat is selected for the convenience of accurate selection of load resistance. When measuring the thermal values of error, the losses are mainly determined at the heat spreaders between thermocouples and the objects where they are mounted. The quality of thermal contact also depends on the surface finish of thermopiles. There is also an uncontrolled heat loss from the side surface of the heat meter due to increased convective heat transfer and heat radiation from the surface of the heat meter to the environment, if the cold side temperature of the module is significantly different from room temperature.

At the “Altec-10002” installation, 36 thermopile samples were investigated and selected (with a height of 5.5 mm and a length of 16.5 mm) for the assembly of annular thermopiles for current source breadboard models. Typical parameters and characteristics of thermopiles for an annular thermopile are given in Table 1.

Table 1

Parameters of elementary thermopiles

Module №	R, Ohm	ΔT, °C	U, V	W, W	η, %
1	2	3	4	5	6
1	0.026	270	0.123	0.351	3.78
2	0.025	270	0.130	0.384	3.77
3	0.023	270	0.109	0.327	3.25
4	0.025	270	0.130	0.384	3.93
5	0.025	270	0.118	0.313	3.62
6	0.025	270	0.130	0.357	3.54
7	0.025	270	0.132	0.403	3.94
8	0.024	270	0.132	0.409	3.82
9	0.026	270	0.120	0.306	3.28
10	0.025	270	0.129	0.348	3.49
11	0.024	270	0.128	0.365	3.31

12	0.025	270	0.123	0.326	3.55
13	0.026	270	0.120	0.282	3.39
14	0.024	270	0.125	0.331	3.43
15	0.026	270	0.131	0.347	3.65
16	0.025	270	0.134	0.395	3.81
17	0.025	270	0.127	0.381	3.78
18	0.025	270	0.126	0.359	3.75
19	0.026	270	0.131	0.367	3.69
20	0.025	270	0.122	0.329	3.51
21	0.025	270	0.132	0.383	3.77
22	0.025	270	0.133	0.392	3.72
23	0.025	270	0.128	0.333	3.35
24	0.025	270	0.135	0.398	3.86
25	0.024	270	0.127	0.349	3.59
26	0.028	270	0.110	0.242	2.90
27	0.026	270	0.119	0.292	3.01
28	0.027	270	0.121	0.296	3.39
29	0.024	270	0.107	0.256	3.13
30	0.026	270	0.128	0.346	3.60
31	0.028	270	0.132	0.343	3.61
32	0.027	270	0.128	0.339	3.56
33	0.026	270	0.128	0.358	3.59
34	0.026	270	0.118	0.301	3.43
35	0.025	270	0.123	0.338	3.50
36	0.025	270	0.121	0.296	3.25

where R is thermopile resistance, ΔT is operating temperature difference on the thermopile, U is thermopile generated voltage, W is thermopile power, η is thermopile efficiency. From single-row thermopiles, annular thermopiles were made, the appearance of which is shown in Fig. 3.

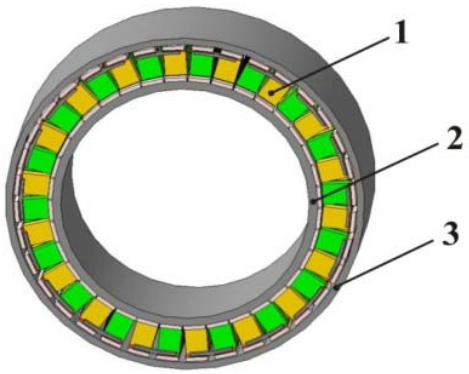

Fig. 3 – Schematic of an annular thermopile:
1 – annular thermopile; 2 – hot heat exchanger ring;
3 – cold heat exchanger ring.

The data presented in Table 1 confirm the efficiency of thermopiles selected for an annular thermopile, as well as the possibility of assuring with their use the initial characteristics of current source breadboard models at the level required by Performance Specification under Contract 3/2019.

Studies of current source breadboard models

Studies of current source breadboard models were performed in accordance with the developed program and the preliminary testing methodology [2]. A heat simulator was used as a heat source. In the course of studies of the electrical parameters of current source breadboard models for compliance with the requirements of the Performance Specification, the dependences of the initial electrical parameters (power P and voltage U) on the temperature gradient ΔT were determined.

Studies of current source breadboard models were performed on the experimental bench the schematic and appearance of which are shown in Fig. 4.

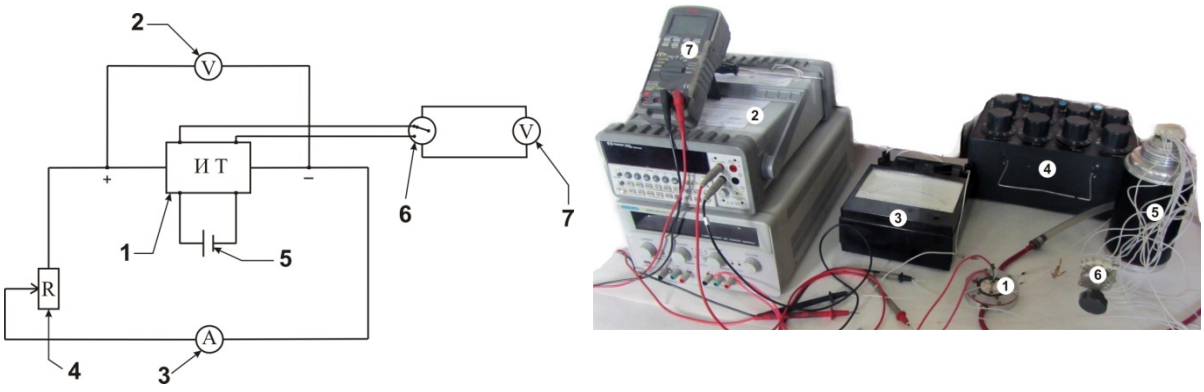

a) *b)*

Fig. 4 – Schematic (a) and appearance (b) of experimental bench for the study of current source breadboard models: 1 – current source breadboard model; 2 – multimeter; 3 – ammeter; 4 – bank of resistors; 5 – power supply; 6 – thermocouple switch; 7 – digital voltmeter; 8 – dewar with ice.

According to the Performance Specification, the output electric power P and the electric voltage U of current source breadboard model should be 2 W and 5 V. Taking into account the electrical parameters given in the Performance Specification, the tests of the current source breadboard model were carried out with an external resistance R = 12.5 Ohm, which was set by the bank of resistors 4. The power of the heat load simulator was increased by the power supply 5. Using a switch 6 and a voltmeter 7, chromel-kopel thermocouples measured the temperatures T_h, T_c of current source heat exchangers with a further determination of the working temperature gradient ΔT on the annular thermopile. In this case, the junction of one thermocouple was placed directly on the hot heat exchanger, and that of the other thermocouple - on the cold heat exchanger. The second junction of the thermocouple was placed in a dewar with ice 8. A multimeter 2 and an ammeter 3 measured the output electric voltage and current strength of a current source breadboard model.

The results of experimental studies of current source breadboard model and the dependences of its electrical parameters on temperature gradient ΔT are given in Fig. 5.

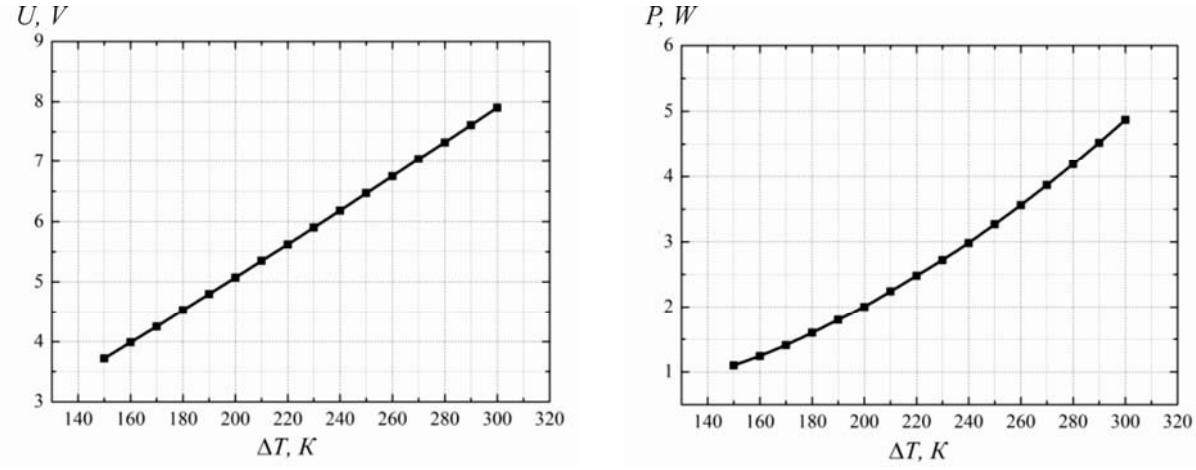

a) *b)*

Fig. 5 – Dependence of electric voltage U (a) and power P (b) of current source breadboard model on the operating temperature gradient ΔT.

From Fig.5 it is seen that with a rise in the temperature gradient ΔT on the thermopile, an increase in the electric voltage U and power P of the breadboard models is observed. In particular, for current source, the required output parameters according to the Performance Specification are already achieved at a working temperature difference of 200 ° C. At the same time, the electric power and voltage of the breadboard model are 2 W and 5 V. With a rise in ΔT, the output characteristics of the current source improve, exceeding the values required by the Performance Specification.

However, it should be borne in mind that in the above-mentioned current source studies, a heat load simulator was used, which provides an almost quasi-stationary operating mode of current source, which will not be ensured when using a pyrotechnic element. When using a pyrotechnic element, more stringent current source operating modes will take place, which will require more heat. The estimated time dependence of the heat source thermal power is shown in Fig. 6.

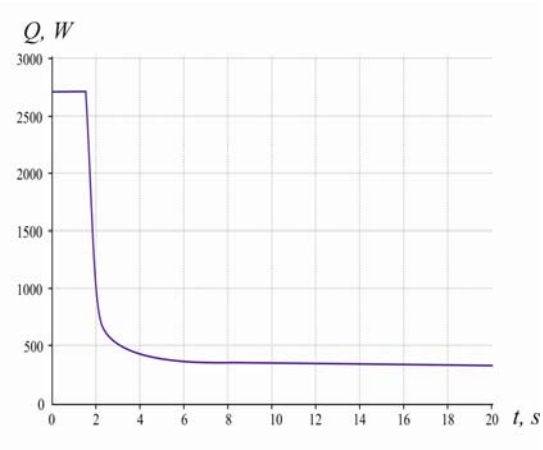

Fig. 6 – Time dependence of thermal power of pyrotechnic heat source.

Conclusion

The results of research confirmed the efficiency of current source breadboard models and the compliance of their electrical parameters with the requirements of the Performance Specification set out in Appendix 1 to Contract 3/2019.

References

1. Anatychuk L.I., Mykytiuk P.D. (2019). Design of an annular thermopile for a single acting current source. *J.Thermoelectricity*, №3, стор. …
2. Program and methods of research on a thermoelectric current source with an annular thermopile. *Contract 3/2019 of 16.04.2019*. Institute of Thermoelectricity.

Submitted 15.052.2019

Анатичук Л.І., *акад. НАН України*[1,2]
Микитюк П.Д. *канд. фіз.-мат. наук*[1,2]
Микитюк О.Ю. *канд. фіз.-мат. наук, доцент*[3]

[1]Інститут термоелектрики НАН і МОН України,
вул. Науки, 1, Чернівці, 58029, Україна,
e-mail: anatych@gmail.com;
[2]Чернівецький національний університет
імені Юрія Федьковича, вул. Коцюбинського 2,
Чернівці, 58012, Україна,
[3]Вищий державний навчальний заклад України
«Буковинський державний медичний університет»,
Театральна площа, 2, Чернівці, 58012, Україна

ДО ПИТАННЯ ВИБОРУ МАТЕРІАЛУ ТЕРМОПАРИ ДЛЯ ТЕРМОПЕРЕТВОРЮВАЧІВ МЕТРОЛОГІЧНОГО ПРИЗНАЧЕННЯ

Наведено результати досліджень термоелектричного джерела струму одноразової дії з кільцевою термоелектричною батареєю. Результати досліджень підтвердили працездатність макетних зразків ДС з кільцевою термобатареєю (ТЕБ) і відповідність їх електричних параметрів вимогам технічного завдання за договором 3/2019. Бібл. 2, рис. 6, табл. 1.
Ключові слова: термоелектрична батарея, джерело струму, номінальна напруга, вихідна потужність.

Анатычук Л.И., *акад. НАН Украины*[1,2]
Микитюк П.Д. *канд. физ.-мат. наук*[1,2]
Микитюк О.Ю. *канд. физ.– мат. наук, доцент*[3]

[1]Институт термоэлектричества НАН и МОН Украины,
ул. Науки, 1, Черновцы, 58029, Украина,
e-mail: anatych@gmail.com;

[2]Черновицкий национальный университет
имени Юрия Федьковича, ул. Коцюбинского 2,
Черновцы, 58012, Украина
[3]Высшее государственное учебное заведение Украины
«Буковинский государственный медицинский университет»,
Театральная площадь, 2, Черновцы, 58002, Украина

ЭКСПЕРИМЕНТАЛЬНЫЕ ИССЛЕДОВАНИЯ ТЕРМОЭЛЕКТРИЧЕСКОГО ИСТОЧНИКА ТОКА С КОЛЬЦЕВОЙ ТЕРМОЭЛЕКТРИЧЕСКОЙ БАТАРЕЕЙ

Приведены результаты исследований термоэлектрического источника тока одноразового действия с кольцевой термоэлектрической батареей. Результаты исследований подтвердили работоспособность макетных образцов ИТс кольцевой термобатареей (ТЭБ) и соответствие их электрических параметров требованиям технического задания по договору 3/2019. Библ. 2, рис. 6, табл. 1.

Ключевые слова*:* термоэлектрическая батарея, источник тока, напряжение, выходная мощность.

References

1. Anatychuk L.I., Mykytiuk P.D. (2019). Design of an annular thermopile for a single acting current source. *J.Thermoelectricity*, №3, стор. …
2. Program and methods of research on a thermoelectric current source with an annular thermopile. *Contract 3/2019 of 16.04.2019*. Institute of Thermoelectricity.

Submitted 15.05.2019

A.V. Prybyla

A.V. Prybyla, *cand. phys. - math. sciences*[1,2]

[1]Institute of Thermoelectricity
of the NAS and MES of Ukraine,
e-mail: anatych@gmail.com
1, Nauky str., Chernivtsi, 58029, Ukraine;
[2]Yu.Fedkovych Chernivtsi National University,
2, Kotsiubynskyi str., Chernivtsi, 58000, Ukraine

DESIGN OF A THERMOELECTRIC COOLING MODULE FOR AN X-RAY DETECTOR

The paper presents the results of designing a thermoelectric multistage thermoelectric cooling module for X-ray detectors. The structure of a thermoelectric cooler as part of an X-ray detector is developed and the possibilities of its practical use are analyzed. Bibl. 12, Fig. 2.
Key words: computer design, thermoelectric cooling, X-ray detector.

Introduction

General characterization of the problem. X-ray methods are widely used for non-destructive microanalytical studies of the structure and composition of materials with high spatial resolution [1]. The current state of nuclear microanalysis methods using focused beams of MeV energy ions with high monoenergeticity ($\Delta E/E=10^{-5}$) allows spatial resolution on the surface of up to 100 nanometers and up to 10 nanometers in the sample thickness. Further enhancement of the resolution substantially depends on the improvement of the analytical characteristics of semiconductor detectors, as well as on the use of wide-aperture position-sensitive radiation detectors of new types [2].

To increase the resolution of x-ray detectors, it is important to solve the problem of ensuring the optimal temperature of their operation [3-9].

It is solved by using semiconductor thermoelectric cooling modules [5-9] to provide the required cooling depth in the minimum working volume of the detector. Thus, single-stage thermoelectric modules are used for shallow cooling (to 250 K). Two-stage thermoelectric cooling modules are used for cooling sensors to operating temperature of 230 K, three-stage modules - to temperature of 210 K, four and five-stage modules – to temperatures below 190 K [10].

Therefore, the purpose of this work is to analyze the capabilities of thermoelectricity for cooling X-ray detectors and to design a multi-stage thermoelectric cooler for X-ray detectors.

Physical model

For the calculations, we used the physical model of a thermoelectric cooler as part of an X-ray detector presented in Fig. 1. It consists of a housing 2 with a beryllium window 1 through which radiation enters the X-ray detector 3. The required temperature and thermal conditions on the surface of the X-ray detector are provided by a multi-stage thermoelectric cooler with an electric power W consisting of n- and p-type thermoelectric material legs 8, electrically conductive interconnect plates 9, ceramic electrical insulation plates 7. A vacuum is created inside the detector housing 4 to reduce heat loss. The heat flow is removed from the thermoelectric cooler through the base of detector housing 5 and its fixture 6.

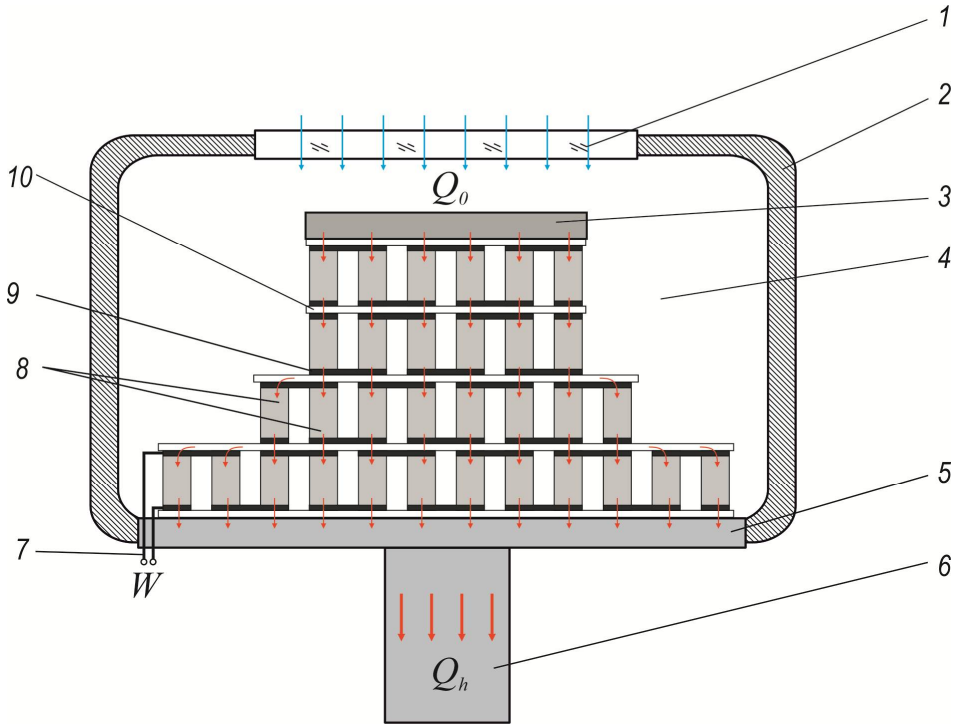

Fig. 1. Physical model of a thermoelectric multi-stage cooler as part of an X-ray radiation detector:
1 - beryllium window; 2 – device housing; 3 – X-ray radiation detector;
4 – internal space of device where vacuum is created; 5 – device housing base;
6 – device fixture; 7 – electrical leads; 8 – legs of n- and p-type thermoelectric material,
9 – electrical interconnect plates, 10 – ceramic electrical insulating plates .

Mathematical and computer descriptions of the model

The system of equations for the description of coefficient of performance of a thermoelectric cooler depending on the parameters of physical model is determined from thermal balance equations:

$$Q_c = \chi_1 (T_c^{(1)} - T_c), \tag{1}$$

$$\begin{cases} Q_h = \chi_3 (T_h^{(2)} - T_h^{(1)}) \\ Q_h = \chi_4 (T_h^{(1)} - T_h) \end{cases}, \tag{2}$$

$$Q_h = Q_c + W_{TE}. \tag{3}$$

Here, $T_c^{(1)}$ is detector surface temperature, T_c is thermoelectric module cold side temperature, χ_1 is thermal contact resistance, $T_h^{(2)}$ is thermoelectric module hot side temperature, $T_h^{(1)}$ is detector base temperature; T_h is temperature of surface to which heat is removed, χ_2 is thermal contact resistance, χ_3 is thermal resistance of heat exchanger on the "hot side" of thermoelectric converter, Q_0 is refrigerating capacity, Q_h is heating capacity.

With regard to (1) – (3), the expression for the coefficient of performance of thermoelectric cooler will be written in the form:

$$\varepsilon_r = \frac{Q_0}{W + W_1} = \frac{\alpha I (T_c + Q_0 N_1) - 0.5 I^2 R - \lambda (T_h - T_c - (Q_h N_2 + Q_0 N_1))}{W + W_1}, \tag{4}$$

where α is differential Seebeck coefficient of material, I is current strength, R is electrical resistance of

thermoelectric module, λ is average thermal conductivity of thermoelectric module legs, W_1 is power consumed to provide heat exchange,

$$N_1 = \frac{(\chi_1 + \chi_2)}{\chi_1 \chi_2},\ N_2 = \frac{(\chi_3 + \chi_4)}{\chi_3 \chi_4}. \tag{5}$$

To design the thermoelectric cooler, the COMSOL Multiphysics software package was used [11]. For this purpose, the equations of the physical model must be presented in a certain form, as will be shown below.

To describe heat and electricity flows, we use the laws of conservation of energy

$$div\vec{E} = 0 \tag{6}$$

and electrical charge

$$div\vec{j} = 0, \tag{7}$$

where

$$\vec{E} = \vec{q} + U\vec{j}, \tag{8}$$

$$\vec{q} = \kappa \nabla T + \alpha T\vec{j}, \tag{9}$$

$$\vec{j} = -\sigma \nabla U - \sigma\alpha \nabla T. \tag{10}$$

Here, $\vec{E}$ is energy flux density, $\vec{q}$ is thermal flux density, $\vec{j}$ is electric current density, U is electric potential, T is temperature, α, σ, κ are the Seebeck coefficient, electrical conductivity and thermal conductivity.

With regard to (8) – (10), one can obtain

$$\vec{E} = -(\kappa + \alpha^2 \sigma T + \alpha U \sigma)\nabla T - (\alpha \sigma T + U\sigma)\nabla U. \tag{11}$$

Then the laws of conservation (5), (6) will take on the form:

$$-\nabla\left[(\kappa + \alpha^2 \sigma T + \alpha U \sigma)\nabla T\right] - \nabla\left[(\alpha \sigma T + U\sigma)\nabla U\right] = 0, \tag{12}$$

$$-\nabla(\sigma\alpha \nabla T) - \nabla(\sigma \nabla U) = 0. \tag{13}$$

The second-order nonlinear differential equations in partial derivatives (12) and (13) determine the distribution of temperature T and potential U in the thermoelectric cooler.

Solving these equations with the use of technology of object-oriented computer simulation [11] and optimal control theory [12] allows finding optimal design of thermoelectric converter and the dependences of its characteristics.

Computer design results

As a result of computer simulation, the structure of a thermoelectric multistage module (Fig. 2) was designed, which provides the possibility of its use to ensure the temperature conditions of the X-ray detector (Table 1).

Thus, a thermoelectric cooler contains 4 stages - 6, 12, 27 and 65 pairs of thermoelectric material legs, its overall dimensions are 12 x 16 x 12 mm, while providing a cooling area of 4 x 8 mm. The dimensions of legs of thermoelectric material based on n- and p-type bismuth telluride (Bi_2Te_3) are 0.6 x

0.6 x 1.8 mm. Insulating plates of aluminum oxide (Al_2O_3) are 0.5 mm thick, electrical interconnects of copper (Cu) with an anti-diffusion layer of nickel (Ni) are 0.1 mm thick.

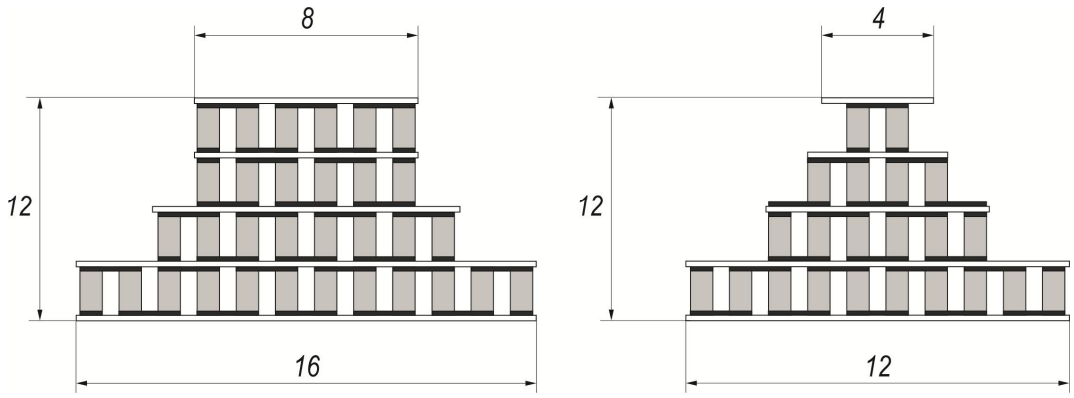

Fig.2. Schematic design of a thermoelectric cooler for an X-ray radiation detector

The estimated cooling capacity of the thermoelectric converter is Q_0 = 57 mW (3 mW - thermal load from the detector plus 54 mW - leakage through radiation). Provided the temperature at the detector $T_c^{(1)}$ = - 70 °C and at the heat sink temperature T_h = +20 °C, the coefficient of performance of the thermoelectric cooler is ε = 0.02. Therefore, the electrical power that will be consumed by this converter is W = 2.85 W.

The results obtained prove the possibilities of using thermoelectric coolers for assuring temperature and thermal conditions for X-ray radiation detectors and outperform the well-known world analogs [10].

Conclusions

1. Computer-aided design of a thermoelectric cooler for X-ray detectors was conducted.
2. The structure and characteristics of a thermoelectric cooler (as part of an X-ray detector) were designed. Thus, the thermoelectric cooler contains 4 stages of Bi_2Te_3 based thermoelectric material with the overall dimensions of 12x16x12 mm while providing a cooling area of 4x8 mm.
3. The electric power of a thermoelectric converter W = 2.85 W was determined, which with the coefficient of performance ε = 0.02 provides for the temperature of detector housing base $T_c^{(1)}$ = -70 °C and ΔT = 90 K.

References

1. Buhay O.M., Drozdenko M.O., Storizhko V.Yu. (2014). Microanalytical X-ray facility in IAP NASU. *Nanotechnology and Nanomaterials. Book of Abstracts.* Lviv.
2. Woldseth R. (1973). *X-Ray energy spectrometry*. Kevex: Scotts Valley, CA.
3. Stone R.E., Barkley V.A. and Fleming J.A. (1986). Performance of a Gamma-ray and X-ray spectrometer using Germanium and Si (Li) detectors cooled by a closed-cycle cryogenic mechanical refrigerator. *IEEE Trans. Nucl. Sci*. NS-33, 1, 299.
4. Broerman E.C., Keyser R.M., Twomey T.R., Upp D.L. *A new cooler for HPGe detector systems, ORTEC*. PerkinElmer Instruments: Inc Oak Ridge TN 37831-0895 USA.
5. Schlesinger TE, James RB. (1995). *Semiconductors and semimetals. Vol. 43. Semiconductors for room temperature nuclear detector applications*. New York: Academic Press.
6. Semiconductors for room-temperature detectors. Applications II. (1998). *Materials Research Society Symposium Proceedings,* Vol. 487. Materials Research Society: Warrendale, PA.
7. Sokolov, A., Loupilov, A., Gostilo, V. (2004). Semiconductor Peltier-cooled detectors for x-ray

fluorescence analysis. *X-Ray Spectrometry, 33(6), 462–465. doi:10.1002/xrs.744.*
8. http://www.rmtltd.ru/applications/photodetectors/xray.php.
9. http://www.amptek.com/wp-content/uploads/2014/04/XR-100T-CdTe-X-ray-and-Gamma-Ray-Detector-Specifications.pdf.
10. Anatychuk L.I., Vikhor L.N. (2013). The limits of thermoelectric cooling for photodetectors. *J. of Thermoelectricity*, 5, 54-58.
11. COMSOL Multiphysics User's Guide (2010). COMSOLAB, 804 p.
12. Anatychuk L.I., Semeniuk V.A. (1992). *Optimalnoie upravleniie svoistvami termoelektricheskikh materialov i priborov [Optimal control over the properties of thermoelectric materials and instruments]*. Chernivtsi: Prut [in Russian].

Submitted 19.05.2019

Прибила А.В., *канд. физ.-мат. наук*[1,2]

[1]Інститут термоелектрики НАН і МОН України,
вул. Науки, 1, Чернівці, 58029, Україна;
e–mail: anatych@gmail.com;
[2]Чернівецький національний університет
ім. Юрія Федьковича, вул. Коцюбинського 2,
Чернівці, 58012, Україна

ПРОЕКТУВАННЯ ТЕРМОЕЛЕКТРИЧНОГО МОДУЛЯ ОХОЛОДЖЕННЯ ДЕТЕКТОРА РЕНТГЕНІВСЬКОГО ВИПРОМІНЮВАННЯ

У роботі наведено результати проектування термоелектричного багатокаскадного термоелектричного модуля охолодження рентгенівських детекторів. Розроблено конструкцію термоелектричного охолоджувача у складі детектора рентгенівського випромінювання та проаналізовано можливості його практичного використання. Бібл. 12, рис. 2 .
Ключові слова: комп'ютерне проектування, термоелектричне охолодження, рентгенівський детектор.

Прибыла А.В., *канд. физ.-мат. наук*[1,2]

[1]Институт термоэлектричества НАН и МОН Украины,
ул. Науки, 1, Черновцы, 58029, Украина,
e–mail: anatych@gmail.com;
[2]Черновицкий национальный університет им. Юрия Федьковича,
ул. Коцюбинского, 2, Черновцы, 58012, Украина

ПРОЕКТИРОВАНИЯ ТЕРМОЭЛЕКТРИЧЕСКОГО МОДУЛЯ ОХЛАЖДЕНИЯ ДЕТЕКТОРА РЕНТГЕНОВСКОГО ИЗЛУЧЕНИЯ

В работе приведены результаты проектирования термоэлектрического многокаскадного термоэлектрического модуля охлаждения рентгеновских детекторов. Разработана конструкция термоэлектрического охладителя в составе детектора рентгеновского излучения и проанализированы возможности его практического использования. Библ. 12, рис. 2.
Ключевые слова: компьютерное проектирование, термоэлектрическое охлаждение, рентгеновский детектор.

References

1. Buhay O.M., Drozdenko M.O., Storizhko V.Yu. (2014). Microanalytical X-ray facility in IAP NASU. *Nanotechnology and Nanomaterials. Book of Abstracts.* Lviv.
2. Woldseth R. (1973). *X-Ray energy spectrometry*. Kevex: Scotts Valley, CA.
3. Stone R.E., Barkley V.A. and Fleming J.A. (1986). Performance of a Gamma-ray and X-ray spectrometer using Germanium and Si (Li) detectors cooled by a closed-cycle cryogenic mechanical refrigerator. *IEEE Trans. Nucl. Sci*. NS-33, 1, 299.
4. Broerman E.C., Keyser R.M., Twomey T.R., Upp D.L. *A new cooler for HPGe detector systems, ORTEC.* PerkinElmer Instruments: Inc Oak Ridge TN 37831-0895 USA.
5. Schlesinger TE, James RB. (1995). *Semiconductors and semimetals. Vol. 43. Semiconductors for room temperature nuclear detector applications*. New York: Academic Press.
6. Semiconductors for room-temperature detectors. Applications II. (1998). *Materials Research Society Symposium Proceedings,* Vol. 487. Materials Research Society: Warrendale, PA.
7. Sokolov, A., Loupilov, A., Gostilo, V. (2004). Semiconductor Peltier-cooled detectors for x-ray fluorescence analysis. *X-Ray Spectrometry, 33(6), 462–465. doi:10.1002/xrs.744.*
8. http://www.rmtltd.ru/applications/photodetectors/xray.php.
9. http://www.amptek.com/wp-content/uploads/2014/04/XR-100T-CdTe-X-ray-and-Gamma-Ray-Detector-Specifications.pdf.
10. Anatychuk L.I., Vikhor L.N. (2013). The limits of thermoelectric cooling for photodetectors. *J. of Thermoelectricity*, 5, 54-58.
11. COMSOL Multiphysics User's Guide (2010). COMSOLAB, 804 p.
12. Anatychuk L.I., Semeniuk V.A. (1992). *Optimalnoie upravleniie svoistvami termoelektricheskikh materialov i priborov [Optimal control over the properties of thermoelectric materials and instruments].* Chernivtsi: Prut [in Russian].

Submitted 19.05.2019

ARTICLE SUBMISSION GUIDELINES

For publication in a specialized journal, scientific works are accepted that have never been printed before. The article should be written on an actual topic, contain the results of an in-depth scientific study, the novelty and justification of scientific conclusions for the purpose of the article (the task in view).

The materials published in the journal are subject to internal and external review which is carried out by members of the editorial board and international editorial board of the journal or experts of the relevant field. Reviewing is done on the basis of confidentiality. In the event of a negative review or substantial remarks, the article may be rejected or returned to the author(s) for revision. In the case when the author(s) disagrees with the opinion of the reviewer, an additional independent review may be done by the editorial board. After the author makes changes in accordance with the comments of the reviewer, the article is signed to print.

The editorial board has the right to refuse to publish manuscripts containing previously published data, as well as materials that do not fit the profile of the journal or materials of research pursued in violation of ethical norms (for instance, conflicts between authors or between authors and organization, plagiarism, etc.). The editorial board of the journal reserves the right to edit and reduce the manuscripts without violating the author's content. Rejected manuscripts are not returned to the authors.

Submission of manuscript to the journal

The manuscript is submitted to the editorial office of the journal in paper form in duplicate and in electronic form on an electronic medium (disc, memory stick). The electronic version of the article shall fully correspond to the paper version. The manuscript must be signed by all co-authors or a responsible representative.

In some cases it is allowed to send an article by e-mail instead of an electronic medium (disc, memory stick).

English-speaking authors submit their manuscripts in English. Russian-speaking and Ukrainian-speaking authors submit their manuscripts in English and in Russian or Ukrainian, respectively. Page format is A4. The number of pages shall not exceed 15 (together with References and extended abstracts). By agreement with the editorial board, the number of pages can be increased.

To the manuscript is added:

1. Official recommendation letter, signed by the head of the institution where the work was carried out.

2. License agreement on the transfer of copyright (the form of the agreement can be obtained from the editorial office of the journal or downloaded from the journal website – Dohovir.pdf). The license agreement comes into force after the acceptance of the article for publication. Signing of the license agreement by the author(s) means that they are acquainted and agree with the terms of the agreement.

3. Information about each of the authors – full name, position, place of work, academic title, academic degree, contact information (phone number, e-mail address), ORCID code (if available). Information about the authors is submitted as follows:

authors from Ukraine - in three languages, namely Ukrainian, Russian and English;

authors from the CIS countries - in two languages, namely Russian and English;

authors from foreign countries – in English.

4. Medium with the text of the article, figures, tables, information about the authors in electronic

form.

5. Colored photo of the author(s). Black-and-white photos are not accepted by the editorial staff. With the number of authors more than two, their photos are not shown.

Requirements for article design

The article should be structured according to the following sections:

- *Introduction*. Contains the problem statement, relevance of the chosen topic, analysis of recent research and publications, purpose and objectives.
- *Presentation of the main research material* and the results obtained.
- *Conclusions* summing up the work and the prospects for further research in this direction.
- *References*.

The first page of the article contains information:

1) in the upper left corner – UDC identifier (for authors from Ukraine and the CIS countries);

2) surname(s) and initials, academic degree and scientific title of the author(s);

3) the name of the institution where the author(s) work, the postal address, telephone number, e-mail address of the author(s);

4) article title;

5) abstract to the article – not more than 1 800 characters. The abstract should reflect the consistent logic of describing the results and describe the main objectives of the study, summarize the most significant results;

6) key words – not more than 8 words.

The text of the article is printed in Times New Roman, font size 11 pt, line spacing 1.2 on A4 size paper, justified alignment. There should be no hyphenation in the article.

Page setup: "mirror margins" – top margin – 2.5 cm, bottom margin – 2.0 cm, inside – 2.0 cm, outside – 3.0 cm, from the edge to page header and page footer – 1.27 cm.

Graphic materials, pictures shall be submitted in color or, as an exception, black and white, in .opj or .cdr formats, .jpg or .tif formats being also permissible. According to author's choice, the tables and partially the text can be also in color.

Figures are printed on separate pages. The text in the figures must be in the font size 10 pt. On the charts, the units of measure are separated by commas. Figures are numbered in the order of their arrangement in the text, parts of the figures are numbered with letters – a, b, .. On the back of the figure, the title of the article, the author (authors) and the figure number are written in pencil. Scanned images and graphs are not allowed to be inserted.

Tables are provided on separate pages and must be executed using the MSWord table editor. Using pseudo-graph characters to design tables is inadmissible.

Formulae shall be typed in Equation or MatType formula editors. Articles with formulae written by hand are not accepted for printing. It is necessary to give definitions of quantities that are first used in the text, and then use the appropriate term.

Captions to figures and tables are printed in the manuscript after the references.

Reference list shall appear at the end of the article. References are numbered consecutively in the order in which they are quoted in the text of the article. References to unpublished and unfinished works are inadmissible.

Attention! In connection with the inclusion of the journal in the international bibliographic abstract database, the reference list should consist of two blocks: CITED LITERATURE and REFERENCES (this requirement also applies to English articles):

CITED LITERATURE – sources in the original language, executed in accordance with the Ukrainian standard of bibliographic description DSTU 8302:2015. With the aid of VAK.in.ua

(http://vak.in.ua) you can automatically, quickly and easily execute your "Cited literature" list in conformity with the requirements of State Certification Commission of Ukraine and prepare references to scientific sources in Ukraine in understandable and unified manner. This portal facilitates the processing of scientific sources when writing your publications, dissertations and other scientific papers.

REFERENCES – the same cited literature list transliterated in Roman alphabet (recommendations according to international bibliographic standard APA-2010, guidelines for drawing up a transliterated reference list "References" are on the site http//www.dse.org.ua, section for authors).

To speed up the publication of the article, please adhere to the following rules:

- in the upper left corner of the first page of the article – the UDC identifier;
- family name and initials of the author(s);
- academic degree, scientific title;

begin a new line, Times New Roman font, size 12 pt, line spacing 1.2, center alignment;

- name of organization, address (street, city, zip code, country), e-mail of the author(s);

begin a new line 1 cm below the name and initials of the author(s), Times New Roman font, size 11 pt, line spacing 1.2, center alignment;

- the title of the article is arranged 1 cm below the name of organization, in capital letters, semi-bold, font Times New Roman, size 12 pt, line spacing 1.2, center alignment. The title of the article shall be concrete and possibly concise;
- the abstract is arranged 1 cm below the title of the article, font Times New Roman, size 10 pt, in italics, line spacing 1.2, justified alignment in Ukrainian or Russian (for Ukrainian-speaking and Russian-speaking authors, respectively);
- key words are arranged below the abstract, font Times New Roman, size 10 pt, line spacing 1.2, justified alignment. The language of the key words corresponds to that of the abstract. Heading "Key words" - font Times New Roman, size 10 pt, semi-bold;
- the main text of the article is arranged 1 cm below the abstract, indent 1 cm, font Times New Roman, size 11 pt, line space spacing 1.2, justified alignment;
- formulae are typed in formula editor, fonts Symbol, Times New Roman. Font size is "normal" – 12 pt, "large index" – 7 pt, "small index" – 5 pt, "large symbol" – 18 pt, "small symbol" – 12 pt. The formula is arranged in the text, center aligned and shall not occupy more than 5/6 of the line width, formulae are numbered in parentheses on the right;
- dimensions of all quantities used in the article are represented in the International System of Units (SI) with the explication of the symbols employed;
- figures are arranged in the text. The figures and pictures shall be clear and contrast; the plot axes – parallel to sheet edges, thus eliminating possible displacement of angles in scaling; figures are submitted in color, black-and-white figures are not accepted by the editorial staff of the journal;
- tables are arranged in the text. The width of the table shall be 1 cm less than the line width. Above the table its ordinary number is indicated, right alignment. Continuous table numbering throughout the text. The title of the table is arranged below its number, center alignment;
- references should appear at the end of the article. References within the text should be

enclosed in square brackets behind the text. References should be numbered in order of first appearance in the text. Examples of various reference types are given below.

Examples of LITERATURE CITED

Journal articles

Anatychuk L.I., Mykhailovsky V.Ya., Maksymuk M.V., Andrusiak I.S. Experimental research on thermoelectric automobile starting pre-heater operated with diesel fuel. *J.Thermoelectricity*. 2016. №4. P.84–94.

Books

Anatychuk L.I. *Thermoelements and thermoelectric devices. Handbook.* Kyiv, Naukova dumka, 1979. 768 p.

Patents

Patent of Ukraine № 85293. Anatychuk L.I., Luste O.J., Nitsovych O.V. Thermoelement.

Conference proceedings

Lysko V.V. *State of the art and expected progress in metrology of thermoelectric materials.* Proceedings of the XVII International Forum on Thermoelectricity (May 14-18, 2017, Belfast). Chernivtsi, 2017. 64 p.

Authors' abstracts

Kobylianskyi R.R. *Thermoelectric devices for treatment of skin diseases*: extended abstract of candidate's thesis. Chernivtsi, 2011. 20 p.

Examples of REFERENCES

Journal articles

Gorskiy P.V. (2015). Ob usloviakh vysokoi dobrotnosti i metodikakh poiska perspektivnykh sverhreshetochnykh termoelektricheskikh materialov [On the conditions of high figure of merit and methods of search for promising superlattice thermoelectric materials]. *Termoelektrichestvo - J.Thermoelectricity,* 3, 5 – 14 [in Russian].

Books

Anatychuk L.I. (2003). *Thermoelectricity. Vol.2. Thermoelectric power converters*. Kyiv, Chernivtsi: Institute of Thermoelectricity.

Patents

Patent of Ukraine № 85293. Anatychuk L. I., Luste O.Ya., Nitsovych O.V. Thermoelements [In Ukrainian].

Conference proceedings

Rifert V.G. Intensification of heat exchange at condensation and evaporation of liquid in 5 flowing-down films. In: *Proc. of the 9th International Conference Heat Transfer.* May 20-25, 1990, Israel.

Authors'abstracts

Mashukov A.O. *Efficiency hospital state of rehabilitation of patients with color carcer.* PhD (Med.) Odesa, 2011 [In Ukrainian].